NTIS # PB2003-106851

SSC-428

IN-SERVICE NON-DESTRUCTIVE EVALUATION OF FATIGUE AND FRACTURE PROPERTIES FOR SHIP STRUCTURE

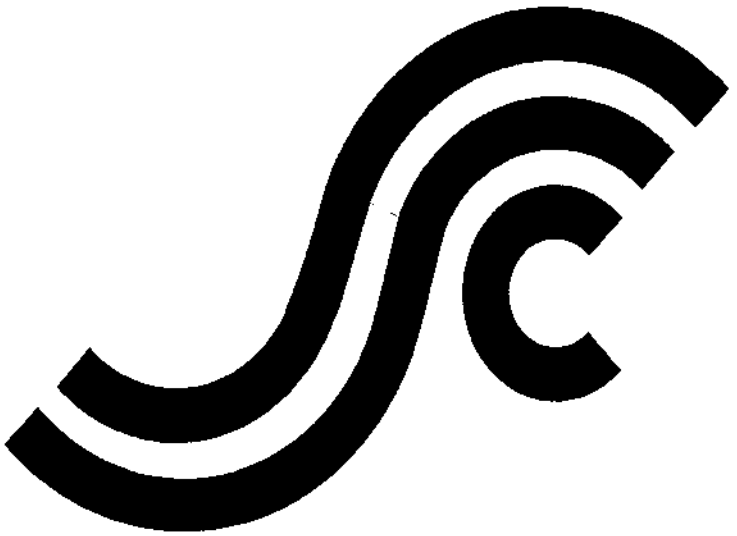

SHIP STRUCTURE COMMITTEE
2003

SHIP STRUCTURE COMMITTEE

RADM Thomas H. Gilmour
U. S. Coast Guard Assistant Commandant,
Marine Safety and Environmental Protection
Chairman, Ship Structure Committee

Mr. W. Thomas Packard
Director,
Survivability and Structural Integrity Group
Naval Sea Systems Command

Dr. Donald Liu
Senior Vice President
American Bureau of Shipping

Mr. Joseph Byrne
Director, Office of Ship Construction
Maritime Administration

Mr.Gerard A. McDonald
Director General, Marine Safety,
Safety & Security
Transport Canada

Mr. Thomas Connors
Director of Engineering
Military Sealift Command

Dr. Neil Pegg
Group Leader - Structural Mechanics
Defence Research & Development Canada - Atlantic

CONTRACTING OFFICER TECHNICAL REP.
Lieutenant Eric M. Cooper / Ms. Dinah Mulligan
U.S. Coast Guard R & D Center

EXECUTIVE DIRECTOR
Lieutenant Eric M. Cooper
U. S. Coast Guard

SHIP STRUCTURE SUB-COMMITTEE

AMERICAN BUREAU OF SHIPPING
Mr. Glenn Ashe
Mr. Yung Shin
Mr. Phil Rynn
Mr. William Hanzalek

DEFENCE RESEARCH & DEVELOPMENT ATLANTIC
Dr David Stredulinsky
Mr. John Porter

MARITIME ADMINISTRATION
Mr. Chao Lin
Mr. Carlos Setterstrom
Mr. Richard Sonnenschein

MILITARY SEALIFT COMMAND
Mr. Joseph Bohr
Mr. Rick A. Anderson
Mr. Michael W. Touma

NAVAL SEA SYSTEMS COMMAND
Mr. Jeffery E. Beach
Mr. Edward E. Kadala
Mr. Allen H. Engle
Mr. Charles L. Null

TRANSPORT CANADA
Mr. Jacek Dubiel

UNITED STATES COAST GUARD
Mr. Rubin Sheinberg
Mr. Robert Sedat
Commander Ray Petow

CANADIAN COAST GUARD
Mr. Daniel Gauvin

Member Agencies:

American Bureau of Shipping
Defence Research Establishment Atlantic
Maritime Administration
Military Sealift Command
Naval Sea Systems Command
Society of Naval Architects & Marine Engineers
Transport Canada
United States Coast Guard

Ship
Structure
Committee

Address Correspondence to:

Executive Director
Ship Structure Committee
U.S. Coast Guard (G-MSE/SSC)
2100 Second Street, SW
Washington, D.C. 20593-0001
Ph: (202) 267-0003
Email: ecooper@comdt.uscg.mil

SSC – 428
SR – 1385

August 2003

IN-SERVICE NON-DESTRUCTIVE EVALUATION OF FATIGUE AND FRACTURE PROPERTIES FOR SHIP STRUCTURE

An extensive literature review was conducted to seek out potential Non-Destructive Evaluation techniques that aid in estimating the residual lives of welded structures. Five potential techniques were then selected for further investigation.

- **Automated Ball Indentation (ABI) Approach**: In-situ fracture toughness assessment.
- **Piezzomagnetism**: Remaining fatigue crack initiation life.
- **Magnetic Winding Magnetometer (MWM) Technique**: Remaining fatigue crack initiation life.
- **Acoustic Emission Technique**: Detection and growth of cracks.
- **Crack Propagation Gauges**: Crack Growth Monitoring.

Of these five techniques, the ABI technique, the acoustic emission technique, and the crack propagation technique were recommended for ship structural applications, although, further investigations are required in the case of the ABI technique. With regards to the piezzomagnetism approach and the MWM technique, detailed laboratory scale investigations are required to assess their feasibility and suitability to assess remaining fatigue crack initiation life in the high cycle fatigue regime.

T. H. GILMOUR
Rear Admiral, U.S. Coast Guard
Chairman, Ship Structure Committee

Technical Report Documentation Page

1. Report No. SSC-428	2. Government Accession No.	3. Recipient's Catalog No.
4. Title and Subtitle In Service Non-Destructive Evaluation of Fatigue and Fracture Properties For Ship Structures		5. Report Date **August 2003** 6. Performing Organization Code
7. Author(s) Dr. S. Tiku		8. Performing Organization Report No. SR-1385
9. Performing Organization Name and Address BMT Fleet Technology Limited 311 Legget Drive Kanata, ON Canada K2K 1Z8 U.S. Coast Guard Research & Development Center 1082 Shennecossett Road Groton, CT 06340-6096		10. Work Unit No. (TRAIS) 11. Contract or Grant No. DTCG -39-97-F-E00342
12. Sponsoring Agency Name and Address Ship Structure Committee C/O Commandant (G-MSE/SSC) United States Coast Guard 2100 Second Street, SW Washington, DC 20593-0001		13. Type of Report and Period Covered Final Report 14. Sponsoring Agency Code **G-M**
15. Supplementary Notes Sponsored by the Ship Structure Committee and its member agencies		
16. Abstract		
17. Key Words	18. Distribution Statement Distribution Unlimited, Available From: National Technical Information Service U.S. Department of Commerce Springfield, VA 22151 Ph. (703) 605-6000	
19. Security Classif. (of this report) Unclassified	20. Security Classif. (of this page) Unclassified	21. No. of Pages 100
		22. Price PC - 29.50 MF - 17.00 E - 8.95

CONVERSION FACTORS

(Approximate conversions to metric measures)

To convert from	To	Function	Value
LENGTH			
inches	Meters	divide	39.3701
inches	Millimeters	multiply by	25.4000
feet	Meters	divide by	3.2808
VOLUME			
cubic feet	cubic meters	divide by	35.3149
cubic inches	cubic meters	divide by	61,024
SECTION MODULUS			
$inches^2$ feet	$centimeters^2$ meters	multiply by	1.9665
$inches^2$ feet	$centimeters^3$	multiply by	196.6448
$inches^3$	$centimeters^3$	multiply by	16.3871
MOMENT OF INERTIA			
$inches^2$ $feet^2$	$centimeters^2$ $meters^2$	divide by	1.6684
$inches^2$ $feet^2$	$centimeters^4$	multiply by	5993.73
$inches^4$	$centimeters^4$	multiply by	41.623
FORCE OR MASS			
long tons	Tonne	multiply by	1.0160
long tons	Kilograms	multiply by	1016.047
pounds	Tonnes	divide by	2204.62
pounds	Kilograms	divide by	2.2046
pounds	Newtons	multiply by	4.4482
PRESSURE OR STRESS			
$pounds/inch^2$	$Newtons/meter^2$ (Pascals)	multiply by	6894.757
kilo $pounds/inch^2$	mega $Newtons/meter^2$ (mega Pascals)	multiply by	6.8947
BENDING OR TORQUE			
foot tons	meter tons	divide by	3.2291
foot pounds	kilogram meters	divide by	7.23285
foot pounds	Newton meters	multiply by	1.35582
ENERGY			
foot pounds	Joules	multiply by	1.355826
STRESS INTENSITY			
kilo $pound/inch^2$ $inch^{½}$ ($ksi\sqrt{in}$)	mega Newton $MNm^{3/2}$	multiply by	1.0998
J-INTEGRAL			
kilo pound/inch	$Joules/mm^2$	multiply by	0.1753
kilo pound/inch	kilo $Joules/m^2$	multiply by	175.3
TEMPERATURE			
Degrees Fahrenheit	Degrees Celsius	subtract & divide by	32 1.8

BMT FTL DOCUMENT QUALITYCONTROL DATA SHEET

REPORT: In Service Non-Destructive Evaluation of Fatigue and Fracture Properties for Ship Structures

DATE: June, 2003

PREPARED BY:

Dr. Sanjay Tiku, Senior Materials Specialist
Dr. Nick Pussegoda, Fatigue and Fracture Analysis Engineer

REVIEWED BY:

A.S. Dinovitzer, Vice-President
Manager-Structural Reliability and Risk

APPROVED BY:

I.F. Glen, President

CONTENTS

LIST OF FIGURES

LIST OF TABLES

EXECUTIVE SUMMARY

BMT Fleet Technology Limited (BMT FTL) was tasked by the Ship Structure Committee under Solicitation No. DTMA91-99-R-00001 to evaluate techniques for "In Service Non-Destructive Evaluation (NDE) of Fatigue and Fracture Properties for Ship Structures". The project had been divided into several tasks starting with an extensive literature review to seek out potential NDE techniques that will aid in estimating the residual lives of welded structures and thus be suitable for fulfilling the objective of this program. Five potential techniques were then selected for further investigation. Four subcontracts were issued to different organizations to assess the suitability of different NDE techniques to meet the required objectives. The techniques, their objectives, and the subcontractors were:

- **Automated Ball Indentation (ABI) Approach**: In-situ fracture toughness assessment.
  An experimental program was developed and the work was carried out by Advanced Technology Corporation (ATC), Oak Ridge, TN and BMT FTL.

- **Piezzomagnetism**: Remaining fatigue crack initiation life.
  An experimental program was initiated and the work was carried out by a graduate student under the guidance of Prof. Sidney Guralnick at the Illinois Institute of Technology.

- **Magnetic Winding Magnetometer (MWM) Technique**: Remaining fatigue crack initiation life.
  An experimental program was developed and the work was carried out by JENTEK Sensors Inc. and BMT FTL.

- **Acoustic Emission Technique**: Detection and growth of cracks.
  A paper study to assess the suitability of an acoustic emission technique for in-situ monitoring on ship structures. The work was carried out by PowerTech Labs, BC.

- **Crack Propagation Gauges**: Crack growth monitoring.
  The work was carried out by BMT FTL to assess the suitability of crack propagation gauges to monitor crack growth along non-planar, rough surfaces in complex geometries such as fillet welds.

Of these five techniques, the ABI technique, the acoustic emission technique and the crack propagation technique were recommended for ship structural applications, although, further investigations are required in the case of the ABI technique. With regards to the piezzomagnetism approach and the MWM technique, detailed laboratory scale investigations are required to assess their feasibility and suitability to assess remaining fatigue crack initiation life in the high cycle fatigue regime.

1. INTRODUCTION

BMT Fleet Technology Limited was tasked by the Ship Structure Committee under Solicitation No. DTMA91-99-R-00001 to evaluate techniques for "In Service Non-Destructive Evaluation (NDE) of Fatigue and Fracture Properties for Ship Structures". The project requirements included carrying out an extensive literature review to seek out potential NDE techniques that will aid in evaluating fatigue and fracture properties of ship structures, select promising techniques for further evaluation, develop experimental programs with different subcontractors to investigate the selected NDE techniques and perform an objective assessment of the capabilities of NDE techniques studied and make recommendations.

The report details the literature review, and includes a brief introduction about different NDE techniques selected, the experimental program results, conclusions and recommendations. The detailed results and the final reports of the subcontractors are produced in their entirety in the Annexes.

1.1 Technical Background

There is an increasing emphasis placed on prolonging the life of the existing aging infrastructure, and this also applies to merchant and naval ships [1,2]. This necessarily entails the application of a damage tolerance (DT) methodology that ensures that an aged structure with accumulated damage can sustain anticipated operational loads without failure or loss of functionality.

Damage Tolerance methodology assumes that crack-like flaws are present in all structures, new or old. The fatigue crack initiation life is therefore neglected and DT analysis is based upon the growth of an assumed reasonable maximum flaw size that could, or is known to, exist in the structure. However, in older ship structures made from steels with limited fracture toughness, the use of such an approach leads to limited residual lives considering the conservative assumptions that are normally made about the input parameters (upper-bound driving force, lower bound material resistance). Therefore, it is important to estimate the fatigue crack initiation life in aging weld structures, even though initiation life estimation is strictly not a part of fracture mechanics-based damage tolerance analysis.

In the context of an aging ship structure, damage tolerance methodology, coupled with initiation life estimation, has the objectives of determining the following at a given point in time [3]:

- Do any fatigue cracks exist in the aged structure?
- If not, how much of the fatigue crack initiation life has already been consumed (accumulated fatigue damage) at a particular critical location, e.g., an uncracked weld toe in a critical structural detail?
- If a fatigue crack is already present at a particular location in the ship structure, at what rate might it grow in service?
    - What is the critical flaw size that might instigate an unstable fracture?

The present work was carried out keeping in mind the above four objectives. At first, a literature review was carried out to identify suitable technologies that could provide appropriate inputs for residual life calculations. Once the NDE techniques and the respective subcontractors were identified to evaluate the techniques, small programs were developed to evaluate the feasibility and effectiveness of the techniques for ship structures applications.

2. LITERATURE REVIEW

The literature review has been divided into three sections according to their intended applications:

1. Crack detection and crack growth measurement;
2. Critical flaw size estimation;
3. Estimation of remaining fatigue crack initiation life.

2.1 Crack Detection and Crack Growth Measurement

2.1.1 Conventional NDI Techniques

Several non-destructive techniques, from the conventional to advanced technology, are available for the detection of flaws in welded structure. Table 2.1 is a simplified breakdown of the complexity and relative requirements of the five most frequently used NDT techniques [4]. Table 2.2 gives a comparison of common non-destructive evaluation methods as judged by the Office of Non-destructive Evaluation, NIST, USA [4].

Table 2.1: The Relative Uses and Merits of Various NDT Methods [4]

	Test method				
	Ultrasonics	X-Ray	Eddy Current	Magnetic Particle	Liquid Penetrant
Capital Cost	Medium to High	High	Low to Medium	Medium	Low
Consumable Cost	Very Low	High	Low	Medium	Medium
Time of Results	Immediate	Delayed	Immediate	Short Delay	Short Delay
Effect of Geometry	Important	Important	Important	Less Important	Less Important
Access Problems	Important	Important	Important	Important	Important
Type of Defect	Internal	Most	External	External	Surface Breaking
Relative Sensitivity	High	Medium	High	Low	Low
Formal Record	Expensive	Standard	Expensive	Unusual	Unusual
Operator Skill	High	High	Medium	Low	Low
Operator Training	Important	Important	Important	Important	
Training Needs	High	High	Medium	Low	Low
Portability of Equipment	High	Low	High to Medium	High to Medium	High
Dependent on Material Composition	Very	Very	Very	Magnetic Only	Little
Ability to Automate	Good	Fair	Good	Fair	Fair
Capabilities	Thickness Gauging	Thickness Gauging	Thickness Gauging	Defects Only	Defects Only

Table 2.2: Comparisons of Various NDI Methods [4]

Method	Characteristics detected	Advantages	Limitations	Example of use
Ultrasonics	Changes in acoustic impedance caused by cracks, nonbonds, inclusions, or interfaces	Can penetrate thick materials; excellent for crack detection; can be automated	Normally requires coupling to material either by contact to surface or immersion in a fluid such as water. Surface needs to be smooth.	Adhesive assemblies for bond integrity; laminations; hydrogen cracking
Radiography	Changes in density from voids, inclusions, material variations; placement of internal parts	Can be used to inspect wide range of materials and thicknesses; versatile; film provides record of inspection	Radiation safety requires precautions; expensive; detection of cracks can be difficult unless perpendicular to x-ray film.	Pipeline welds for penetration, inclusions, voids; internal defects in castings
Visual-optical	Surface characteristics such as finish, scratches, cracks, or color; strain in transparent materials; corrosion	Often convenient; can be automated	Can be applied only to surfaces, through surface openings, or to transparent material	Paper, wood, or metal for surface finish and uniformity
Eddy current	Changes in electrical conductivity caused by material variations, cracks, voids, or inclusions	Readily automated; moderate cost	Limited to electrically conducting materials; limited penetration depth	Heat exchanger tubes for wall thinning and cracks
Liquid penetrant	Surface openings due to cracks, porosity, seams, or folds	Inexpensive, easy to use, readily portable, sensitive to small surface flaws	Flaw must be open to surface. Not useful on porous materials or rough surfaces	Turbine blades for surface cracks or porosity; grinding cracks
Magnetic particles	Leakage magnetic flux caused by surface or near-surface cracks, voids, inclusions, material or geometry changes	Inexpensive or moderate cost, sensitive both to surface and near-surface flaws	Limited to ferromagnetic material; surface preparation and post-inspection demagnetization may be required	Railroad wheels for cracks; large castings

The Federal Highway Administration (FHWA) sponsored a study to select and develop a practical method for the reliable non-destructive detection of fatigue cracks in the steel members of in-service bridges [5]. Table 2.3 is a summary of the 14 potential non-destructive methods evaluated [5].

After a process of elimination based on the ratings, five techniques, (Barkhausen noise, eddy current, magnetic field disturbance, magnetoabsorbtion and ultrasonics), were short-listed for further evaluation. After further testing, two methods were identified as best suited for the detection and quantification of cracks. These were: ultrasonics for rapid scanning of likely areas and AC magnetic field disturbance for quantification of crack lengths. Following these recommendations, a new system, NUMAC (New Ultrasonic and Magnetic Analyser for Cracks) was developed and delivered to FHWA [6]. This system was designed to detect and quantify fatigue cracks in steel bridges, even when covered with paint. It was realised that the system is a contact system requiring the inspector to place a transducer on the bridge within a foot or so of the crack, making this a very slow process [6].

Table 2.3: Summary of Ratings of Non-Destructive Methods – (FHWA Sponsored Study)

No.	Method	Sensitivity				Adaptability to Field Use						Instrumentation of Method					Remarks
		A	B	C	D	E	F	G	H	I	J	K	L	M	N	P	Q
		In Welds	In Joints	Sub-surface	Discrim-ination	Vibra-tion	Temper-ature	Power Requirements	Safety Requirements	Access	Surface Prep.	Com-plexity	Auto-mation	Operator Dependant	Operator Interpreta-tion	Within Scope of Contract	
1	Acoustic emission	b	c	A	E	F	E	M	L	E	M	H	G	L	L	P	Difficult to apply load and have assurance of repeatable emissions.
2	Acoustic birefringence	c	d	A	G	P	F	M	L	F	H	H	P	H	H	P	
3	Barkhausen noise	b	d	A	G	F	E	M	L	G	M	M	F	M	M	F	
4	Eddy current	b	d	A	F	G	G	M	L	E	L	M	G	M	H	G	Many difficulties encountered in practical application to ferromagnetic materials.
5	Holography	b	d	A	F	P	P	M	M	F	H	H	F	H	M	P	
6	Infrared	c	d	A	N	F	P	H	L	F	H	H	G	M	L	P	
7	Magnetic field disturbance	a	d	A	F-G	G	G	L-M	L	F-G	L-M	M	G	L	L	G	Includes both AC and DC methods.
8	Magnetic particle	a	d	A	P	G	G	M	M	F	M	L	P	H	H	E	Magnetic rubber technique provides permanent record but not useful as a survey tool.
9	Magnetic absorption	b	d	A	F	G	G	M	L	F	M	M	G	M	H	G	
10	Mossbauer effect	c	d	A	F	P	F	M	M	F	M	M	F	M	M	P	
11	Penetrants	b	d	NA	N	G	F	L-M	L	F	H	L	P	H	H	E	
12	Ultrasonics	a	b	A	F	G	G	L-M	L	F	M	M	F	M	H	G	
13	Radiography	c	c	A	F	F	G	H	H	P	L	M	P	H	H	E	
14	X-ray Diffraction	b	d	A	G	P	G	M	M	P	M	M	F	H	H	F	

RATING SYSTEM

Columns A & B (crack length)
- a = 3-7 mm
- b = 7-13 mm
- c = 13-25 mm
- d = >25 mm

Column C
- A - applicable
- NA = not applicable

Columns D,E,F,I,L,P
- E = Excellent
- G = Good
- F = Fair
- P = Poor
- N = None

Columns G,H,J,K,M,N
- L = Low
- M = Moderate
- H = High

One of the reasons ultrasonic testing was selected was because of its capability for rapid scanning of areas. Acoustic emission (AE) is a much faster technique than ultrasonics, and its main advantage compared to other inspection techniques is its capability of volumetric inspection. Taking a closer look at Table 2.3, the performance of the acoustic emission technique seems encouraging. For example, its sensitivity for crack length measurement is 7-13 mm in welds and 13-25 mm in joints. It is an applicable method for detecting sub-surface cracks. For adaptability to field use, its performance has been rated as fair in cases of vibration and excellent in cases of temperature variations. Power requirements are moderate, safety requirements are low, surface preparations are moderate and accessibility is not a problem. From the instrumentation perspective, it has been termed to be high in complexity, good in automation, and low in operator dependence and operator interpretation. However, it was rated as poor within the scope of the contract without giving any details. The results of another study carried out by FHWA to evaluate the capabilities and utility of AE for fatigue crack detection and monitoring demonstrated that AE can be useful for the evaluation of a fatigue cracks but the available systems were not engineered for bridge monitoring [6].

The acoustic emission technique relies on stress waves produced by sudden changes or movements in stressed materials. Sudden changes or movements such as crack growth or plastic deformation act as stress wave sources. The stress waves radiate out into the structure and are sensed by a sensitive piezoelectric transducer. The piezoelectric transducer delivers an electric signal proportional to the stress wave to a nearby pre-amplifier and then to the main signal processing unit. The common range of operation is 100 kHz to 2 MHz [7]. As the stress imposed on the material increases, many sources of stress waves (emissions) are activated. The signals captured by one or more sensors are amplified and measured. The sources of the acoustic energy are disturbances in the elastic stress field and hence without stress there will be no emission. An acoustic emission inspection can therefore only be carried out when the specimen or the structure is under load. As such, the acoustic emission technique is thus suitable for on-line measurement.

The main differences between the acoustic emission and the other NDI methods are: (i) the signal has its origin in the material itself and not in an external source and (ii) the acoustic emission detects movements while other techniques detect existing geometrical discontinuities [8,9]. A major benefit of the acoustic emission method is that it allows the whole volume of the structure to be inspected in a single loading operation; the only requirement is that a suitable number of fixed sensors, typically placed four to twenty feet apart, must be used. The main disadvantages of the technique are (i) it is very sensitive to noise. Many external sources of acoustic emissions with no relation to cracking or plastic deformation (e.g., rivets) can mask the overall signal measured by the transducers, and (ii) the structure/specimen must be under stress. The major challenge in AE testing aboard ships will be to separate the signal from the noise (engine vibrations, sloshing liquids, dropped hammer, etc.).

However, criteria can be developed to filter out the unwanted sound waves from the signal emanating from cracks. For example, Akhtar et al [10] were successful in separating the AE signals from fatigue cracks in natural gas steel cylinders from those arising from other sources. Similarly, AE signals associated with osteoporosis in human bones have recently been separated from other AE events [11]. As well, AE has been successfully applied for non-destructive examination of nuclear and other pressure vessels [12].

The Carderock Division, Naval Surface Warfare center, (NSWCCD) is actively involved in the non-destructive inspection and evaluation of US Navy surface vessel shipboard systems and equipment [13]. Some of the technologies employed along with their applications are described below:

1. *Acoustic Emission*
   Applications: Airflasks, Fuel tanks, Hull voids and Hull structures.
2. *Eddy Current*
   Applications: Non-ferromagnetic Tubing, Auxiliary Condensers, Main Condensers.
3. *Infrared Thermography*
   Applications: Building Rooftops, Building Envelopes, HVAC Systems, Steam Systems and Pollution Abatement, Deck Non-Skid Material, Coatings, Furnace Interiors, Insulation, Boiler Casing Integrity, Blowers, Heat Exchangers, Wire Rope, Bearings, Oil Leaks.
4. *Laser Shearography*
   Applications: Submarine Special Hull Treatment Tiles, Sonar Domes.
5. *Remote Field Testing*
   Applications: Ferromagnetic Tubing, Main Boilers, Auxiliary Boiler.

There are several other non-traditional, non-destructive techniques available which could be used on ship structures directly, namely direct current potential difference (DCPD), alternating current potential difference (ACPD), alternating current field measurement (ACFM) and crack propagation gauges, as explained below.

2.1.2 Other Techniques for Monitoring Crack Growth

(a) Direct Current Potential Drop (DCPD)

In DCPD, a direct current is injected into the specimen. The current is distributed uniformly in the specimen (volume). Since the current flows uniformly throughout the specimen volume, the amount of current required depends on the size and resistivity of the specimen. Currents up to 100 amperes have been used [14]. High DC currents however, can result in specimen heating. High currents also require high capacity power amplifiers and therefore heavy equipment. Additionally, DCPD suffers from the problems of thermo-electric emf that can be of the same magnitude as the DC signals [15]. On the other hand, the technique is simple to use and the electronics and instrumentation are also fairly simple. The many disadvantages of DCPD have been recently eliminated in part by using the pulsed DC measurement method [15].

DCPD has been used for monitoring short crack growth in steels and superalloys [16-19]. Donald et al [20] have illustrated the magnitude of potential differences measured on a standard specimen type (CT) sample having a width of 50 mm, thickness of 7.67 mm and a crack length of 11 mm for a direct current of 10 amperes. For aluminum (Al) alloys, the potential difference measured was 0.1 mV, whereas for steel and titanium the potential differences were 0.6 mV and 3.5 mV respectively. It was also shown that 0.1 μV change was observed for a crack extension of 0.66 mm in Al alloys, 0.11 mm for steel and 0.022 mm for titanium. Burgers et al [21] observed that the sensitivity of DCPD to crack extension also depends on the initial crack length. For a crack 1 mm in length, a crack extension of 0.4 mm may be resolved, whereas for a crack of 30 mm, a crack extension of 0.013 mm may be resolved.

In the case of the DCPD, the specimen volume is very important. This is one of the governing factors in determining the sensitivity of the system. Therefore, the DCPD technique is mostly used on pre-cracked (EDM) small specimens and the problem is in fact reduced to measuring crack growth rates as accurately as possible.

BMT FTL is involved in the prototype development of DCPD systems for field use. The Canadian Navy has sponsored limited work at BMT FTL to produce a portable magnetically mounted prototype potential drop probe system based on the Local Field Direct Current Potential Drop (LFDCPD) laboratory system used at BMT FTL. Since the field is localized, the specimen volume is not important. The system injects currents in pulses and data acquired is the difference of the voltage at peak current and zero current, thus minimizing the problem of thermal emf. The LFDCPD system developed at BMT FTL is based on the same physical principles as the DCPD techniques used by others but requires much less current and can therefore be made much more compact. The system will be used as a shipboard hull monitoring system for the continuous monitoring of the propagation of fatigue cracks detected in service. The main advantage of this system is its very short installation time. With multiple probes, it can generate excellent crack shape predictions as has been illustrated in the open literature.

The sensor developed for the Canadian Navy shown in Figure 2.1 is mounted on the specimen used for evaluating the assembled sensor. The sensor uses four spring loaded gold plated contact probes with the two outer ones providing the current input to the test component and the inner ones used to measure the potential drop across their span. The probes themselves are electrically insulated from the holder by nylon inserts. The steel holder contains two permanent magnet inserts to affix assembled sensor to the test piece or the structural component.

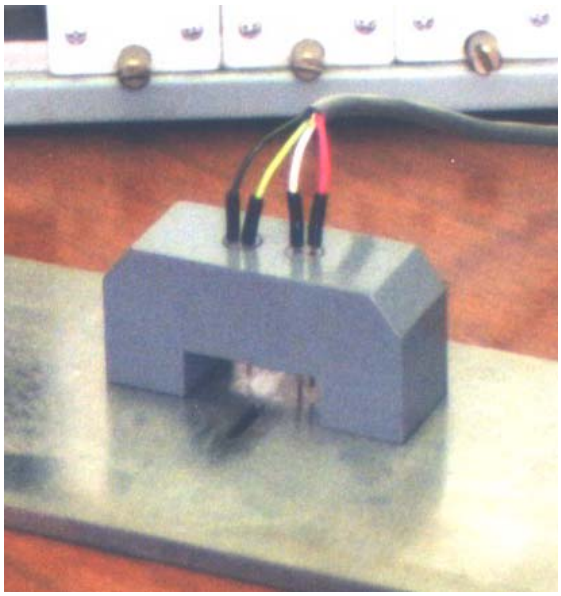

Figure 2.1: Magnetically Mounted Potential Drop Sensor for Monitoring Crack Growth Onboard Ships

Laboratory experiments have been conducted to demonstrate that the magnetically mounted probe can measure crack growth rates with adequate sensitivity. For example, it is seen in Figure 2.2, that there is an increase in the normalized potential difference (NPD) with an increase in the number of cycles, where

$$NPD = \frac{PD_i}{PD_0}\frac{PD_{\mathrm{Re}\,f0}}{PD_{\mathrm{Re}\,fi}}$$

and PD_I and PD_0 are the I'th and first PD measurement and PD_{ref} are the reference probe values. Normalizing in this fashion accounts for changes caused by temperature and voltage fluctuations.

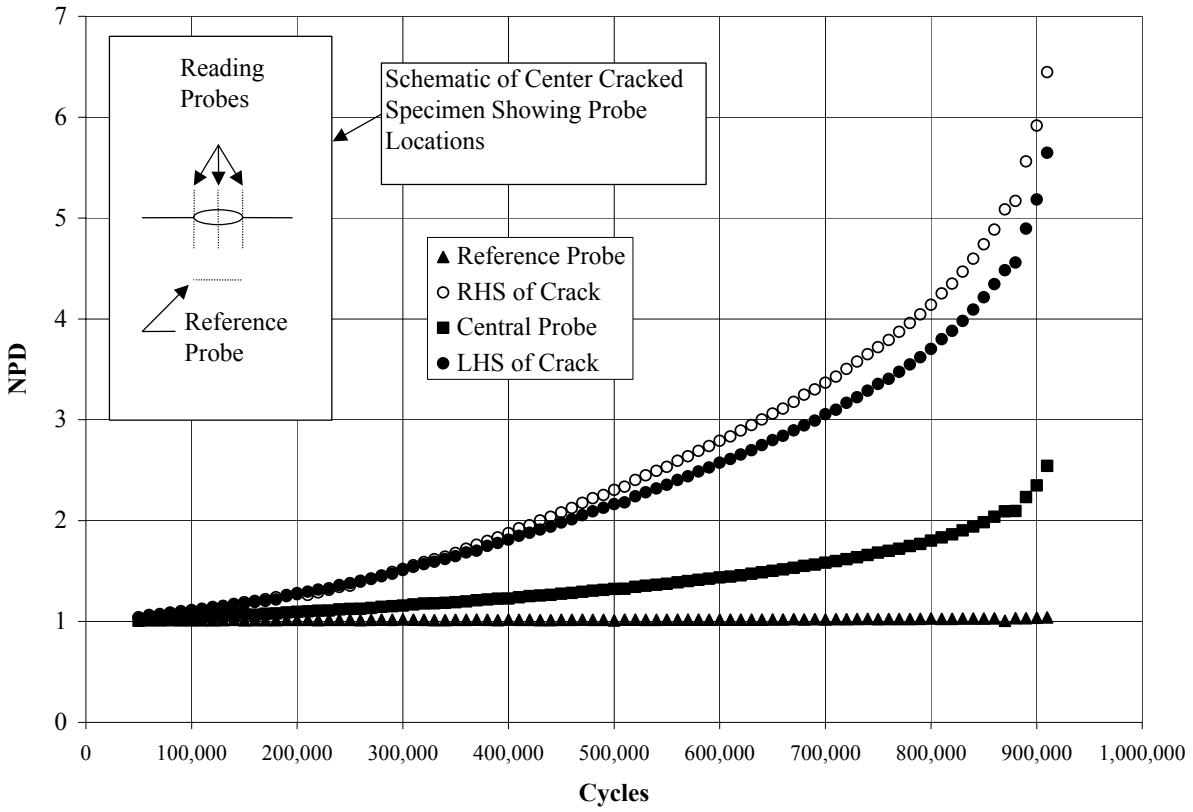

Figure 2.2: Normalized Potential Crack Growth During Fatigue Test

(b) Alternating Current Potential Difference (ACPD)

ACPD has generated considerable interest since the Damage Tolerant Design (DTD) methodology came into existence. With the ACPD, an alternating current (AC) is injected into the specimen and the resulting potential difference is measured across two points on the surface. The current distributes uniformly at the surface, but is confined to a narrow region in the thickness direction and this effect is known as the skin effect [22]. The skin effect results in an increased sensitivity in detecting surface cracks because of the presence of higher current densities compared to DCPD. The sensitivity can be increased by increasing the current frequency since this results in an enhanced skin effect. In ACPD, small currents, from 200 mA to 1 amperes are usually sufficient. Therefore, the ACPD has two distinct advantages over DCPD. First, the specimen thickness is not important and therefore large coupons can be tested. Secondly, small amounts of currents are injected, therefore, specimen heating is not a problem. Moreover, ACPD is not affected by the thermal emf as in the case of DCPD.

Increasing the frequency leads to an increased sensitivity, but there is an associated drawback to this, as there is a magnetic field present of increasing strength. The probes used for the measurement of the potentials can be affected by the induced magnetic field caused by the high frequency AC. Thus, the probes are measuring both the surface voltage and an induced voltage.

Veropest et al [23] used a 40 kHz current frequency and reported the detection of surface micro-cracks of 0.0066 mm^2 area in steel wires, but recommended the use of 10 kHz frequency for accurate and reproducible crack growth measurements. They showed that by increasing the frequency, the induction effect becomes stronger. Watt [24] used the ACPD technique in a wide range of titanium alloys. He applied the technique to monitor crack propagation in single edge notch (SEN) and CT specimens. He also applied the technique for crack detection in small SEN specimens and during fatigue testing of T butt welds. He used his ACPD system up to 8 kHz frequency and reported that lead interaction problems were exacerbated at higher frequencies (10 kHz and above).

Hwang and Ballinger [25] used an ACPD system that was capable of generating a current at a frequency of up to 230 kHz. However, their experiments were conducted at frequencies of up to 203 kHz. They reported a sensitivity of 50 μm for multiple crack initiation using a probe spacing of 10 mm in a Ni base superalloy. For single crack initiation, they observed a decrease in sensitivity. To achieve the same sensitivity of 50 μm crack depth, the probe spacing was reduced to 1.2 mm. They also observed that long term signal stability is achieved if (i) rigid probe attachments are used, (ii) the signal is pre-amplified close to the specimen and, (iii) adequate lead grounding and shielding are employed. They concluded that ACPD is more suitable for constant load than for dynamic loading. They observed that the problem of induced signal in the probe wires becomes more important above 100 kHz current frequency.

Gendron et al [26,27] used the technique successfully for on-line crack initiation and crack growth measurements in coated and uncoated blades of Ni-based superalloys during thermal fatigue experiments carried out in a high velocity burner rig. The maximum temperature of the flame was around 1323^{o} C and gas velocity was around Mach 0.4. The resolution of the ACPD technique for crack detection (at the leading and trailing edges) was reported to be 125 μm under the harsh testing conditions of the experiments.

Charlesworth and Dover [28] used their system for crack measurement under water with no modifications. The testing was carried-out on a tubular welded T-joint in which a fatigue crack was introduced. The measurements were carried-out both in air and water. They reported a negligible difference in the measurements in both cases. Hwang and Ballinger [25] also performed measurements in water at high temperatures up to 350° C under both static and dynamic loading. The AC currents used ranged between 1 to 1.4 amperes with frequencies between 17 to 203 kHz. They found the ACPD technique to be compatible with aggressive environments.

Dover et al [29] were the first to use the ACPD as a NDI tool on offshore structural components. The equipment used was limited to a maximum frequency of 6 kHz and 1 ampere current. They reported that the system was capable of measuring cracks of any size. However, no data or results were presented. They also described another low frequency (50 Hz), instrument for NDI application of offshore structures. The smallest crack size that could be detected with the unit was reported to be 25 mm in length.

Watt [24] has also reported using the ACPD as a NDI tool for a wide range of items of various complexities including large structural items. However, no results pertaining to its performance were reported.

ACPD technique has also been used to characterize the short crack growth behaviour of naturally initiated fatigue cracks in 7075 Al alloy (for a ≥ 40 μm crack depth) [30]. The technique has also been used to monitor on-line damage on a CF-18 aircraft during full scale testing at Canadair, Bombardier under International Follow on Structural Test Program (IFOSTP) [30]. The sensors were installed at fracture critical locations on CF-18 aircraft and were able to measure the response of the structure to load cycling. A crack was also detected by the sensors on one of the critical locations monitored by the ACPD technique. The crack was detected at the fracture critical location almost 2500 spectrum flight hours (SFH) (~ five years in real life) before any other established technique (visual inspection, Eddy Current, Liquid Penetration and acoustic emission) utilized by the Department of National Defence (DND)/Canadair was able to detect the crack. The magnitude of the signal was able to size the cracks using calibration curves established in the laboratory experiments.

(c) Alternating Current Field Measurement (ACFM)

ACFM technique is a non-contact technique. A current is induced in the part to be inspected and the corresponding magnetic fields measured. In this regard, the technique is similar to eddy current but the probe design is similar to the ACPD technique. The ACFM technique has been used for automated inspection of drillstring threaded connections, where the technique allowed a rapid scanning through oil and oxide layers [29]. It has been used on underwater tubular intersections to demonstrate the ability of the technique to detect cracks 1mm or deeper at a weld toe and to give length and depth estimates accurate to within 5 mm and 1mm, respectively, for simple crack shapes [29].

(d) Crack Propagation Gauges

Crack propagation gauges are a commercial product available from several companies, and for the most part, have been used in laboratory studies of crack growth rate, especially when the crack growth rates are high (crack arrest tests) and not amenable to measurements by other techniques (optical, compliance). However, the gauges are suitable for measuring slow crack growth rates in a field environment as well. Such gauges can be wire type or foil type, and the progression of a surface crack through the gauge bonded to a surface increases the total resistance that can be easily measured. Because of the nature of these measurements, temperature compensation and long-term electrical stability are not major issues.

The gauge can be installed at the crack tip itself so that crack growth monitoring can commence more or less immediately. Alternatively, if crack growth over a specified time interval or a critical flaw size for the location has been calculated, the gauge could be installed a certain distance ahead of the current tip (with suitable safety factor on the critical crack size) to provide a warning that an appropriate repair/maintenance action is required.

The two main prerequisites for the use of crack growth gauges are (i) the location of the crack and the crack tips must be known beforehand (by ultrasonic or other means) and (ii) the gauge itself and associated wiring are protected from damage in service. Also, it will need to be demonstrated that the gauge can be reliably installed on irregular surfaces near plate intersections (fillet and corner joints). Another drawback of crack gauges is their labour intensive installation. Further, the extent of crack growth that can be monitored is limited by the size of the gauge (40 mm maximum) unless several gauges are placed along the anticipated crack path.

2.2 Critical Flaw Size/Residual Strength Estimation

Besides the yield strength of the material where the crack resides, the two most important parameters required for critical flaw size calculation are the fracture toughness, a material property, and the magnitude of the residual stresses present. As far as the surface residual stresses are concerned, these can be reliably determined using a portable x-ray diffractometer. This should be adequate when the flaw tip is away from the weld in the base material since the residual stresses (assembly and fabrication) can be expected to be more or less uniform through the thickness and simple gradients may be estimated by taking measurements on both the surfaces. Near the weld zone, the residual stresses can have complex through thickness distribution and therefore the x-ray diffraction measurements will be of somewhat limited value.

(a) Automated Ball Indentation (ABI)

It is only recently that a portable Stress-Strain Microprobe^{TM} has been developed which, using an automated ball indentation (ABI) technique, can help calculate yield and ultimate tensile strength as well as the fracture toughness as a function of temperature [31]. The theoretical basis of the technique is described in several publications [32,33], and for the time being Figures 2.3 and 2.4 show a very promising agreement between ABI predicted strength and fracture toughness properties and those determined experimentally. It should be noted, however, that calculations required for predicting material tensile and fracture toughness properties do need certain experimentally determined material data, the most important of these being the critical fracture stress which is determined by a tensile test at a low temperature, e.g., at liquid nitrogen temperature.

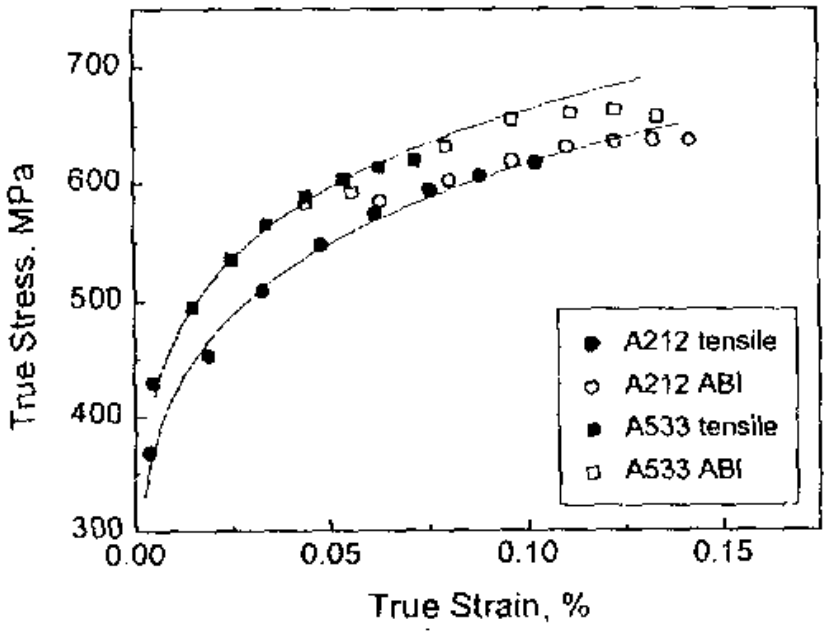

Figure 2.3: Correlation between ABI and Tensile Data for A212B and A533B Steels

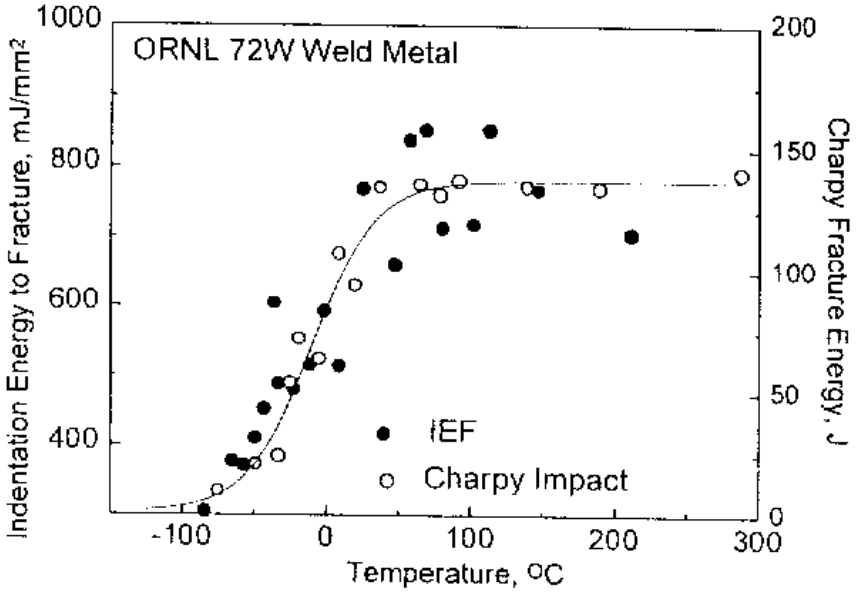

Figure 2.4: Variation in Indentation Energy to Fracture and Charpy Energy with Test Temperature

(b) Ultrasonic Technique

The characteristics of sound propagation through any material are dependent on virtually all physical aspects of the medium: atomic constituents, grain size, shape, and structure, phase boundaries, elastic constants, presence of flaws or dislocations etc.

At least in theory, a detailed knowledge of a material's structure should allow the determination of impulse response or vice versa. The use and potential offered by ultrasonic velocity and attenuation measurements to determine and/or monitor material properties have been explored by several researchers [34-38]. Empirical evidence has been presented to show that there is a close relation between ultrasonic attenuation properties and fracture toughness properties of polycrystalline metallic materials. For example, Figure 2.5 illustrates the correlation between ultrasonic attenuation factor and fracture toughness [34] and Figure 2.6 demonstrates the correlation between ultrasonic attenuation and plain strain stress intensity factor, ductile fracture appearance transition temperature (FATT) and shelf energy of the Charpy-V curve (KV) [36]. The problems encountered in the ultrasonic attenuation measurements are related to an inconsistent level of acoustic coupling, standardization of transducer design and performance, and design and availability of broad band equipment capable of rapid frequency domain calculations [35]. Moreover, the ultrasonic attenuation measurements have been correlated with the plain strain fracture toughness (LEFM) in relatively brittle materials and it needs to be seen whether this technique will be applicable to tougher structural steels displaying elastic plastic fracture. Also, its applicability for the field measurements as well as at lower temperatures needs to be determined.

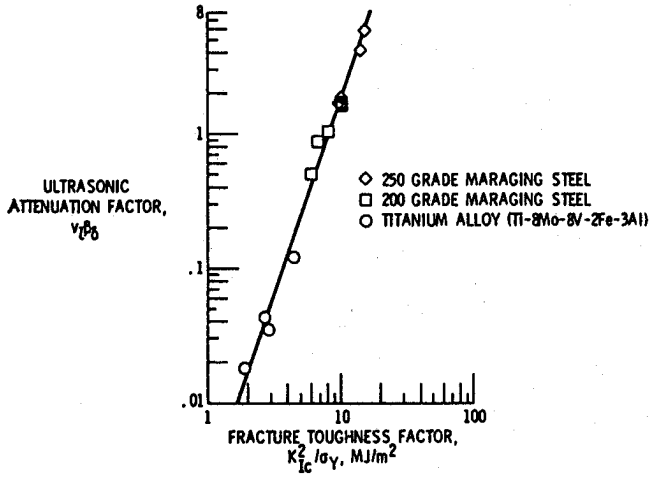

Figure 2.5: Correlation of Ultrasonic Attenuation Factor $v_1\beta_\delta$ and Fracture Toughness factor $K^2{}_1C/\sigma_y$.

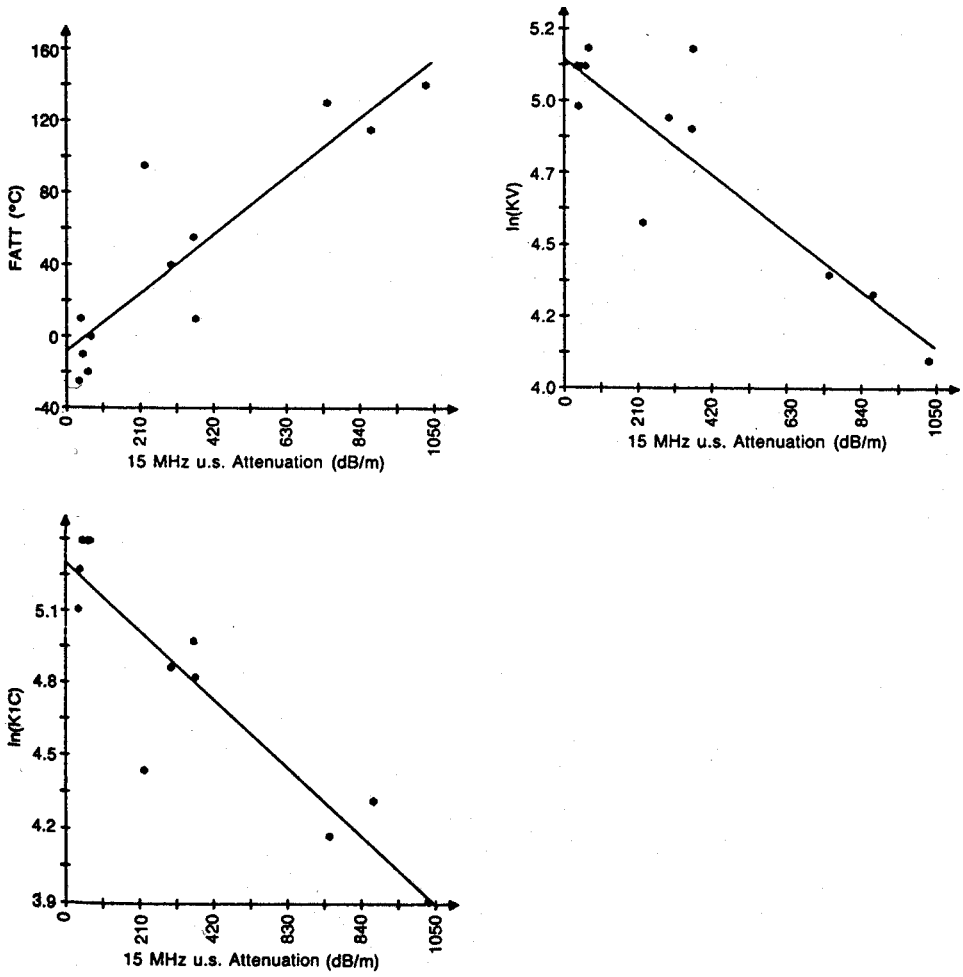

Figure 2.6: Correlation between Ultrasonic (u.s.) Attenuation at 15 MHz and the FATT, ln KV and ln K_{IC} Values of all Samples

2.3 Estimation of Remaining Fatigue Crack Initiation Life

(a) X-ray diffraction line broadening analysis:

The use of x-ray diffraction to determine the absolute magnitude of total elastic surface stress (applied + residual) is well established. The technique relies on the fact that the magnitudes of the elastic stress and the lattice spacing are related and the latter can be accurately calculated from the shift in the angular position of the x-ray diffraction peak.

What is less commonly appreciated is that when a metal or alloy is plastically deformed, then in addition to the changes in the lattice spacing consistent with the elastic component of applied and residual stresses, there is a distortion of the lattice planes (micro-strain). This distortion is such that the lattice spacing, on a micro-level, changes randomly from grain to grain and within a grain. This leads to broadening of the x-ray diffraction peak signifying increases and decreases in lattice spacing with the average value remaining the same as for the stress free lattice. In reality however, both elastic macrostrains and non-uniform microstrain may be present so that peak shift and broadening occur simultaneously.

It should be noted that even for a completely lattice distortion free material, the diffraction peak has some width (broadening) associated with it due to the imperfect nature of the x-ray optics. Methodologies have been developed to separate this "instrumental broadening" from the observed broadening to obtain that due to the lattice distortion in the sample. From the latter, a microstrain and a domain size parameter may be calculated which in turn are a reflection of the nature of imperfections in the crystal lattice caused by plastic deformation, heat treatment, surface mechanical treatment, etc. Williamson and Smallman [39] have developed an analysis approach that can be used to deduce the nature of the dislocation substructure (predominantly random dislocations or subgrains) from microstrain and domain size, from which an estimate of the plastic strain/fatigue damage could be inferred.

The line broadening analysis technique has been used by Kurita [40] to develop a correlation between line broadening and hardness of induction hardened components (Figure 2.7) and used it as a quality control tool for large components. Following the same strategy, Kurita and Chiaki [41] were able to establish a relationship between the equivalent plastic strain introduced by tension, compression or torsion and the resulting line broadening (Figure 2.8).

Similarly, Goto [42] has obtained, in a laboratory environment, a reasonably linear relation between the magnitude of line broadening and the fatigue strength of 17-4 PH steel in heat treated and shot peened condition. In addition, the technique has been used to reveal other conditions where the compressive residual stress layer introduced by shot peening had been wholly or partially destroyed by heating and/or machining, or by polishing, Figure 2.9. More importantly, he was able to use Figure 2.9 as a calibration curve for a quality assurance objective, i.e., to have a high degree of confidence, prior to placing the component in service, that the required fatigue performance would be realized.

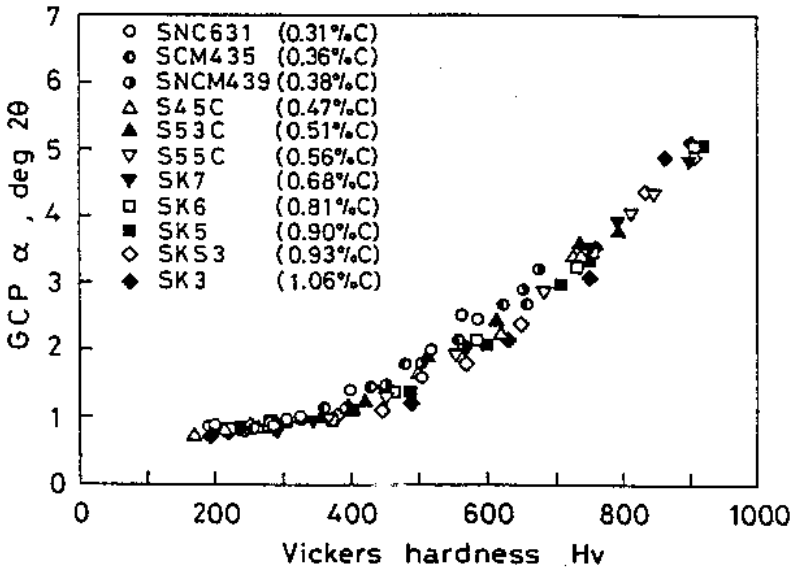

Figure 2.7(a): Increase in GCP Alpha (Line Broadening) with Increasing Vickers Hardness for Quenched and Tempered Steels

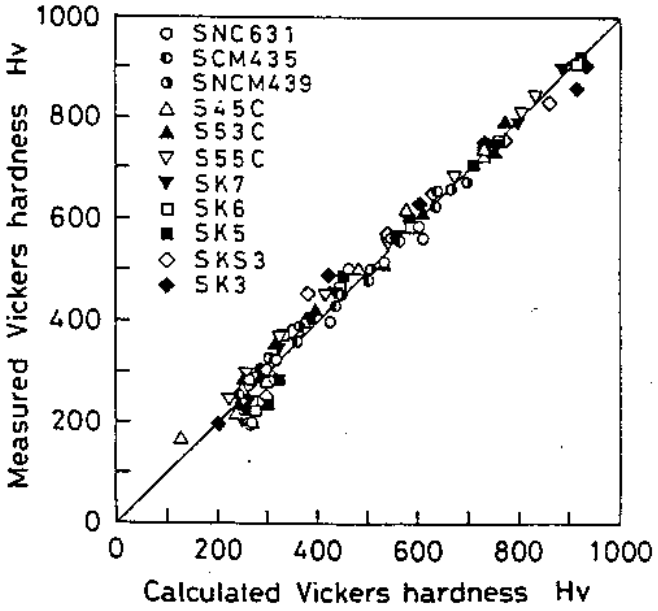

Figure 2.7(b): Correlation between the Measured Hardness and that Calculated from GCP Alpha for Quenched and Tempered Steels

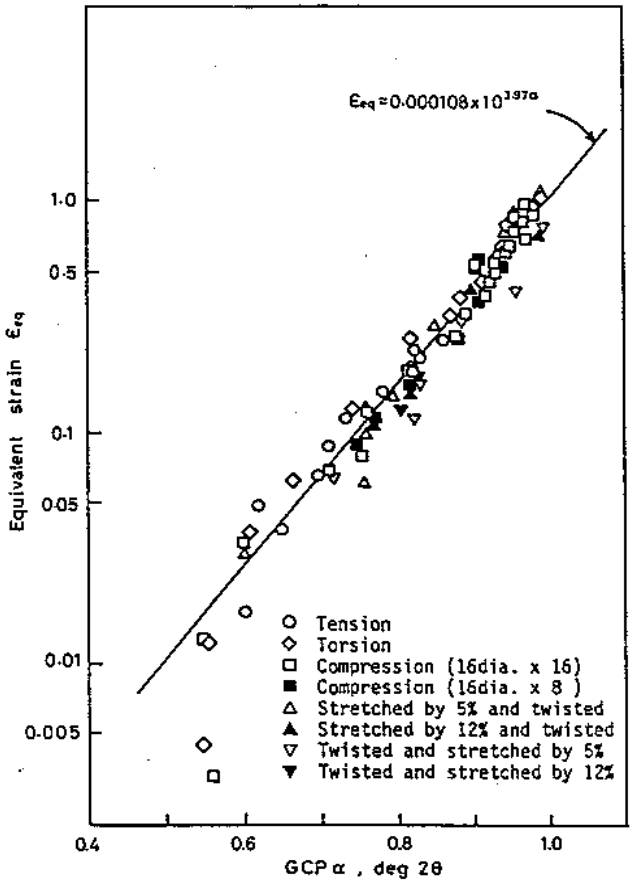

Figure 2.8: Equivalent Plastic Strain applied by Various Methods as a Function of GCP Alpha

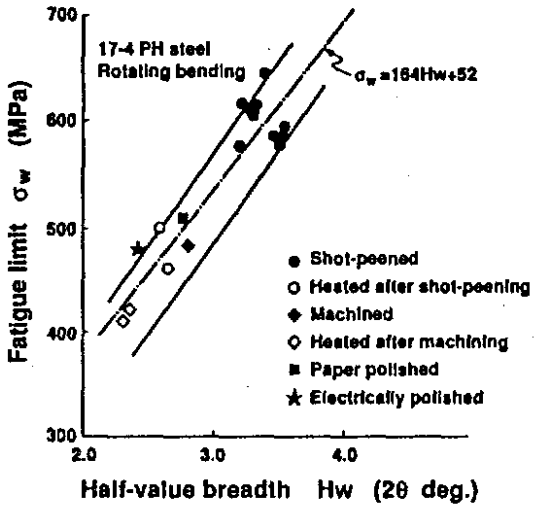

Figure 2.9: Fatigue Limit versus Half-Value Breadth (17-4PH Steel)

Goto also tried to assess the accumulation of fatigue damage by monitoring the changes in residual stress and line broadening with fatigue life [42]. As seen in Figure 2.10, this was not particularly successful because significant changes in these parameters occur in the first or the last 10% of the fatigue life. A similar conclusion was arrived at by Pangborn et al [43] who, for Al alloys, found that the line broadening was more sensitive to "fatigue damage" in the first and last 10% to 15% of the fatigue life. They attributed this to the observation that in the middle 70% to 80% of the life, the fatigue damage accumulated in the specimen interior rather than at the surface layer sampled by the x-ray technique.

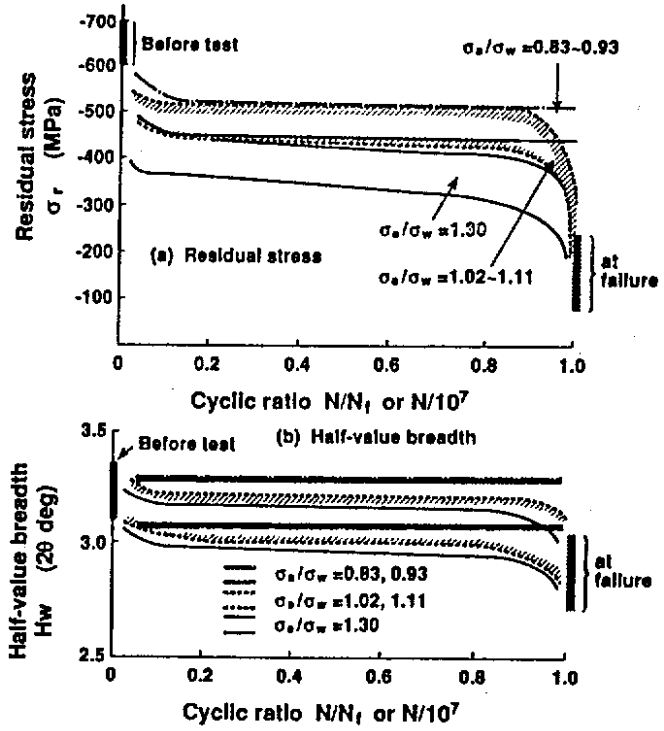

Figure 2.10: Changes in Residual Stress and Half Value Breadth during High Cycle Fatigue of the Specimens Shot Peened under Five Different Conditions (17-4 PH steel)

More recently, Isobe et al [44] have again used the line broadening technique to assess fatigue damage in machined, homogeneous material laboratory specimens, using conventional x-ray diffraction procedures. They were successful in observing changes in various measures of line broadening (peak intensity, peak integral intensity and FWHM ratios) although the relationships were not linear or monotonic. It seems at first that since these investigators conducted their fatigue tests in the low cycle regime (less than half a million cycles), the fatigue damage could be more uniformly distributed across the specimen cross-section.

Pangborn et al [45] carried out fatigue tests at both LCF and HCF conditions and used the line broadening analysis to compare the results. Figure 2.11 shows the results for the waspalloy subjected to LCF at low and high temperatures. As can be seen in the Figure2.11, the line broadening is continuously increasing with the number of cycles, and the line broadening increases more for specimens cycled at higher temperatures. However, when the same approach was applied to the Inconel 718 HCF specimens, the results were quite different as shown in Figure 2.12. It is clear from the results that after the first 10% of the fatigue life there was little change in the broadening for the rest of the 90% of the fatigue life. These results indicate that the standard line broadening approach may not be suitable for HCF testing conditions.

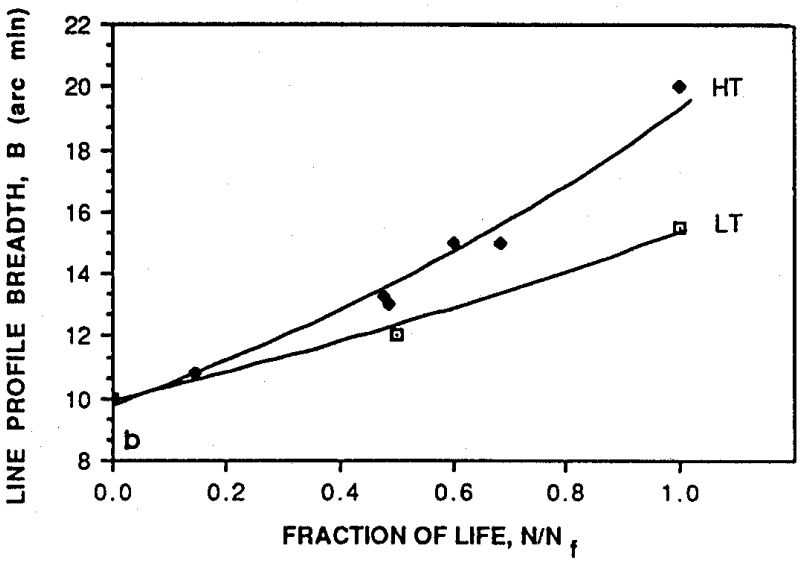

Figure 2.11: Line Broadening of Waspalloy Fatigued in Torsion

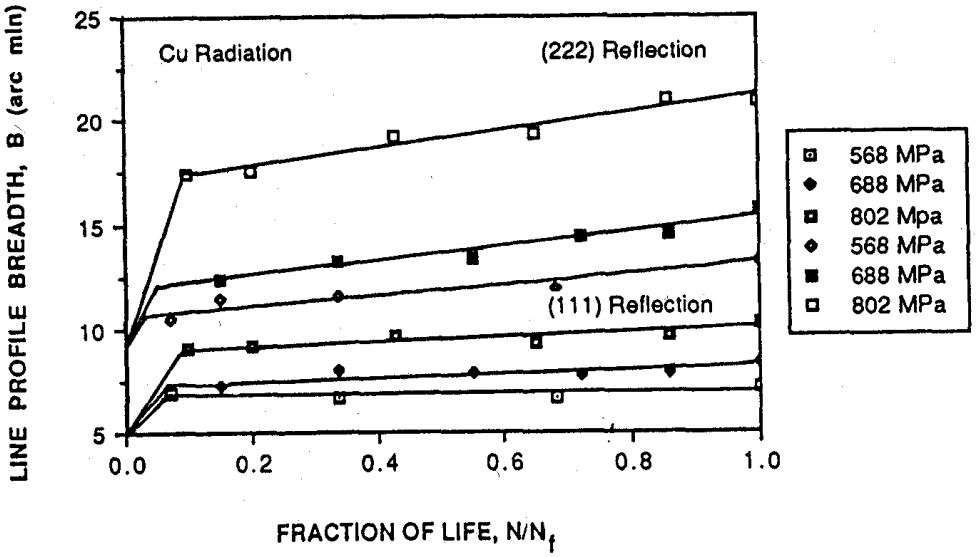

Figure 2.12: Line Broadening of Inconel 718 Fatigued in Tension-Tension

The authors [45] also used another technique called CARCA (computer assisted rocking curve analysis) to study the fatigue damage during HCF. CARCA involves a modification of x-ray double crystal diffractometry. In CARCA technique, the primary x-ray beam is first reflected from a flat, monochromating crystal to produce a parallel beam incident on the specimen. This reduces the number of reflecting grains such that they are individually resolved using a position sensitive detector as shown in Figure 2.13. By rotating the specimen in increments of 3-5 minutes of arc, and recording the reflecting intensities at each position, the rocking curves for each of the grains can be generated so as to obtain an adequate statistical sampling of the deformation. The idea is to exclude those grains, which, at low stress amplitudes, undergo little or no distortion during the cycling and the grains exhibiting broadening above a chosen threshold are included in the analysis. Figure 2.14 shows the results and as can be seen normalized average rocking curve widths show a steep increase over the fatigue life. Moreover, the data lies within a narrow scatter band irrespective of the applied loads or loading condition (constant or spectrum). This curve for HCF is comparable to that shown in Figure 2.11 for LCF. The technique may be suitable for small specimens in the laboratory studies; however, it may be impossible to implement the technique on large structures since one may have to scan very large areas to locate the grains with high deformation.

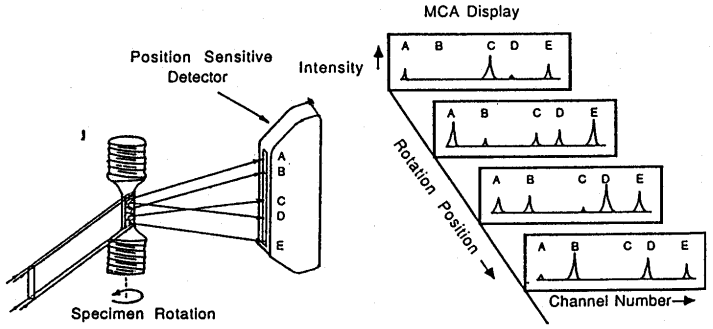

Figure 2.13: Construction of Rocking Curves for Reflecting Grains from a Polycrystalline Fatigued Specimen

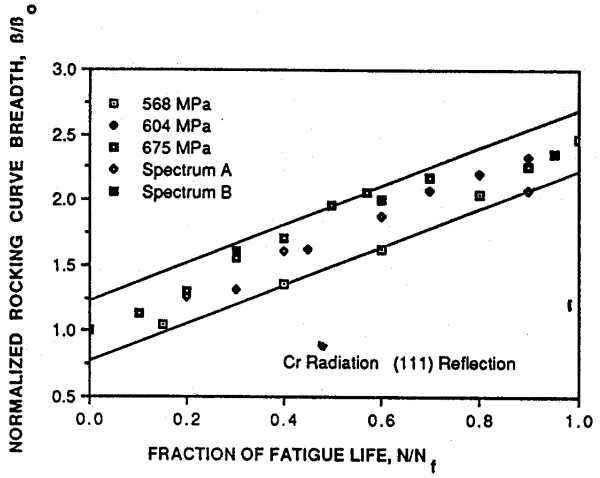

Figure 2.14: Dependence of Normalized Rocking Curve Breadths on Fraction of Fatigue Life for Inconel 718.

(b) Fatigue induced Piezomagnetism

Guralnick [46] at Illinois Institute of Technology has recently been studying piezomagnetism as a non-destructive measure of the fatigue process in metals. Piezomagnetism is the change in the intrinsic magnetization of a material subjected to mechanical actions such as tension, compression, and cyclic loading. In the case of cyclic loading, microplastic processes such as generation of dislocations and other defects, modification of grain texture, etc., alter the arrangement of the ferromagnetic domain structure and affect the intensity of the associated magnetic fields.

These magnetic effects can be fairly substantial and relatively easily measured in a ferromagnetic material like steel. Laboratory investigations already completed at Illinois Institute of Technology (IIT) indicate that magnetic hysteresis is a reliable indicator of the evolution of fatigue damage in steel. Magnetic hysteresis measurements have been found to closely correlate with relevant mechanical stress versus strain measurements in specimens subject to cyclic loading. The laboratory investigations to date, however, focussed on the low and medium cycle regimes, and the potential of the approach in the high cycle fatigue regime needs to be explored.

(c) Meandering Winding Magnetometer

The Meandering Winding Magnetometer (MWM) is an advanced eddy current sensor developed and marketed by JENTEK sensors Inc [47-50]. The MWM is a planar conformable eddy current sensor that was designed to support quantitative and autonomous data interpretation methods. These methods, called grid measurement methods, permit crack detection without the use of crack standards, and provide quantitative images of absolute electrical properties (conductivity and permeability) [47,48]. It has been said that the MWM sensor geometry with flat rectangular meandering windings provides the following advantages [49]:

(i) Accurate modeling of sensor response;
(ii) Ability to determine absolute properties such as electrical conductivity and magnetic permeability;
(iii) Ability to perform one-sided magnetic anisotropy measurements;
(iv) Accurate determinations of lift-off, i.e. proximity to conductive surface;
(v) Ability to conform to curved surfaces, including areas of double curvature;
(vi) Additional control over the depth of sensitivity through the spatial winding wavelength;
(vii) Ability to be permanently mounted in poorly accessible locations for on-line monitoring of damage;
(viii) Ability to scan with and without direct contact with a component.

One of the advantages of the MWM sensors has been its ability to scan large areas. It is being used at ALCOA for rapid scanning of steel roll surfaces without contact to detect cracks at up to 2 ft./second.

Figure 2.15 shows the MWM electrical conductivity measurements as a function of percent fatigue life for Al 2024 and stainless steel**.** Figure 2.16 shows the MWM measurements along the gauge length of the fatigue-damaged specimens. As can be seen with increase in the fatigue life consumed, the conductivity measurements are decreasing in the middle of the specimens. These were the areas where cracks were seen later. These results are quite promising. Moreover, the technique can be used on-line, off-line, for rapid scans and as a non-contact technique. However, most of the fatigue testing has been carried out under LCF conditions and on the aerospace materials (Al alloys, superalloys, and stainless steel) that are non-magnetic.

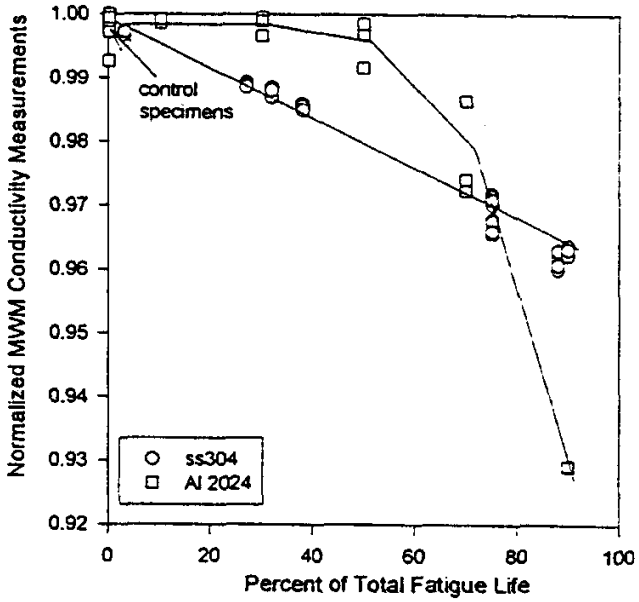

Figure 2.15: MWM Electrical Conductivity Measurements as a Function of Percent of Fatigue Life

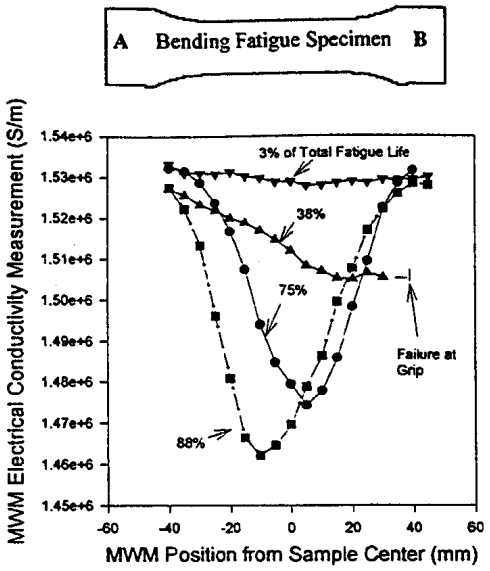

(a) 304 Stainless Steel

Figure 2.16(a): Measurements made on four 304 stainless steel, hourglass specimens fatigued to 3%, 38%, 75% and 88% of total fatigue life.

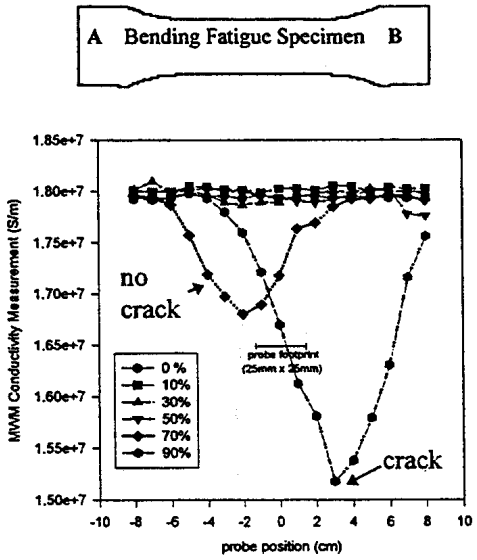

(b) Al 2024

Figure 2.16(b): Measurements made on six 2024 aluminium, hourglass specimens fatigued to 0%, 10%, 30%, 50%, 70% and 90% of total fatigue life.

d) Other Techniques

A Fatigue Damage Indicator [51], comprising three elements with different fatigue lives, is marketed by a French company, STAS, with the objective of monitoring the fraction of the expected fatigue life that is consumed at any point in time. However, for calibration purposes, it requires that the expected life of the joint be known beforehand, but that unfortunately is not the case for aging structures. The indicator's main function is to overcome the difficulties associated with the calculation of expected fatigue lives under variable amplitude loading even though the expected life under constant amplitude loading is known. However, the gauges are not suitable for fatigue lives greater than 10^6 cycles [43], which rules out its application for ship structures.

Similarly, the use of Infrared Thermography to quickly and non-destructively determine the fatigue limit of steel connecting rods has been demonstrated [52]. Again, however, the technique is based on the fatigue damage and the resulting heat energy dissipation occurring at any point in time and does not give any idea of the already accumulated fatigue damage.

2.4 Summary

A literature search and review was performed to seek out the potential NDE techniques that will aid in estimating the residual lives of welded structures. The search was focused in the following three areas.

1. Crack detection and crack growth measurement;
2. Critical flaw size estimation;
3. Estimation of remaining fatigue crack initiation life.

In each of the above areas, several NDE techniques have been identified and discussed and the following, Table 2.4, is a summary of their advantages and disadvantages in the context of their applicability to ship structures.

Table 2.4: Summary of Advantages/Disadvantages of Various NDE Techniques

Crack Detection and Crack Growth Measurement		
Technique	Advantages	Disadvantages
Acoustic Emission	Fast technique. Capability of Volumetric Inspection.	Extraneous noise problems.
Ultrasonics	Extensively used on structures. Demonstrated Industrial Applications.	Slow.
Eddy Current	Extensively used in the laboratory and field applications. Non-contact technique.	Slow. Lift-off problems.
Crack propagation Gauges	Simple technique. Demonstrated in LCF conditions	Applicability to welded structures/irregular surfaces unknown. Location of the crack has to be known beforehand.
Direct Current Potential Difference	Simple technique. Extensively used in laboratory studies. Can be used on line as well as off-line. Automation fairly simple	Contact Technique. Crack location should be known otherwise a wide area would have to be instrumented. Capability in field applications unknown.
Alternating Current Potential Difference	Very Sensitive technique. Capability of strain as well as crack measurements Can be used off-line as well as on-line. Demonstrated in the laboratory as well as field applications.	Contact Technique. Crack location should be known otherwise a wide area would have to be instrumented. Probe design very critical.
Alternating Current Field Measurement	Non-contact technique.	Will be affected by lift-off.

Critical Flaw Size Estimation		
Automated Ball Indentation	Demonstrated Industrial Applications. Applicable to tougher steels.	Destructive tests need to be carried out to calculate critical fracture stress
Ultrasonics attenuation	Easily Available. Familiarity with the equipment.	Applicability to tougher steels not demonstrated.
Estimation of Remaining Fatigue Crack Initiation Life		
X-ray Diffraction	Portable equipment available. Used on Ship structures. Applicable in LCF conditions.	Applicability to HCF questionable Skilled Operator & Interpretation required.
Fatigue induced Piezomagnetism	Applicability in LCF and Intermediate fatigue demonstrated. More sensitive to magnetic materials.	HCF capability not demonstrated Still a laboratory tool.
Meandering Winding Magnetometer	Scanning Capability (up to 900 mm/sec (3 ft./sec)) Can be used on-line as well as off-line Has been used on Al alloys and stainless steels	Applicability on magnetic materials unknown. Applicability in HCF conditions unknown.
Fatigue Damage Indicator	Applicability in LCF demonstrated.	Not applicable in HCF conditions
Infrared Thermography	Fast technique. Used for evaluating fatigue limits.	Cannot determine fatigue life consumed.

2.5 Recommendations

After reviewing and assessing the relative potential and merits of different NDE techniques the following five have been selected for further evaluation:

1. Acoustic Emission for crack detection and monitoring.
2. Crack propagation gauges for crack growth monitoring.
3. Automated Ball Indentation (ABI) technique for fracture toughness measurement.
4. Fatigue induced piezomagnetism approach to determine remaining fatigue crack evaluation life.
5. Magnetic Winding Magnetometer (MWM) technique to evaluate remaining fatigue crack initiation life.

The acoustic emission technique has been selected because of its capability to carry out volumetric inspection. The complete ship structure can be inspected very quickly. Acoustic emission sensors are typically placed approximately 4-20 feet apart and by triangulation technique the crack locations and crack growth can be readily monitored. This is the advantage that no other crack detection and/or crack growth monitoring technique offers. However, the main disadvantage of the technique is its sensitivity to noise. Many external sources of acoustic emissions with no relation to cracking or plastic deformation (e.g., rivets) can mask the overall signal measured by the transducers. Therefore, a major challenge in AE testing aboard ships will be to separate the signal from the noise. However, based on recent advances in instrumentation and analysis, it is believed that criteria can be developed to filter out the unwanted sound waves (noise) from the signal emanating from cracks. The objective of this program will be to evaluate the feasibility of the acoustic emission approach to detect flaws and monitor crack growth in ship structures.

Crack propagation gauges have been selected to evaluate crack growth rates because of their simplicity. The gauges can be mounted at the crack tips so that the crack growth monitoring can commence more or less immediately. Although the local field direct current potential difference (LFDCPD) technique is better, fairly simple and more robust than the crack propagation gauges and has a relatively short installation time, it is already being evaluated in a separate program and not considered for this program.

The Automated Ball Indentation (ABI) technique has been selected for fracture toughness measurement. In this category, the only other technique found was ultrasonic testing. However, the application of the technique has been demonstrated in relatively brittle material (LEFM) and it needs to be seen whether it would be applicable to tougher structural steels. On the other hand, the ABI technique seems to be very promising. It has been used to evaluate fracture toughness in structural ferrous base metals as well as weld metals.

There are three potential techniques to evaluate remaining fatigue crack initiation life: X rays, Fatigue Induced Piezomagnetism and Magnetic Winding Magnetometer. X-ray diffraction and piezomagnetism have been used to evaluate initiation life for LCF. The standard line broadening approach in the x-ray diffraction technique has been shown not to work in HCF testing conditions and thus was not included for further evaluation in this program.

The applicability of the piezomagnetism approach in HCF conditions is unknown. The magnetic winding magnetometers have also been used only in LCF conditions and on aluminium alloys and stainless steels and their applicability is also unknown in HCF conditions and on magnetic materials. On the other hand, the MWM technique can be used for both, on-line and off-line measurements and also has scanning capabilities. Commercial equipment is available for MWM, but the piezomagnetism approach is at a relatively early stage and at present it is confined to laboratory studies. Considering all these facts, and the objective of the program, the piezomagnetism approach and the MWM technique were selected for further evaluation.

3. EVALUATION OF THE AUTOMATED BALL INDENTATION (ABI) APPROACH

3.1 Objective

The objective of these experiments was to carry out a preliminary evaluation of the Automated Ball Indentation™ (ABI) test technique as an NDE method for the estimation of fracture toughness of:

i) Ship structural steels.
ii) Typical ship welds.

In order to assess the results of the ABI method, full thickness fracture toughness tests were also conducted for comparison.

3.2 Material Characterization

3.2.1 Base Materials

Two steel plates with a specified minimum yield strength of 350 MPa (50 ksi) were selected. The nominal plate thickness was 25 mm (1 inch), and the chemical compositions were as given in Table 3.1. Microstructures are presented in Figure 3.1, with steel A displaying a slightly coarser ferrite grain size and a larger area fraction of the second phase (pearlite) as compared with steel B. The latter observation is consistent with the higher carbon content of steel A. The average ferritic grain size of steel A is estimated to be close to ASTM #8 and the grain size of steel B is smaller than that of steel A.

Table 3.1: Chemical Composition of Base Metal, (wt%)

Steel	C	Mn	P	S	Si	Cu	Ni	Cr	Al	V
A	0.16	1.06	0.016	<0.01	0.27	0.013	0.01	0.038	0.044	0.033
B	0.08	1.4	0.012	0.007	0.31	0.21	0.18	0.02	0.032	0.057

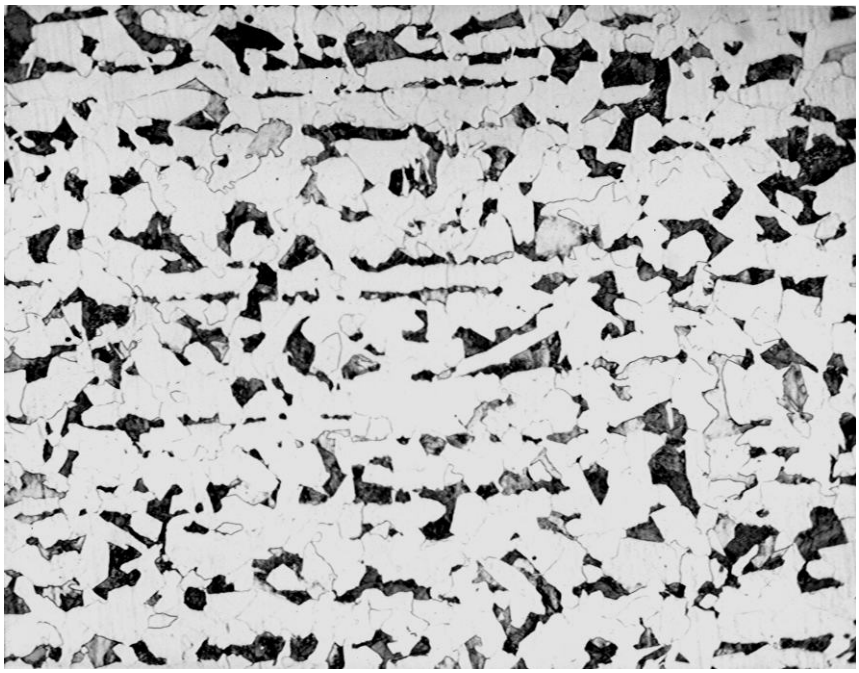

(a)

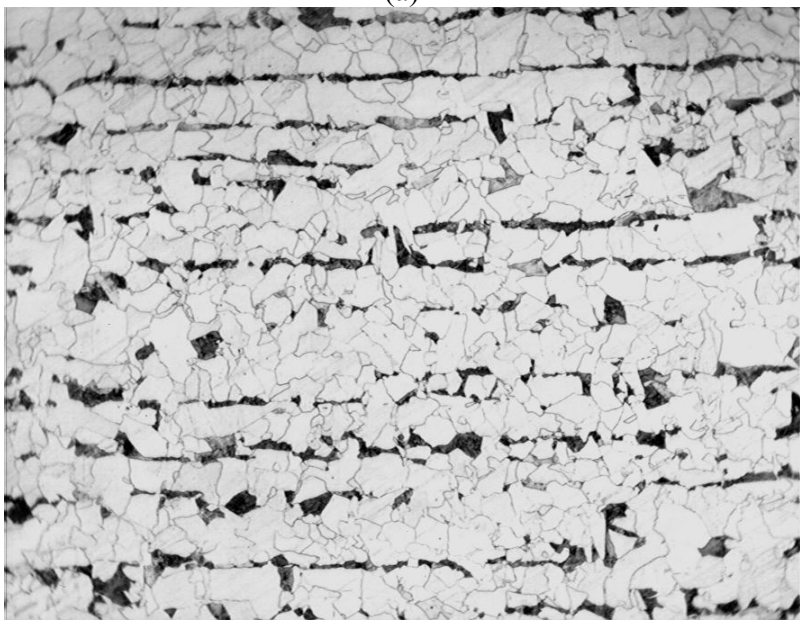

(b)

Figure 3.1: Microstructure of the base materials; (a) steel A, and (b) steel B. Magnification 200X

To complete the material characterization of the base metal, the following tests were performed:

i) Full thickness tensile testing in the L-T orientation. These were done at quasi-static rate at room temperature (22^{o}C). The results are presented in Table 3.2.

ii) Full thickness (10 x 10 mm) Charpy V-notch testing, in accordance with ASTM E23. Transition curves were obtained in L-T orientation, from specimens extracted from the

T/4 location with respect to the plate thickness. The results are presented in Figure 3.2. Steel B has a better toughness as shown by the lower transition temperature and higher upper shelf absorbed energy.

iii)

Table 3.2: Tensile Properties

Steel	Yield strength*, (MPa)	Tensile strength, (MPa)	Elongation,+ (%)
A	357	530	45.5
B	381	473	52.5

* the yield strength is the lower yield strength as both steels exhibit the Luder's yield plateau.
+ based on a 50 mm gauge length

Yield strength is increased with smaller ferrite grain size (Hall-Petch equation). Therefore we would expect steel B to have a higher YS compared to A. The TS increases with vol. fraction of pearlite in low C steels, via "2nd phase" hardening. Steel A has a higher vol. fraction of pearlite (microstructure) and higher C content.

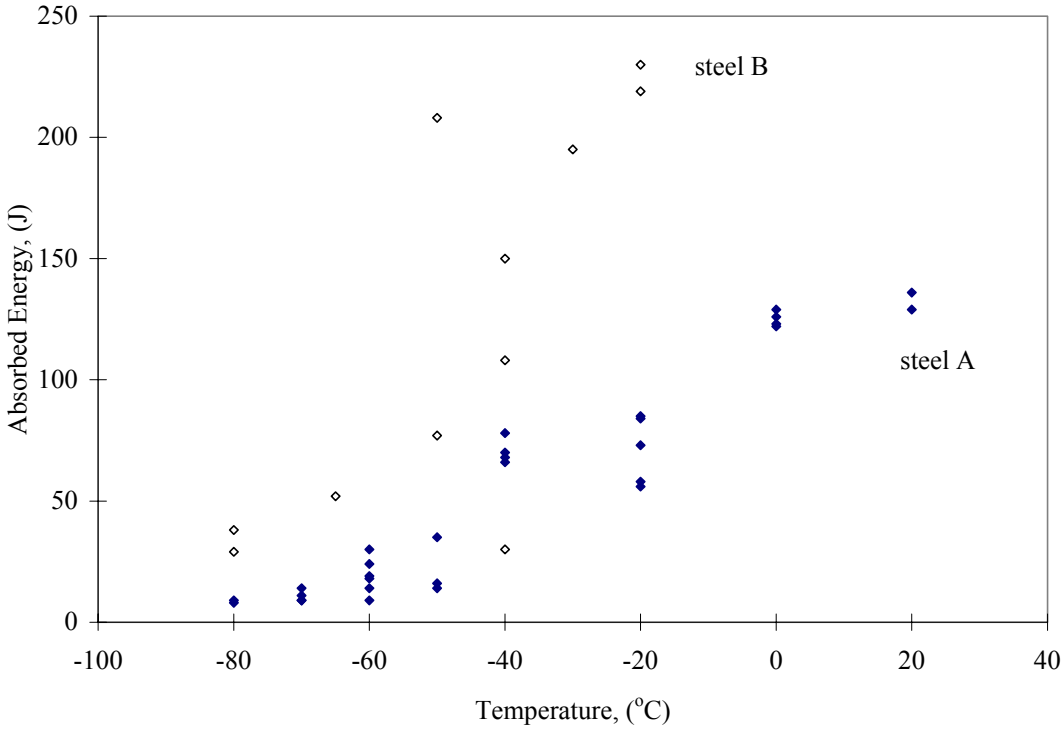

Figure 3.2: Charpy Fracture Transition Results for the Base Metals

Based on the mechanical properties and chemical compositions reported above, both steels are seen to conform to ABS Grade DH 36 steel requirements.

3.2.2 Weld Metal

The weld procedure employed was based on information obtained from the Naval Surface Warfare Center (NSWC), Carderock, and pertained to a previous SSC project vice USSSC [53].

The groove geometry was a single-V butt joint (BSV.1) and the welds were made on 20 mm thick DH 36 Grade ship plate, using either shielded metal arc (SMA) weld or flux cored arc (FCA) weld procedures. These procedures are representative of shipyard practice. See Appendix A for the details of the welding parameters. Figure 3.3, shows a macro-section of the SMA weld.

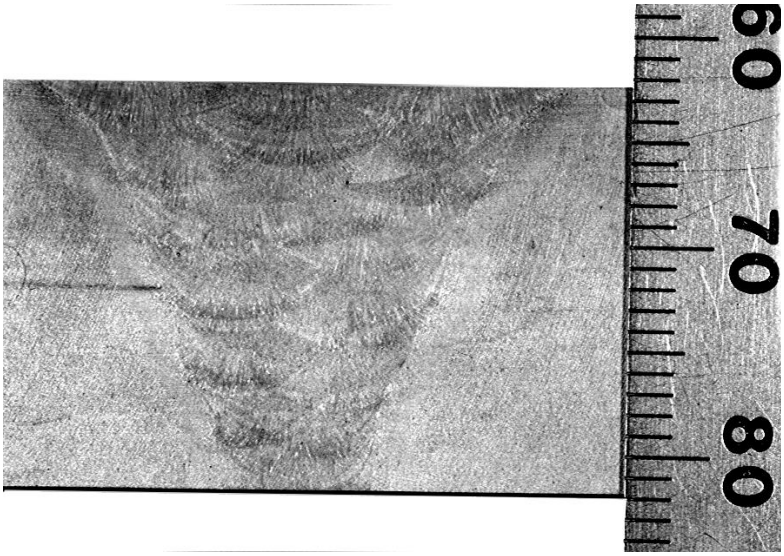

Figure 3.3: Macro-Section of the Multi-Pass Weld, after Removal of the Backing Bar and Cap Reinforcement

Full thickness Charpy V-notch specimens were extracted from the sub-surface location sampling the top half of the weld. Transition curves were obtained from specimens notched in the through thickness direction at the weld centerline. The results are presented in Figure 3.4. The SMAW material has better toughness as shown by the lower transition temperature.

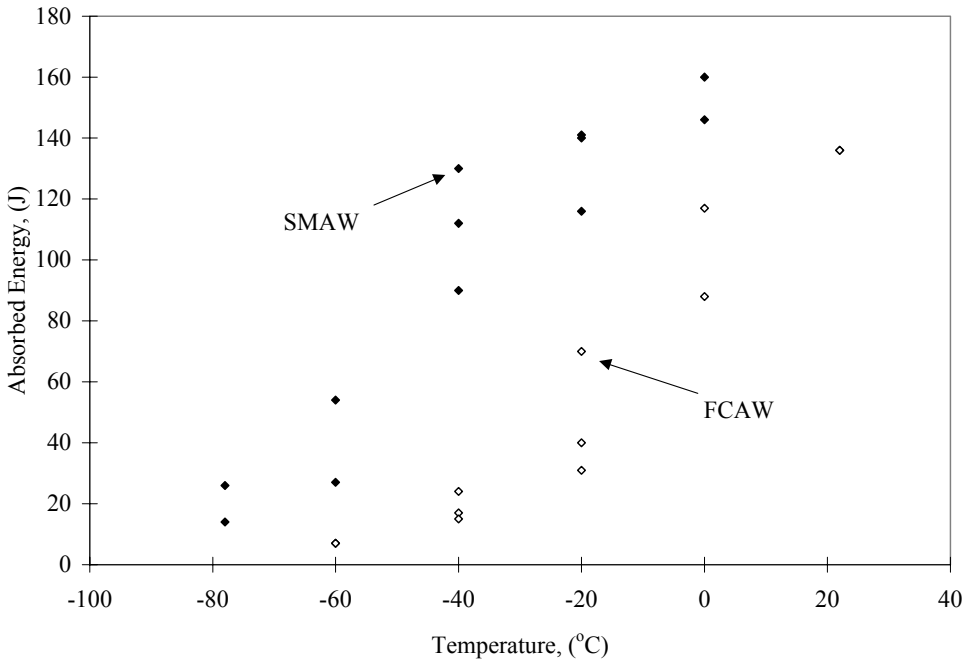

Figure 3.4: Charpy Fracture Transition Results for the SMA and FCA Weld Metals

3.3 Destructive Fracture Toughness Testing

3.3.1 Base Metals

The test procedure was selected to obtain fracture toughness in terms of K_{Jc} [54] values so that a direct comparison could be carried out with fracture toughness values estimated by the ABI method. Full plate thickness SEN(B) specimens, in the L-T orientation, were machined to the standard dimensions (B X 2B) [54]. Crack starter notches were machined using a 1.6 mm (1/16") thick cutter.

A fatigue pre-crack, 2 to 3 mm long, was grown from the machined notch, using a servo-hydraulic machine to have a total crack depth of half the sample width (W) (i.e., up to about a/W = 0.5). In an automated pre-cracking procedure, load shedding was employed to maintain the maximum stress intensity factor (K_f) at a lower value than that allowed in ASTM E1921, and minimum to maximum load ratio was (R-ratio) 0.1 or less. At the completion of pre-cracking, manual load-unload cycles were employed to ensure the crack length was at the predetermined point using specimen compliance.

The specimens were side grooved to a depth of 0.1B in line with the machined notch. During this procedure, the specimen was held only on one side of the crack to ensure that the plastic zone of crack tip was not altered. As recommended, proper seating of the specimen was checked by load-unload cycling in the elastic range [54] and monotonic loading tests were performed in the servo-hydraulic machine until an unstable event took place as detected by audible load drop.

At test temperatures, where instability was not expected, periodic unloading was performed with the objective of developing a J-resistance curve. The quasi-static loading rate was within the requirements of ASTM 1921. The load-CMOD plot was monitored in real time and post-test analysis was performed to determine K_{Jc} or develop the J-R curve with in-house software capabilities, in accordance with ASTM E1921 and ASTM E1820 [55].

The specimen temperature was controlled within ± 2^{o}C during the test with a calibrated thermocouple, spot welded to the specimen very close to the crack plane, and connected to a temperature controller. The cooling medium was liquid nitrogen spray, regulated by a solenoid energized by the controller. Sufficient time was allowed, in accordance with ASTM E 1921, for the specimen to cool through the thickness after the surface reached the test temperature. The calibrated MTS clip gauge used to monitor the CMOD was protected from the liquid nitrogen spray by a transparent enclosure. Triplicate specimens were tested at selected test temperatures and in this way the method deviated from the standard procedure of ASTM E1921 [54]. The selection was dictated by lowest anticipated hull temperature of vessels operating in the North Atlantic. ASTM E 1921 is for obtaining the reference temperature (T_o) and the master curve, and for this it is recommended that testing be performed at a single temperature close to T_o.

When the expected slow stable crack growth was greater than 0.5 mm, the final crack length was marked by heat tinting and the specimens were broken after immersion in liquid nitrogen. In all specimens the initial crack length (a_o) was determined in accordance with ASTM E1921. In those specimens that were heat tinted both a_o and the final crack length (a_f) were determined.

For those tests that produced unstable crack extension, the K_{Jc} determined was validated in accordance with the standard, i.e., the crack straightness requirements for a_o were met, K_{Jc} was lower than the K_{Jc} (limit) and the stable crack extension was below 1 mm. Nearly all unstable fractures gave valid K_{Jc} values, (see Table 3.3a). In tests that did not result in instability, J-R curves were developed and when the requirements of ASTM 1820 were met, J_Q was determined and checked if the qualifying value (J_Q) can be validated as a J_{1C}. A typical J-R plot with the validation requirements to obtain J_Q is presented in Appendix B.

Table 3.3(a): Results of Fracture Toughness Tests for the Base Metals

ID	T °C	a_{oq} (predicted) (mm)	a_o (measured) (mm)	$J_{elastic}$ (kJm^{-2})	$J_{plastic}$ (kJm^{-2})	J_{total}^{+} (kJm^{-2})	K_{Jc} ($MPam^{-2}$)	$K_{Jc(limit)}$ ($MPam^{-2}$)	Comments
A1		31.50	31.27	27.04	345.32	372.36			No fracture
A2	0	32.50	31.28	30.81	804.04	834.85		249	J_{1c}*
A4		27.20	26.87	33.97	101.93	135.90	166.91		
A5	-20	26.70	26.63	30.41	59.18	89.59	135.52	270	
A6		27.50	26.79	42.05	288.76	330.81	260.42		
A7		27.00	25.96	21.26	11.70	32.96	82.20		
A8	-40	27.00	26.83	38.74	284.66	323.40	257.48	285	
A9		26.70	26.46	37.32	190.30	227.62	216.02		
B1		31.30	31.42	35.30	872.75	908.05			
B2	0	32.00	31.52	32.96	440.59	473.55		236.80	No fracture
B4		26.03	25.33	38.60	1041.5	1080.1			No fracture
B5	-20	27.26	26.62	35.41	334.51	369.92	275.38	270.10	
B6		27.60	26.52	44.69	652.32	697.01	378		invalid
B7		27.00	26.78	46.17	861.67	907.85			No fracture
B9	-40	27.00	26.57	37.84	278.38	316.22	254.61	278.24	
B3		31.52	31.39	27.0	738.78	765.8		396.21	

$^{+}$ J_{total} is calculated in accordance with ASTM E 1921, i.e., J is not corrected for crack growth,

*J_{1C} for this specimen from steel A is 310 kJm^{-2}. The equivalent K_{J1c} is 252 $MPa\sqrt{m}$.

3.3.2 Weld Metals

Similar to the base metal, SEN(B) type 3-point bend specimens were machined with the weld at the center of the specimen length. The backing bar and the cap weld reinforcement were removed (see Figure 3.5) and the through-thickness machined notch, for the crack starter, was cut at the weld centerline.

All of the weld specimens were pre-compressed to 1% or less of the specimen thickness, using a 25 mm diameter indentor, which is recommended for more even fatigue crack growth of weld samples [56]. Multi-pass welds have a non-uniform residual stress distribution through the thickness, and this leads to uneven fatigue crack growth in-validating the fracture toughness results. Lateral pre-compression led to a straight fatigue crack fronts, and an example is presented in Figure 3.5.

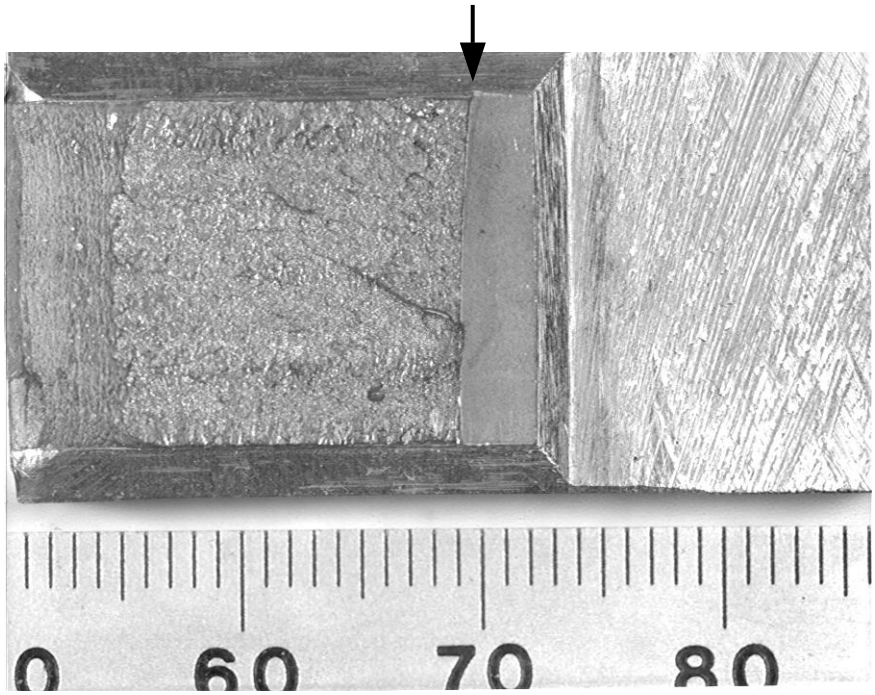

Figure 3.5: Fracture Face of a SEN(B) Specimen S9 from SMAW. This Fatigue Crack Front is Marked by the Arrow

The remainder of the destructive fracture toughness test procedure was as described for the base metals in Section 3.3.1. In brief, after automated fatigue pre-cracking, the specimens were side grooved and tested either by monotonic loading or its variant with periodic unloading for crack growth prediction when a J-R curve was to be developed due to the absence of unstable fracture. The results are presented in Table 3.3b. The additional column on the right gives the K_{Jc} values corrected for (1T) size in accordance with ASTM E1921. Such a correction was not performed on the case of the base metal results, as the specimen thickness was 26 mm (1 inch).

Table 3.3(b): Results of Fracture Toughness Tests for the Weld Metals. (F-denoted FCAW, and S denotes SMAW)

ID	T	a_{oq} (predicted)	a_o (measured)	J_{total}^+	K_{Jc}	$K_{Jc(limit)}$	K_{Jc} (1T)
	^oC	(mm)	(mm)	(kJm^{-2})	($MPam^{-2}$)	($MPam^{-2}$)	
F1	-40	19.01	18.94	16.56	58.29	272	55.6
F6		18.75	19.02	33.40	82.75		78.4
F10		18.62	18.90	10.45	46.29		44.4
F5	-20	19.96	18.92	32.09	81.11	269	76.8
F7		18.92	19.14	65.34	115.73		109.0
F9		19.06	18.94	22.47	67.87		64.5
F3	0	18.89	18.66	116.86	154.78	265	145.3
F4		19.10	18.89	120.72	157.31		147.7
F8		19.06	18.77	57.11	108.19		102.0
S1	-40	18.83	18.70	173.36	188.51	274	176.7
S2		18.60	18.48	23.02	68.70		65.3
S8		18.92	18.83	68.30	118.33		111.4
S3	-20	19.04	18.93	265.82	233.44	272	218.5
S4		18.99	18.95	238.35	221.04		207.0
S9		19.11	18.95	88.93	135.01		127.0
S5	0	19.10	18.92	1286.2		269	No fracture
S6		19.33	18.90	1330.9			
S10		19.15	18.87	844.70			

$^+$ J_{total} is calculated in accordance with ASTM E 1921, i.e., J is not corrected for crack growth,

Unstable fractures were obtained for all tests except for the SMAW specimens tested at 0^oC. All of the specimens that produced unstable fracture had valid K_{Jc} values. J_Q values were determined for the SMAW specimens tested at 0^oC; of these only specimen S10 produced a valid J_{ic} of 260 kJm^{-2}. The equivalent K_{J1c} is 230 $MPa\sqrt{m}$. A typical J-R plot with the validation requirements to obtain J_Q is presented in Appendix B.

3.4. Non-Destructive Fracture Toughness Testing

.3.4.1 Base Metal

Full thickness plate steel coupons were sent to Advanced Technology Corporation (ATC), with the rolling direction marked on the plate surface. At ATC tensile tests in the L-T orientation were carried out first on miniature specimens at a number of temperatures, including –196^{o}C to obtain the critical fracture stress, and other baseline information. This data was then used to convert raw data from the ABI stress-strain microprobe (SSM)^{TM} method to fracture toughness values (K_{Jc}).

The ABI indentations were made normal to the plate surface, and in this way differed with the L-T orientation of specimens used in destructive fracture toughness measurements. The ABI method simulated the non-destructive testing that would be performed in the field on a ship plate structural element. The strain rate in the ABI method was similar to the quasi-static rate of the destructive fracture toughness tests. The detailed results are attached in Appendix C (report from ATC).

3.4.2 Weld Metal

Radiography was performed before extracting 35 mm length samples from the welds. The samples were then machined to remove the weld reinforcement, macro-etched to clearly outline the weld fusion boundary and shipped to ATC with the ID marked. Miniature tensile specimens were EDM machined with the loading axis perpendicular to the weld axis, and these were used for obtaining the baseline information including critical fracture stress required to determine the fracture toughness values (K_{Jc}).

As the focus of this task was comparison of fracture toughness values obtained from each method, i.e., ABI and destructive, the ABI testing was performed on weld material in the middle one-third thickness of the weld. This is because in full thickness fracture toughness tests, unstable fracture initiation most likely occurs in the center region of the specimen on account of the high constraint in that region. In contrast to the base material, the ABI SSM indentations were performed in the same orientation as the fracture toughness tests. Some indentation tests were carried out on the surface layers of the weld to observe any significant differences in these layers compared to the toughness in the center region. The detailed results are attached in Appendix C (report from ATC).

3.5 Comparison of Destructive and Non-Destructive Fracture Toughness Results

3.5.1 Base Metal

The direct way of comparing results would be to superimpose the fracture toughness (K_{Jc}) results from destructive tests on the master curves determined by the ABI method. This is because it has been demonstrated that the ABI method can be used to develop a master curve for ferritic steel that is in reasonable agreement with the master curve determined by destructive tests in accordance with ASTM E 1921-97 [57]. Figures 3.6(a) and 3.6(b) show this comparison for steels A and B, respectively, and the agreement is reasonable for steel A. For steel B, on the other hand, unstable fracture was only obtained in two specimens (Figure 3.6b). This indicates that within limitations of the number of destructive tests performed, the test temperature range appears to be above where cleavage instability occurs. Therefore, for a meaningful comparison both types of tests, destructive and non-destructive, need to be performed in a lower temperature range incorporating T_o [57]. The comparison in Figure 3.6(b) also shows that when the ABI method is employed at temperatures above those recommended in ASTM E 1921, the results would lead to conservative K_{Jc} values.

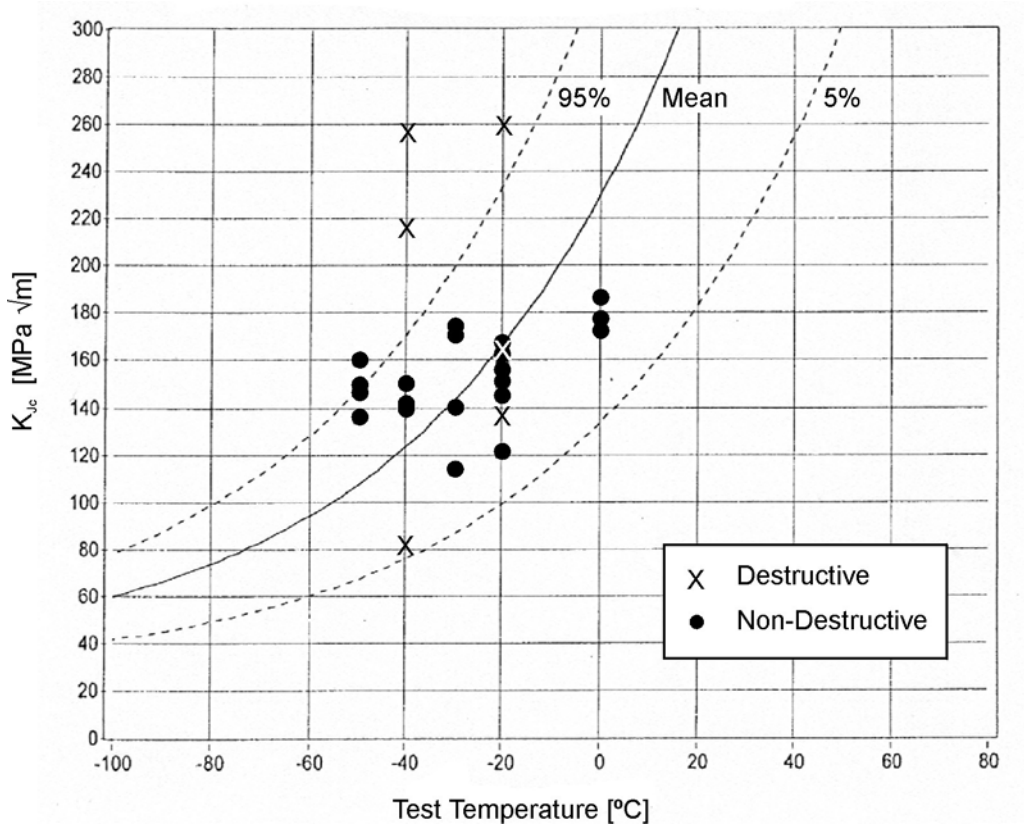

Figure 3.6(a): Results of Destructive Tests Superimposed on the Master Curves (Mean, 5th and 95th Percentile) Determined by the Non-Destructive ABI Method, for Steel A. Unstable Fracture was not Obtained at 0°C

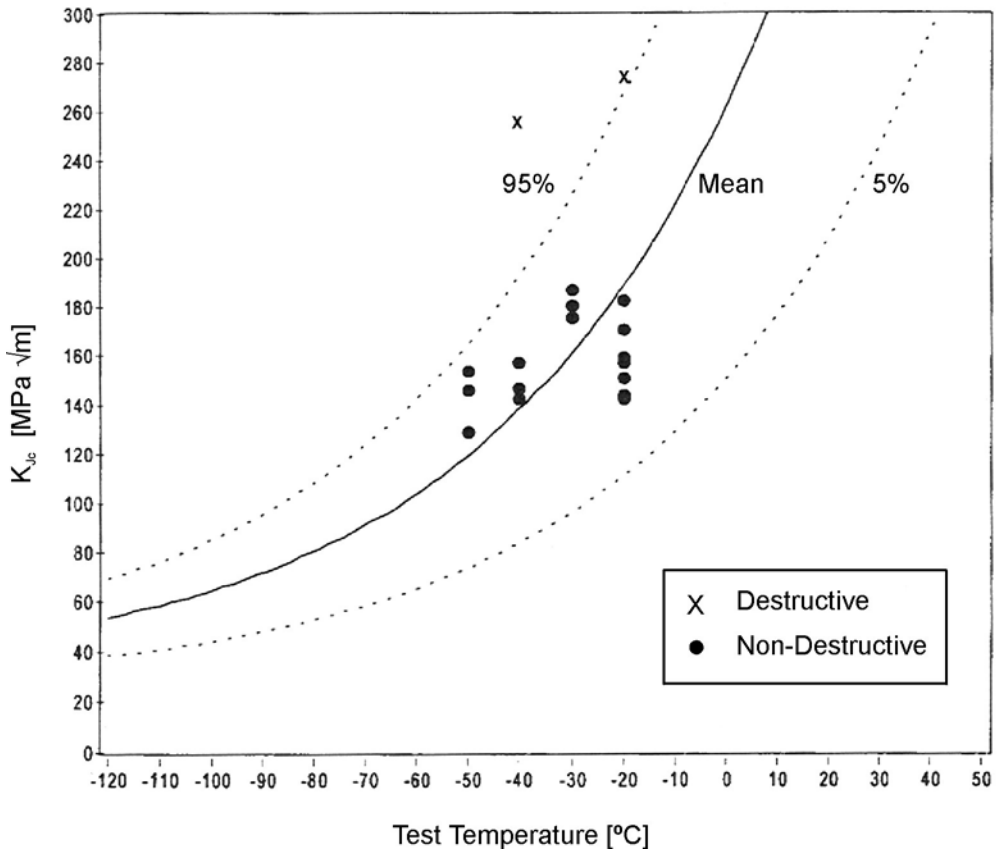

Figure 3.6(b): Results of Destructive Tests Superimposed on the Master Curves Determined by the Non-Destructive ABI Method, for Steel B. Only Two Unstable Fractures were Obtained

The K_{Jc} values of fracture toughness were determined using the critical fracture stress (σ_f) at -196°C (Appendix C). This method can lead to conservative fracture toughness estimates, when the critical fracture stress at higher test temperatures are much greater than the value at -196°C [57]. Therefore, it is recommended that ABI testing be performed in a temperature close to the reference temperature to obtain a more realistic master curve [57]. Testing at temperatures below -40°C, however, was not carried out, as the focus in this program was to perform tests within the practical range for the ship operating conditions.

3.5.2 Weld Metal

A very good agreement between results from the non-destructive and destructive determinations for the SMA weld is demonstrated in Figure 3.7(a). In this case, a correction was employed to account for the effect of temperature on the σ_f, based on previous work that showed σ_f begins to increase above -100°C [57]. In contrast, the conventional fracture toughness results of the FCA weld make the ABI results look non-conservative as the K_{Jc} values of the destructive tests center around the 5th percentile of the reference curve derived from the ABI data (Figure 3.7(b). Ideally, the K_{Jc} data should center around the 50% percentile, i.e., the mean master curve.

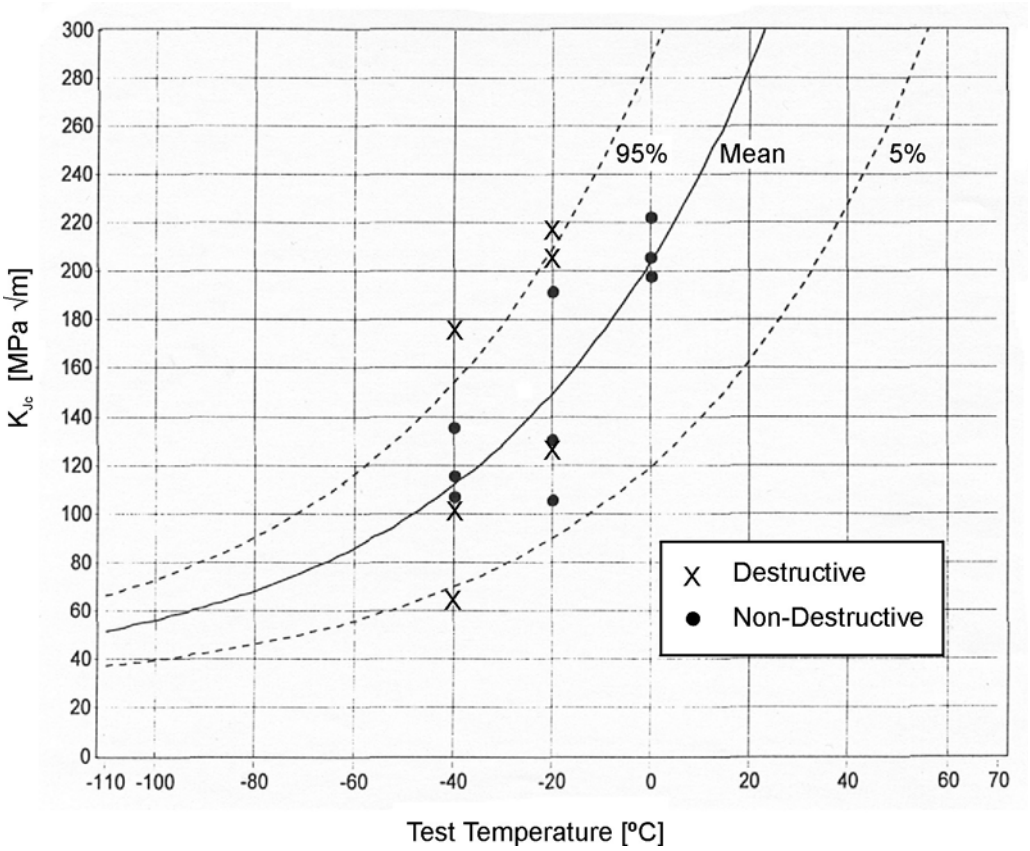

Figure 3.7(a): Results of Destructive Tests Superimposed on the Master Curves Determined by the Non-Destructive ABI Method, for SMA Weld. Unstable Fracture was not Obtained at 0^{o}C

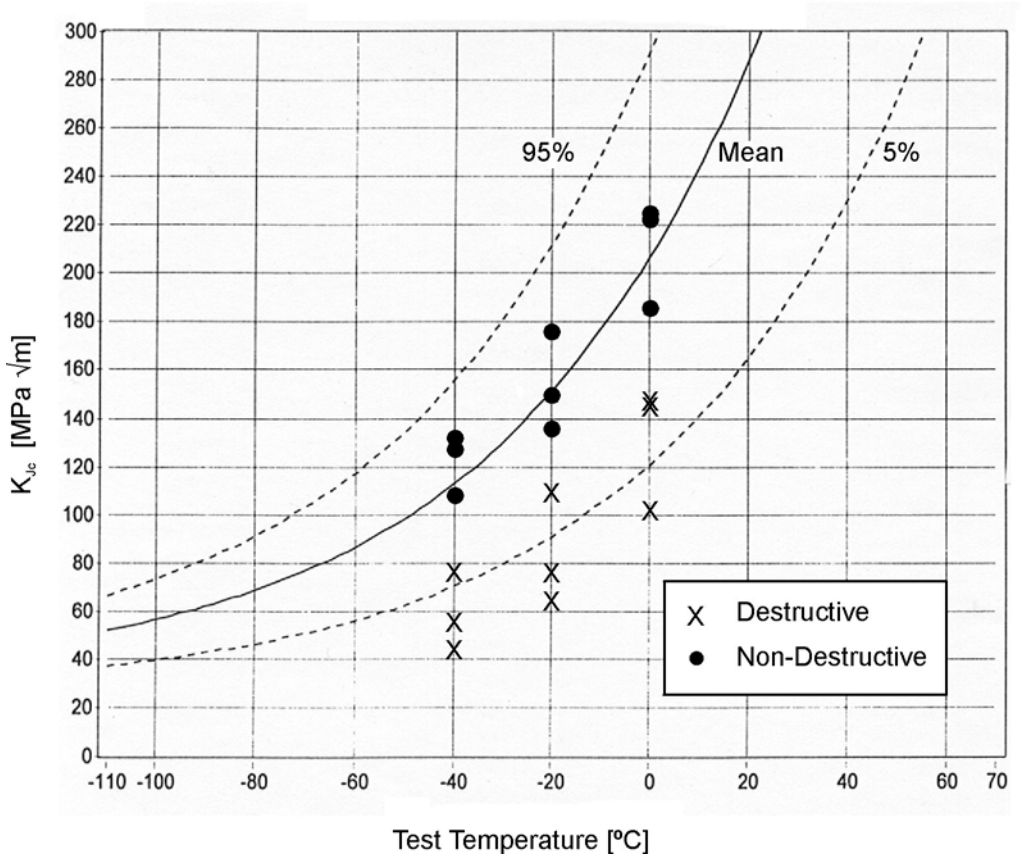

Figure 3.7(b): Results of Destructive Tests Superimposed on the Master Curves Determined by the Non-Destructive ABI Method, for FCA Weld

An alternative method of conducting this comparison would have been to determine the reference temperature by each approach, i.e., destructive and non-destructive, and then derive for each type of weld, a normalized plot, with respect to the reference temperature (T_o). Figures 3.8(a) and 3.8(b) present this data and a very good agreement is displayed when considering the increase in toughness with temperature.

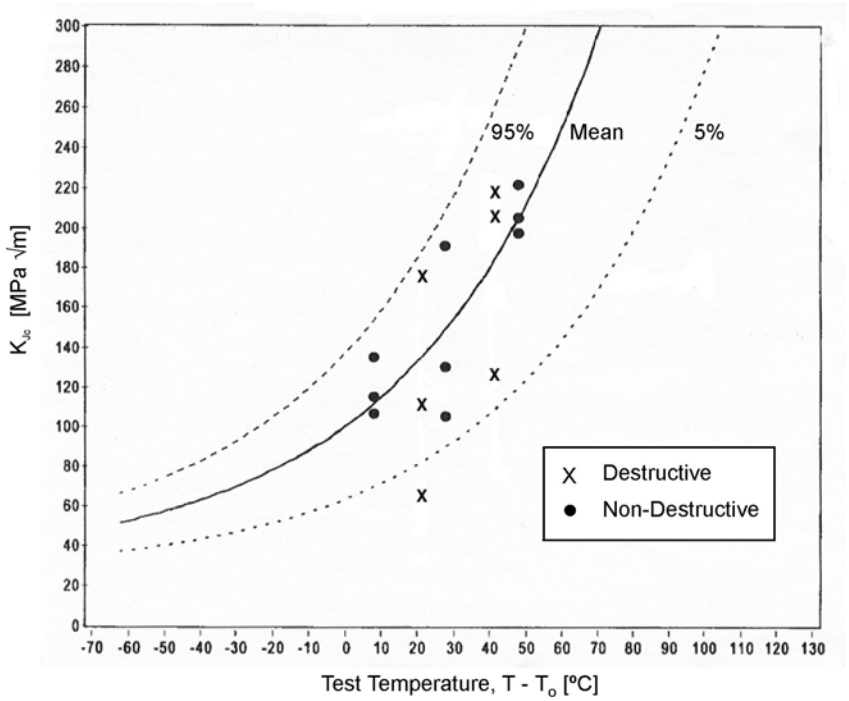

Figure 3.8(a): Normalized Plot, for SMA Weld. Reference Temperatures for Destructive Test Results and Non-Destructive Test Results are -62°C and -48°C, respectively.

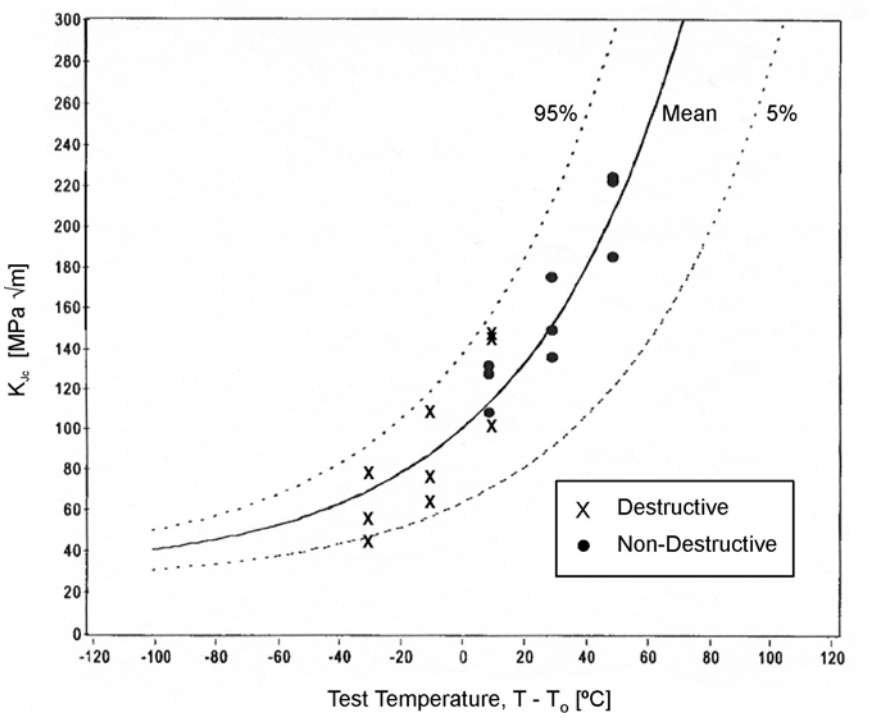

Figure 3.8(b): Normalized Plot, for FCA Weld. Reference Temperatures for Destructive Tests Results and Non-Destructive Test Results are -9°C and -49°C, respectively.

The reference temperature was determined using the multi-temperature method allowed in ASTM E1921. When this alternative method of calculating the reference temperature is employed, the expected scatter band for T_o determination is within 20°C (clause 12 ASTM E1921). For the SMA weld, the difference in T_o calculated for two methods is 14°C, and therefore, destructive and non-destructive results are comparable. However, for the FCA weld, the difference is greater than the scatter band, i.e., 40°C. A plausible explanation would be that the non-destructive evaluations for the FCAW were performed in a localized weld region that has better toughness than the lowest toughness regions of the full thickness weld. Clause 1.6 in ASTM E 1921 standard requires that for multi-pass welds, the heterogeneity and associated local brittle zones is not amenable to the statistical analysis methods employed in the standard. So it is possible that the two sets of data, that is, from the destructive tests and the ABI estimates, are not covered by the same distribution.

3.5.3 Normalized Plots for Steel A

Using the alternative method described above for weld metal, destructive and non-destructive results for steel A can be compared as there is sufficient K_{Jc} data points to determine T_o for the destructive tests. Figure 3.9 displays this comparison.

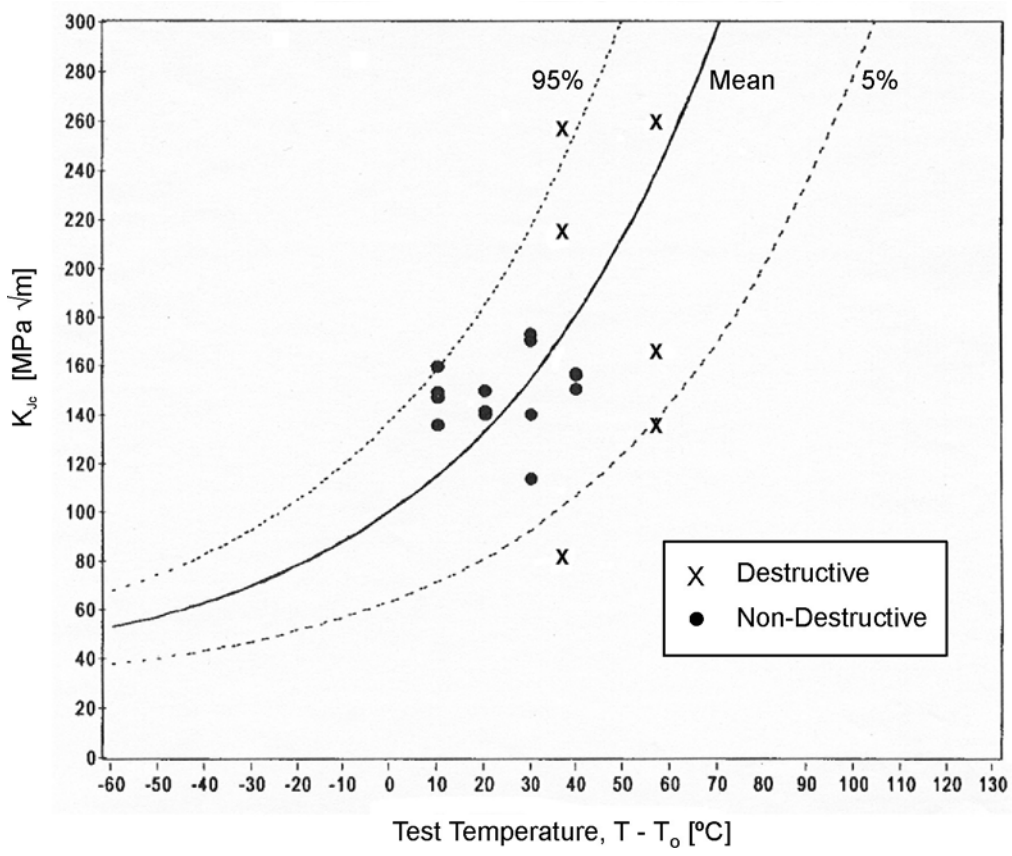

Figure 3.9: Normalized Plot, for Steel A. Reference Temperatures for Destructive Test Results and Non-Destructive Test Results are -77°C and -60°C, respectively.

3.6 Concluding Remarks

The comparison of fracture toughness results from the non-destructive ABI method and destructive method was based on determination of toughness in accordance with ASTM E1921. This is because it has been demonstrated that the ABI method can be used to develop a master curve for ferritic steel that is in reasonable agreement with the master curve determined by destructive tests in accordance with ASTM E 1921-97 [57]. (It should be also noted that this ASTM method allows a probabilistic fracture mechanics approach to be implemented.) The comparison in the current work shows the following:

- For the base materials, meaningful comparison is possible only for steel A, since for steel B there were insufficient K_{Jc} data points due to its high toughness at the test temperatures of interest. The reference temperature calculated from the destructive tests for steel A is -77^{o}C compared to -60^{o}C from the non-destructive tests and is within the 20^{o}C scatter band [54]. In this way, the results from both methods are comparable for steel A.

- For the welds, the fracture toughness results from both methods for the SMA weld metal show agreement, whereas, for the FCA weld metal the destructive test results indicate lower toughness compared to the ABI non-destructive evaluation.

The broader objective of this task was to evaluate the applicability of the ABI non-destructive method for estimation of fracture toughness of structural details in a ship. (Being a non-destructive method, the evaluations need to be limited to testing local regions close to the surface.) The findings from this work can be used to arrive at limitations of the ABI method from this perspective as described below with some alternative strategies to overcome them.

For the base metal, the test temperatures at which reliable toughness (K_{Jc}) data can be obtained has to be within ± 50^{o}C of T_o (reference temperature) [54]. (This limitation is from the ASTM method itself, as the fracture event needs to be a brittle instability without excessive plasticity at the crack tip and also subject to weak-link statistics [54].) For steel B, the destructive test results indicate that this requirement was not met when testing at the design temperature, and therefore, for steels having a lower transition temperature with respect to the design temperature, testing needs to be carried out close to T_o for a proper comparison. It can be argued that beyond the upper limit of this temperature unstable brittle fracture is unlikely and therefore the limit state for failure is that of plastic collapse where toughness is not required. Alternatively, the master curve could be used to determine K_{Jc} values beyond the upper limit in case of the likelihood of unstable fracture. The lower limit will be below the operational temperatures in the North Sea for ship steels manufactured after 1970.

For the weld metal the typical variability in toughness of multi-pass welds is in the through-thickness direction. The ABI method will be used to measure only the sub-surface toughness in field application, as outlined above. This is not a limitation of the method, but rather a limitation from the application where only the surface of the weld is available for testing. As seen in this preliminary work, this can result in non-conservative fracture toughness from the localized nature of the automated ball indentation (ABI) method. A way to overcome this practical difficulty would be to develop a database of ABI sub-surface toughness vs. full thickness destructive toughness for typical ship welds. To improve the reliability of such a database, a parallel microstructural and macrostructural record needs to be made. This database will provide an empirical method to avoid non-conservatism or over- conservatism when only the surface of the weld is accessible for evaluation.

The preliminary work shows that an estimate of the reference temperature will help in selecting the temperature range so that non-destructive testing will give reliable fracture toughness data. Further work is required to determine the temperature envelope where reliable fracture toughness values can be obtained for field application as outlined in Section 9.0.

4. EVALUATION OF THE PIEZZOMAGNETISM APPROACH

4.1 Objective

The objective of the experimental program was to evaluate the feasibility of using magnetic measurements to assess fatigue damage accumulation and thus be able to determine the remaining fatigue crack initiation life.

4.2 Approach

The work was divided into two segments. First, a literature review was carried out by Mr. T. Erber and Prof. S. Guralnick, Illinois Institute of Technology, Chicago, IL. The review focused on the overview of the magnetostriction and piezzomagnetism effects and then looked at the possibility of using piezzomagnetism as an indicator of fatigue. The second phase of the work involved experimental studies and was carried out under a Masters program by Mr. Junwon Son under the guidance of Prof. S. Guralnick.

4.3 Experimental Program

The material chosen for testing was 1018 steel. The specimen design was in accordance with ASTM E 606 specification for strain life tests and is shown in Figure 4.1. The fatigue testing was carried out on MTS servo-hydraulic test systems. Standard 12.5mm (0.5-inch) MTS strain gauge extensometer was used to carry out strain measurements. The strain range used varied from 3.8 mm/mm-3.42 mm/mm (.15in/in-0.135in/in). The total cycles to failure varied from 2,844 to 862,983 cycles depending on the strain range used, with one test terminated at 842,121 cycles. Most of the tests were carried out in the low cycle fatigue regime.

Magnetic measurements were carried out by fluxgate magnetometers (HP 3529A/428B and APS 428C) with a field range of 0.1 mG-10G. A mu-metal shielded cylindrical flux gate probe of 6.85 mm (0.27 inch) diameter, 82.55 mm (3.25 inch) long and weighing approximately 30 grams was used to pick up the variations in the magnetic field during fatigue cycling. Strain and magnetic field variations were collected simultaneously for each cycle during the test.

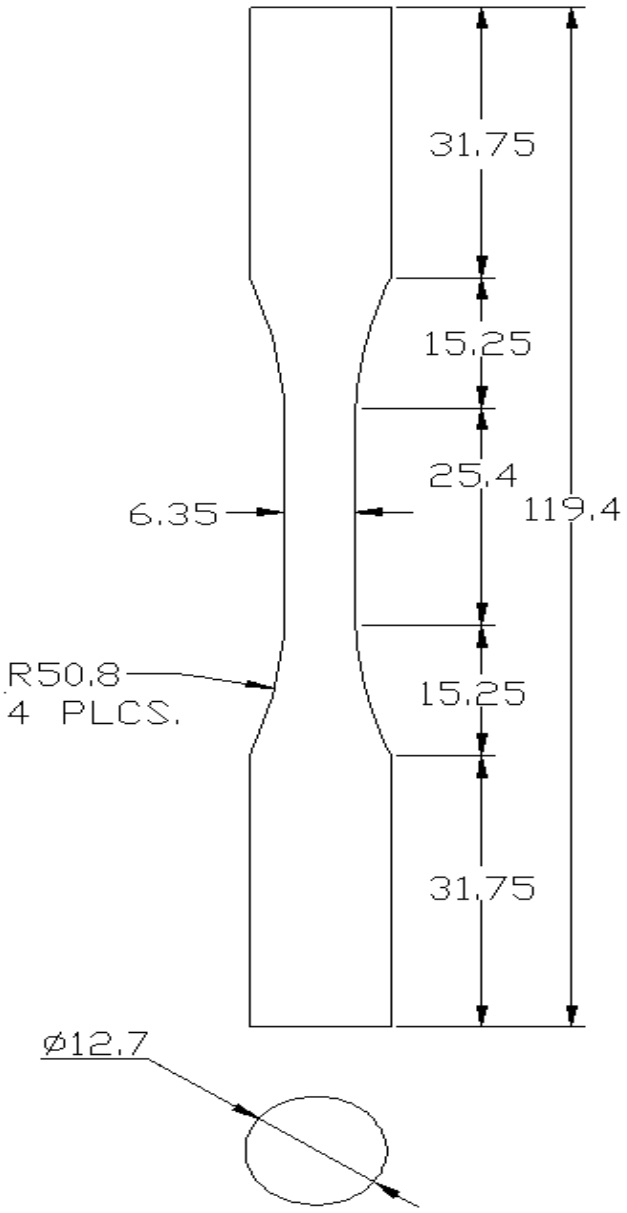

Figure 4.1: Schematic of the Fatigue Test Specimen

4.4 Results

Figure 4.2(a) shows the application of strain with time, and Figures 4.2(b) and 4.2(c) show the corresponding stress versus strain cycle, and magnetic field, B versus the number of fatigue cycles respectively. The B field is simply measured as a function of time, and in turn related to the number of cycles. The mechanical hysteresis loop area or the energy loss (U) was calculated for each individual fatigue cycle. The energy loss per cycle was plotted against the magnetic field measurements.

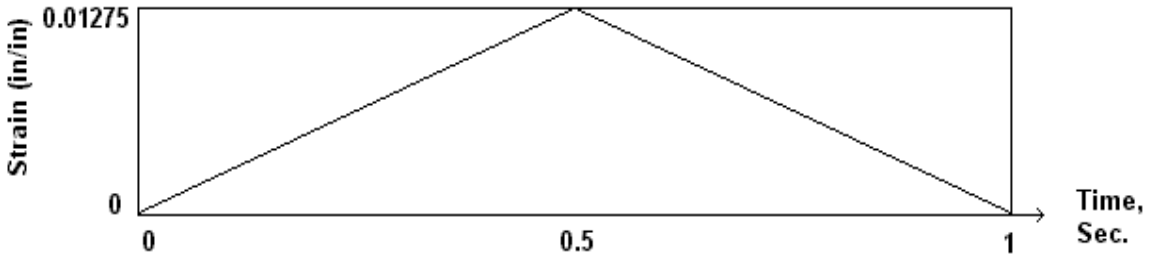

Figure 4.2(a): Schematic of Strain Application versus Time

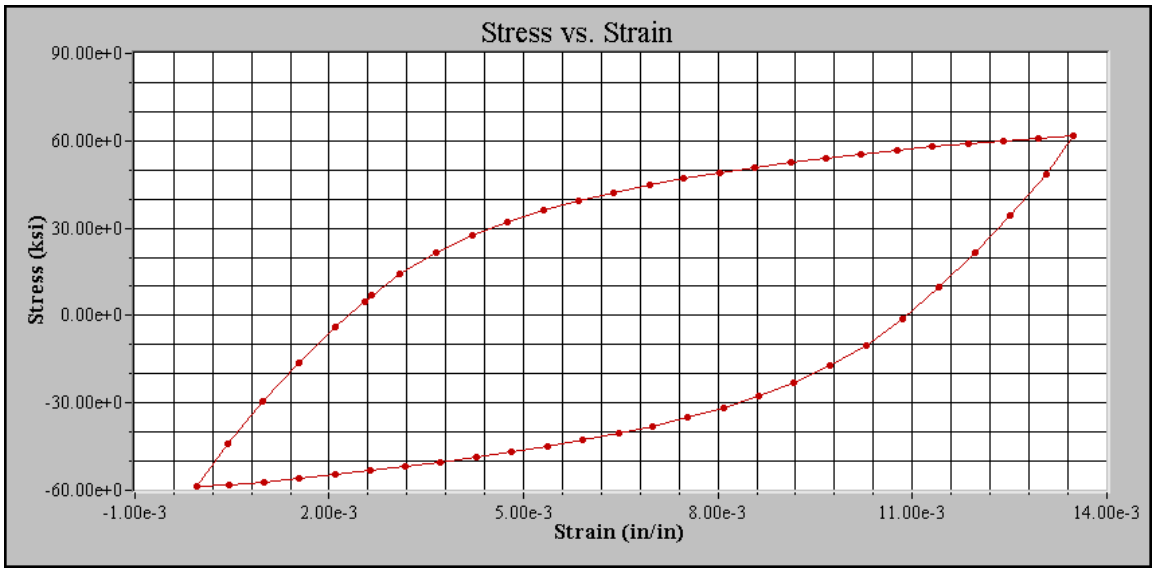

Figure 4.2(b): Mechanical Hysteresis Loop Corresponding to the Strain Application (Figure 4.2(a)).

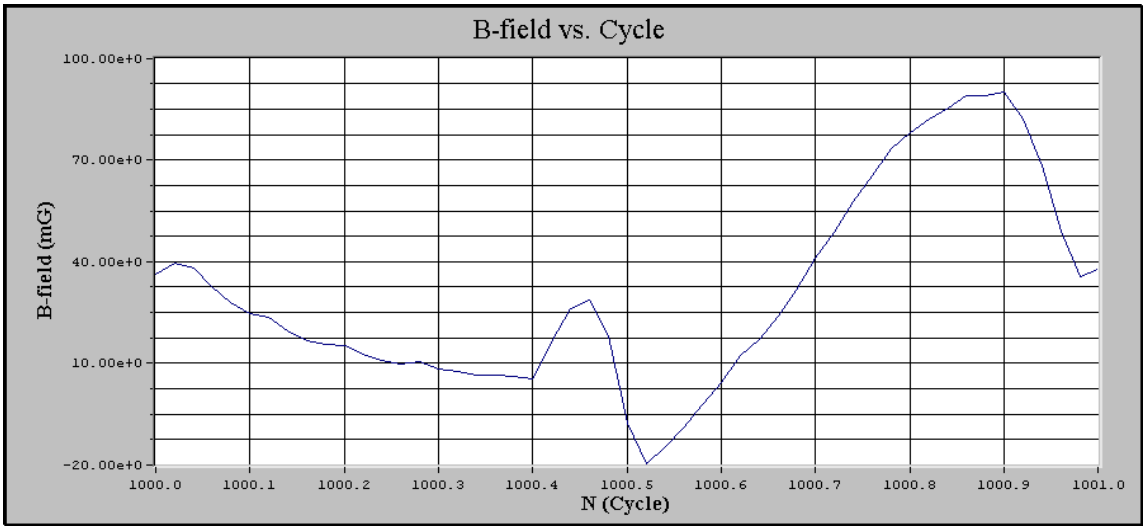

Figure 4.2(c): B Field Measurements Corresponding to Strain Cycle (Figure 4.2a)

Figure 4.3(a) is a schematic of the different stages of evolution of hysteresis with the number of cycles. The first and second slope down regions are denoted region 1 and region 3, respectively and the horizontal region is denoted as region 2. Figure 4.3(b) is another schematic showing the maximum and minimum B field measurements obtained at each cycle along with the mechanical hysteresis loss per cycle. There is a corresponding relationship between the hysteresis loss and the magnetic field measurements and that stages 2 and 3 begin almost at the same number of cycles for either the hysteresis loss or B field measurements. The entire fatigue process was thus divided into four stages: (1) Accommodation of stresses and some initiation of micro-cracks (2) Slip band growth through localized plasticity, (3) Generalized plasticity macro-crack initiation and growth and (4) Macro-Crack growth and complete rupture.

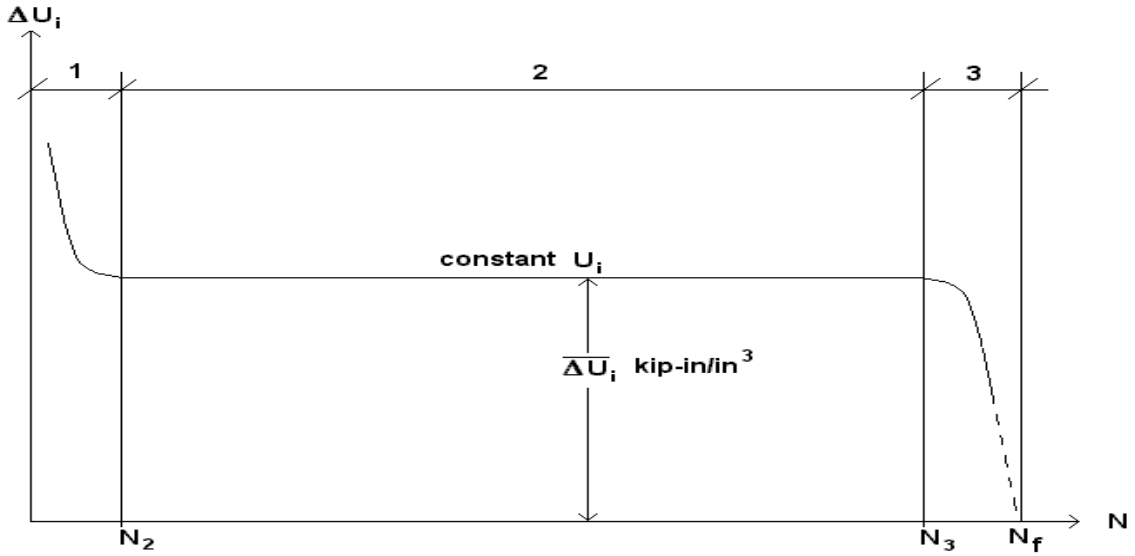

Figure 4.3(a): Different Stages in the Evolution of Mechanical Hysteresis with Number of Cycles

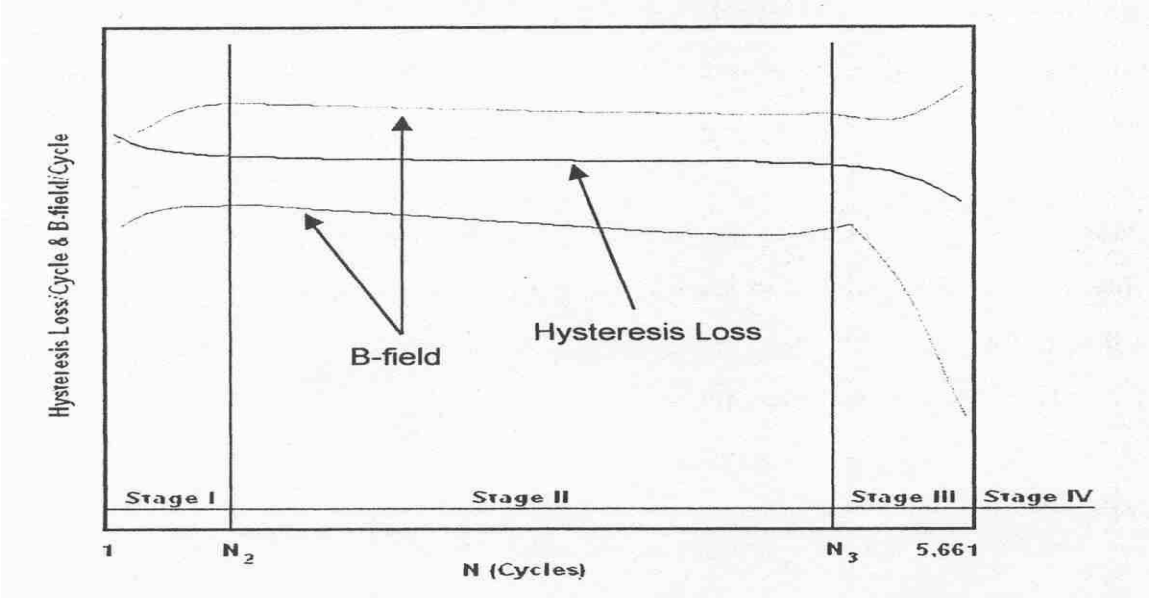

Figure 4.3(b): Stages of Mechanical Hysteresis and B Field versus Number of Cycles

Figures 4.4(a) and 4.4(b) show a couple of examples of the test data for specimens failing in low cycle fatigue and high cycle fatigue regimes respectively. The symbol dU/N is the mechanical hysteresis or energy loss per cycle and Bt/n and Bb/n are the maximum and minimum magnetic field measurements per cycle. For low cycle fatigue, Figure 4.4(a), the mechanical hysteresis measurements are mirrored by analogous changes in the magnetic field measurements. However, for high cycle fatigue the specimen practically showed no mechanical hysteresis but did show substantial magnetic field activity. The measurement of magnetic field activity in a high cycle fatigue environment was one of the significant observations made in this program. The following observations were made by the author:

a) If the width of the B field measurements is narrowing, then the number of cycles of stress applications previously accumulated is smaller than $N_{2;}$.
b) If the width is constant then it is between N_2 and $N_{3;}$.
c) If the width of the B field measurements is widening, then the number of cycles of stress applications previously accumulated is greater than N_3.

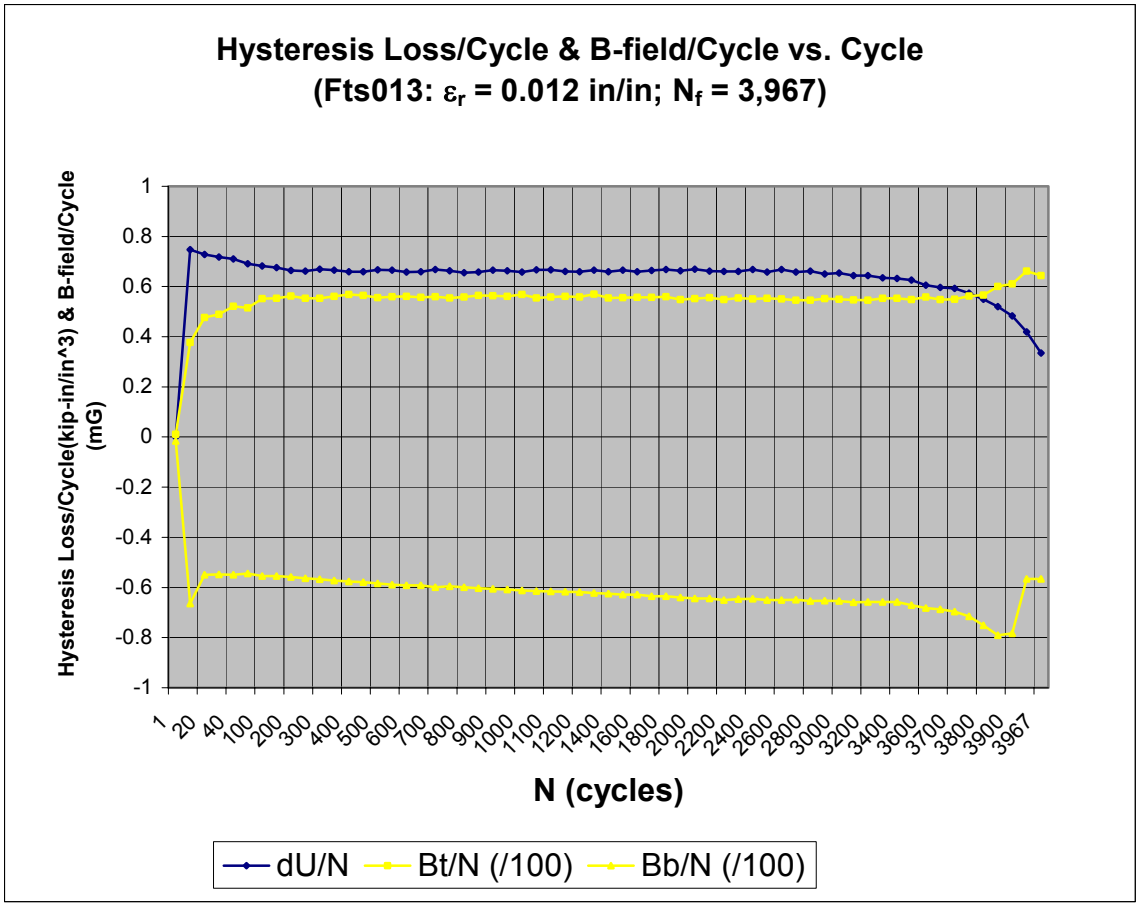

Figure 4.4(a): Hysteresis Loss and B Field/Cycle versus Number of Cycles (Low Cycle Fatigue)

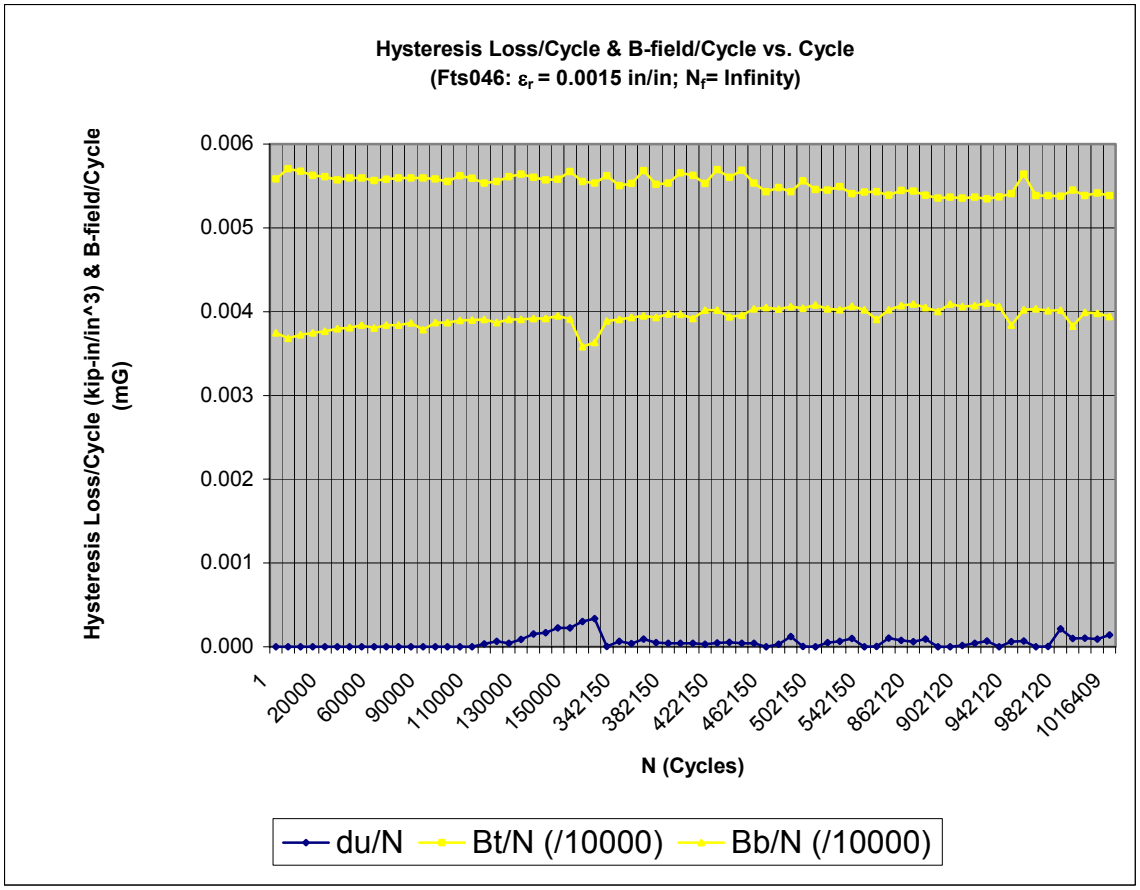

Figure 4.4(b): Hysteresis Loss and B Field/Cycle versus Number of Cycles (High Cycle Fatigue)

4.5 Concluding Remarks

- Most of the experiments in the present program were carried out in the low cycle fatigue regime where as high cycle fatigue is of greater interest in the context of fatigue damage in ship structures. The measurement of magnetic field activity at high cycle fatigue is a very encouraging result and demonstrates that the piezzomagnetism technique is very sensitive compared to the mechanical hysteresis measurements.
- The technique at present is still in the development stages and as such is not ready for commercial or field applications.
- Looking closely at all the data, it was observed that the first stage up to N_2 cycles has a range between 4.5%-56.1% of N_f and at stage 3 the fatigue life already consumed varies between 75-98%. This implies that if one is measuring a constant B field 75-98% of the fatigue life may already have been consumed, thus severely limiting the useful application of this technique.

5. EVALUATION OF THE MEANDERING WINDING MAGNETOMETER (PROPRIETARY)

5.1 Objective

The objective of this program was to evaluate the feasibility of using the magnetic winding magnetometer (MWM) technique to estimate the remaining fatigue crack initiation life.

5.2 Approach

The work was divided into five major components as detailed below and carried out by JENTEK Sensors Inc and BMT FTL.

a) Fabrication of welded specimens: Carried out by BMT FTL;
b) Base line magnetic permeability measurements using MWM sensors on all specimens: Carried out by JENTEK Sensors Inc.;
c) Preliminary fatigue testing to establish fatigue crack initiation life and subsequently subjecting the specimens to different percentages of fatigue crack initiation life: Carried out by BMT FTL.
d) Sorting of specimens using the MWM technique on the basis of anticipated remaining fatigue crack initiation life: Carried out by JENTEK Sensors Inc.
e) Testing these specimens to determine the actual remaining fatigue crack initiation life and compare it with MWM results: Carried out by BMT FTL.

5.3 Experimental Program

5.3.1 Specimen Fabrication

Algoma 100 quench and tempered steel plate was used for fabricating specimens. The chemical composition is shown in Table 5.1. Three panels, 609 x 355 x 19 mm (24 x 14 x 0.75 inches) each, were used in the present program. Pulsed Gas Metal Arc Welding (GMAW) was used to deposit single weld beads 609 mm (24 inches) long at the middle of the three panels and on both sides, thus simulating butt-welded joints. The heat input was kept at 1.88 kJ/mm (47.7kJ/in), the wire used was ER100S-1 (1.2 mm/0.05 inches) and the shielding gas used was Arcal 211 (Ar-CO_2-He). 101 mm (4 inches) wide middle tension specimens were then fabricated from the welded panel by saw cutting and machining. The weld bead on one side was ground flush with the parent metal surface to avoid fatigue crack initiation on this side. The weld reinforcement on the other side was ground flush only at the edges of the plate so that the cracks did not initiate at the corners of the weld toe.

Further, one of the two weld toes was also ground and hammer peened to ensure that the fatigue cracks did not initiate at this toe. Thus, only one weld toe per specimen was left untouched. Figure 5.1 shows a schematic of the middle tension specimen. The untouched weld toe was used to establish fatigue crack initiation life and carry out MWM measurements. DCPD probes were spot welded across the untouched weld toe as shown in Figure 5.2 to monitor fatigue crack initiation. There were a total of ten active probes about 9 mm apart installed along the weld. One probe was installed away from the weld on the base metal for use as a reference probe.

Table 5.1: Chemical Composition of Base Metal, (wt%).

C	Mn	P	S	Si	Cu	Ni	Cr	Mo	Ni
0.17	1.27	0.008	0.007	0.25	0.08	0.01	0.08	0.13	0.01

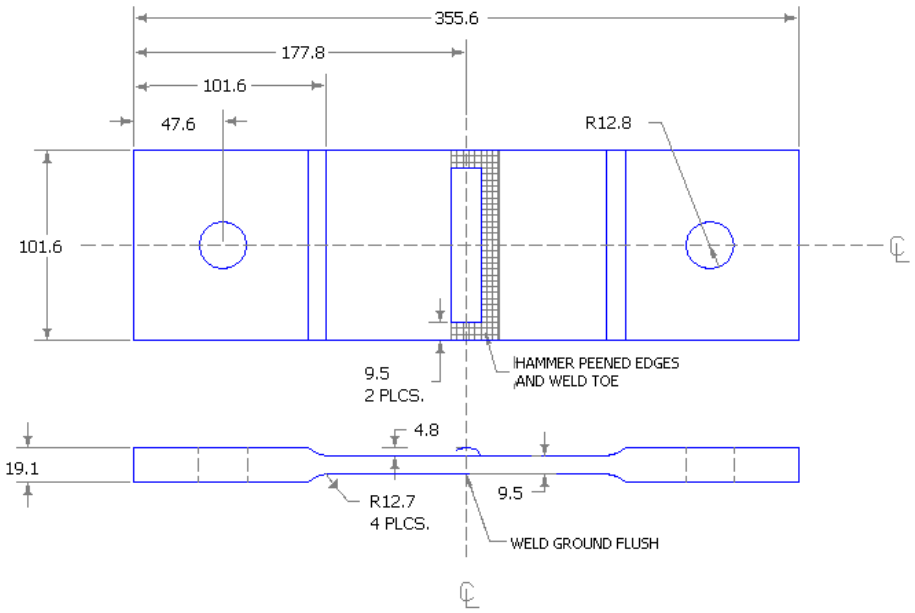

Figure 5.1: Schematic of the MT Specimen used in the Present Program

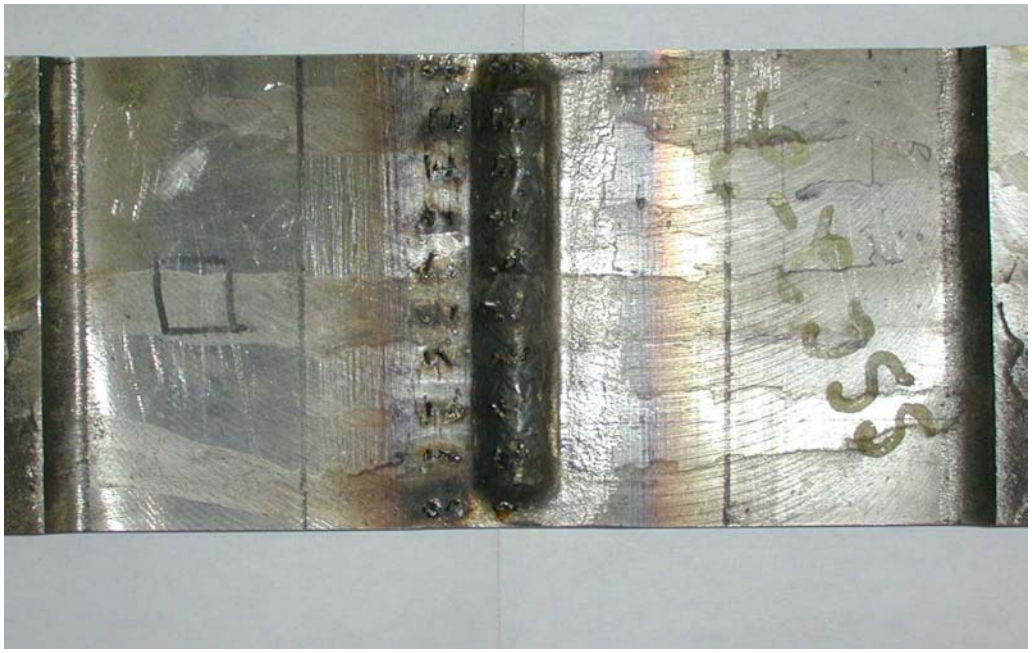

Figure 5.2: Photograph of a Specimen Showing Spot Welded Probes across one Weld Toe. The Other Weld Toe is Ground and Hammer Peened

5.3.2 Permeability Measurements using MWM Technique

All fabricated specimens were shipped to JENTEK Sensors Inc. to carry out base line measurements as well as look for the variability in the measurements between different specimens using the MWM technique. Figure 5.3 shows an example of permeability measurements transverse to the weld with the MWM sensor. In the figure, the weld axis is at position 5.5. Six specimens (1-1, 1-3, 2-2, 2-3, 2-5 and 3-3) were identified by JENTEK for remaining fatigue crack initiation life prediction based on initial extensive measurements. The plan was to test the specimens to establish the fatigue crack initiation life. The six specimens identified by JENTEK would then be subjected to different fractions of fatigue crack initiation life and then sent back to JENTEK so that they can sort the specimens using the MWM technique.

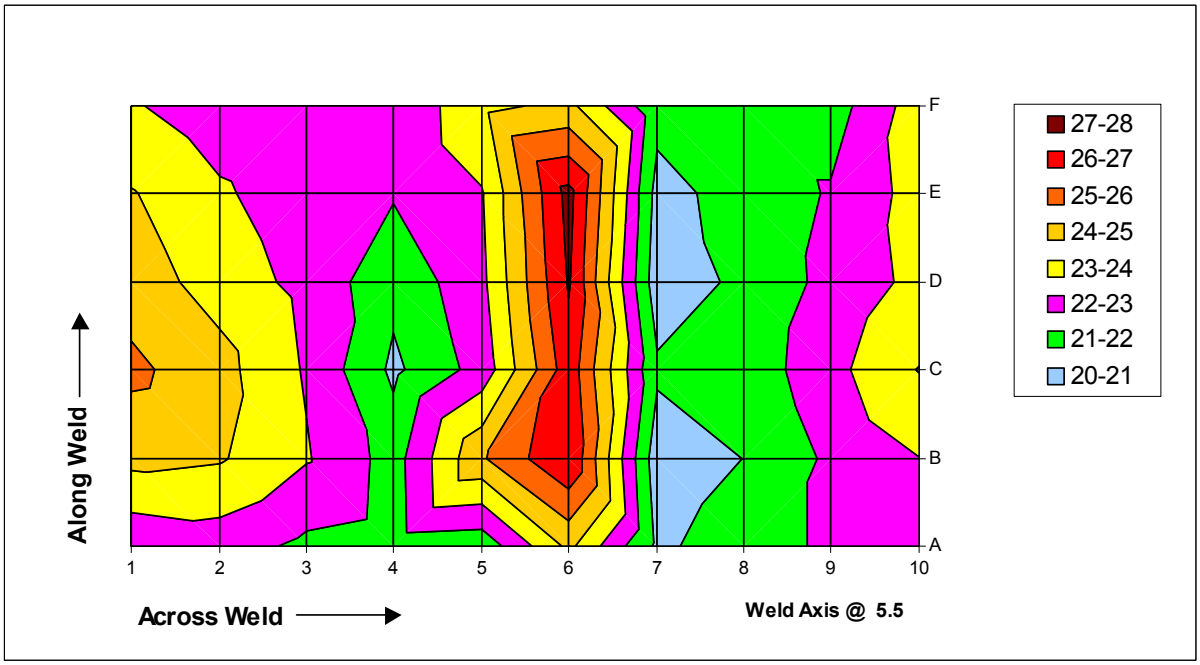

Figure 5.3: Example of Permeability Measurements Carried out Transverse to the Weld with MWM Sensor

5.3.3 Fatigue Testing

The specimens were subjected to constant amplitude fatigue testing at a positive stress ratio, R=0.1 and at a frequency of 8-10 Hz. A localized DCPD technique was used to monitor the weld toe for fatigue crack initiation and crack growth. Figure 5.4 shows a photograph of an instrumented specimen installed in the testing rig. The DCPD measurements were carried out every 2000 cycles. Figure 5.5(a) shows a plot of normalized potential difference measurements versus number of cycles for all the channels and Figure 5.5(b) shows a plot of channel 12 and

reference PD. There is an increase in the PD values as soon as the probes start to see the crack. The ink staining technique was also used to mark the crack front. All the channels are showing small continuous fluctuations (noise) in the NPD values. During the test it was discovered that the reference probe was not properly welded and because of that reference probe values varied a lot. Since the normalization of the active channels was carried out with respect to the reference probe, the small fluctuations are seen in all the active channels. Figures 5.6(a) and 5.6(b) show the plots of raw PD value for channel 12 and reference probe respectively. The channel 12 PD values are very stable and do not show the fluctuations as seen in the earlier Figures, 5.5(a) and 5.5(b). The reference probe values, Figure 5.6(b) on the other hand are varying a lot.

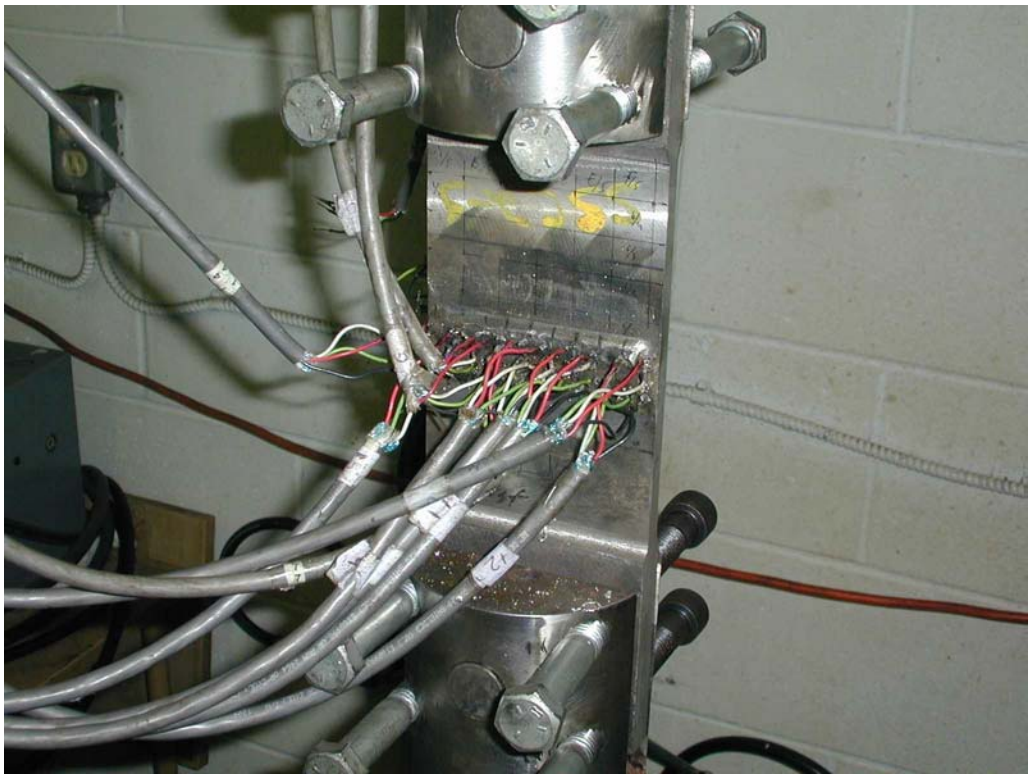

Figure 5.4: Specimen with PD Probes Installed in the Fatigue Testing Rig

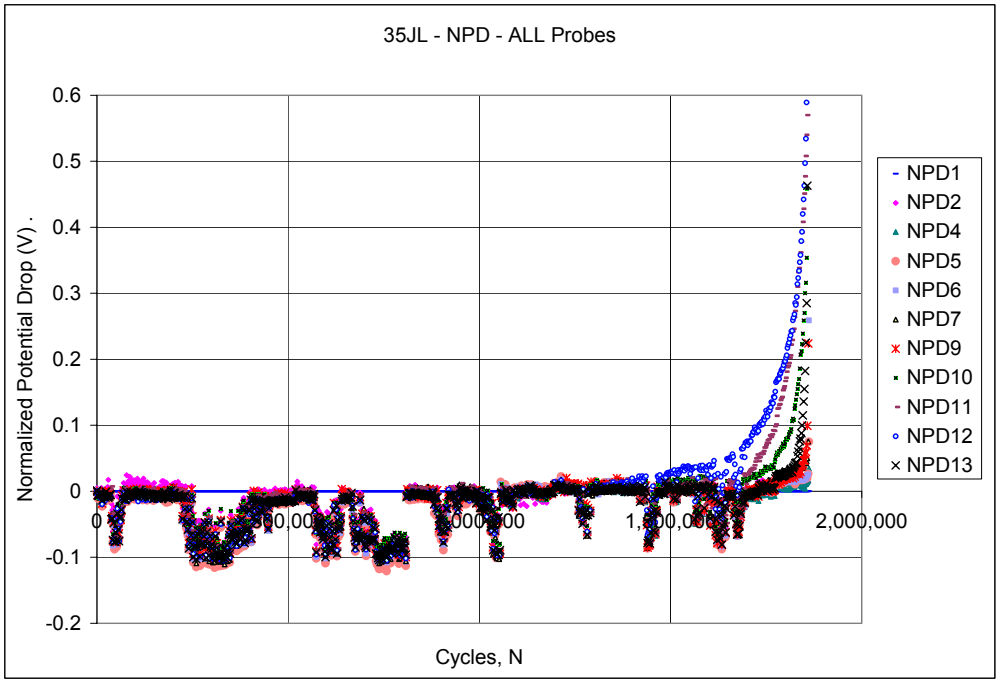

Figure 5.5(a): NPD Readings versus Number of Cycles

Figure 5.5(b): NPD Readings versus Number of Cycles (Channel 12 and Reference Probe)

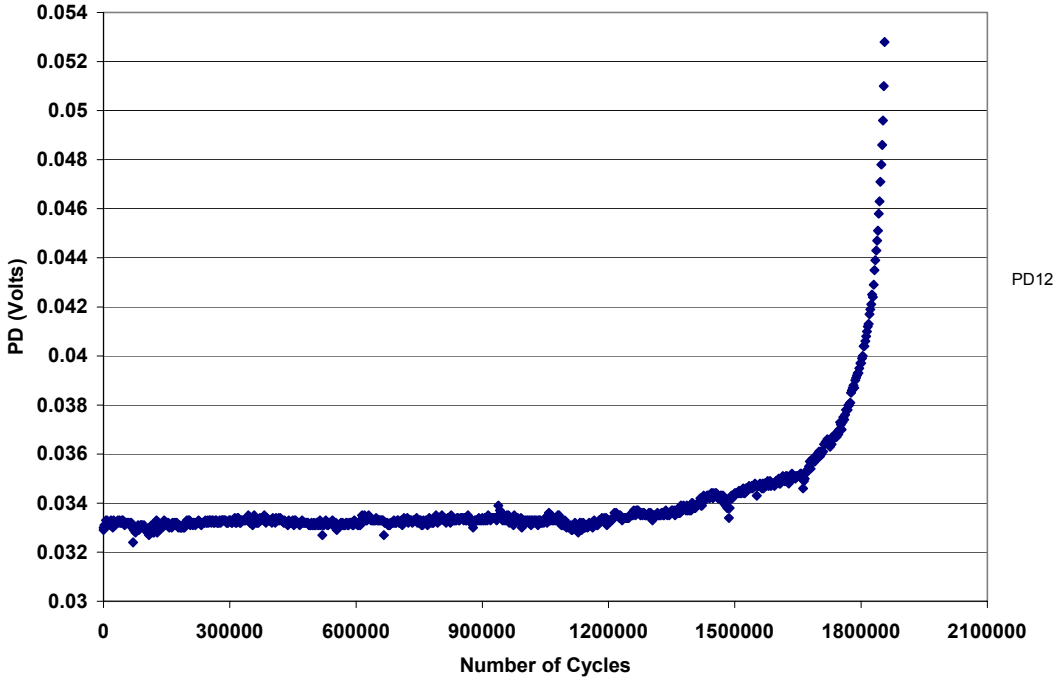

Figure 5.6(a): Raw PD Readings versus Number of Cycles (Channel 12)

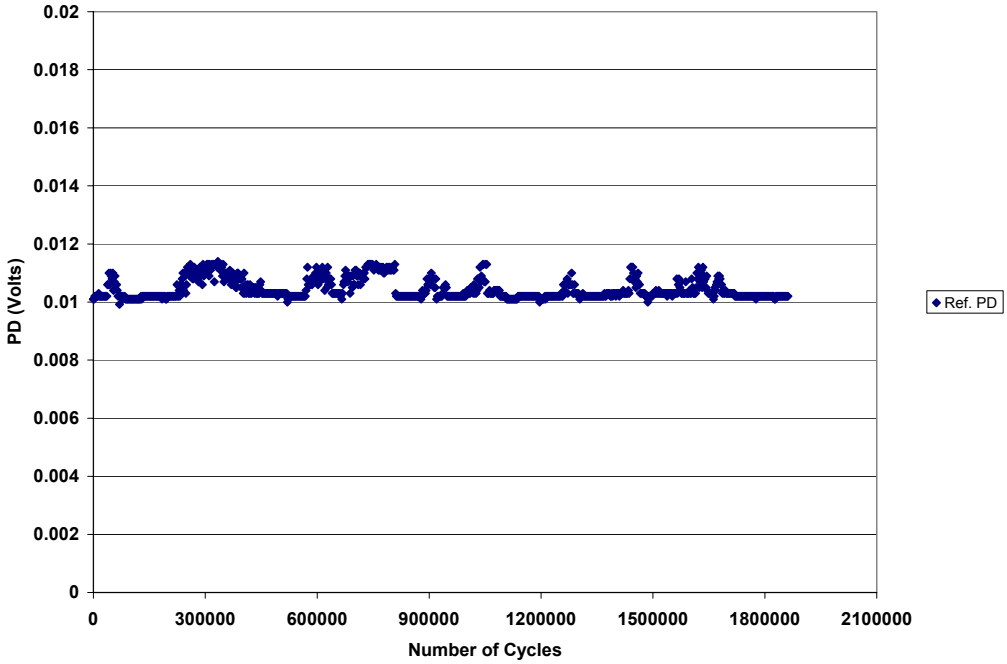

Figure 5.6(b): Raw PD Readings versus Number of Cycles (Reference Probe)

Five specimens were fatigue tested to establish the fatigue crack initiation life. Different stress range values were chosen initially with the objective of finding the stress range for a fatigue crack initiation life of approximately one million cycles. The stress range was found to be 135

MPa. One additional specimen (2-4) was subjected to fatigue cycling until a fatigue crack had initiated and propagated to a length of 8-10 mm and a depth of 0.5-1 mm.

The six specimens identified by JENTEK were then subjected to fatigue cycling to different fractions of fatigue crack initiation life (one million cycles). Table 5.2 shows the specimen identification along with the percentage of fatigue crack initiation life already consumed.

Table 5.2: Details of the Percentage Fatigue Crack Initiation Life Already Consumed

Specimen Identification	Percentage of Fatigue Crack Initiation Life Already Consumed. (Number of fatigue cycles seen by the specimen)
1-1	50% (500,000 cycles)
1-3	50% (500,000 cycles)
2-2	65% (650,000 cycles)
2-3	85% (850,000 cycles)
2-5	65% (650,000 cycles)
3-3	58% (580,000 cycles)
2-4	Specimen with a crack (2.4 Million Cycles)

The above six specimens were shipped to JENTEK without providing them with any details about the fatigue cycling experienced by the specimen. The specimen (2-4) was also sent to JENTEK Sensors Inc. and they were informed that it had a fatigue crack. The approximate size and the location of the fatigue crack were also provided. This was done so that they can establish upper bound base line measurement.

5.3.4 Determination of Remaining Fatigue Crack Initiation Life using the MWM Technique

The results are **"Proprietary and Confidential"** and are for limited disclosure to Canadian and United States governments (provided under separate cover). Appendix E details the summary and conclusions of JENTEK Sensors Inc. about the MWM evaluation carried out in this program.

5.4 Determination of the Remaining Fatigue Crack Initiation Life

The percentage of fatigue crack initiation life consumed as shown in Table 5.2 is based on the average of five destructive tests carried out at BMT FTL and there can be significant variations in the fatigue crack initiation lives in individual specimens. Therefore, the true remaining fatigue crack initiation life could only be established by carrying out further fatigue testing of the specimens. As a result, the specimens on which MWM measurements were carried out and for which JENTEK had provided a relative ranking, were fatigue tested to determine the true fatigue crack initiation life of individual specimens and compare it with the results provided by JENTEK Sensors Inc. The four specimens (2-2, 2-3, 2-5 and 3-3) were thus subjected to the same fatigue loading conditions (stress range = 135 MPa at stress ratio, R=0.1) to establish the remaining fatigue crack initiation life. The results are provided in Table 5.3. Specimen 2-4 was not tested as it already had a fatigue crack as mentioned in the previous section.

Table 5.3: True Remaining Fatigue Crack Initiation Life of Individual Specimens

Specimen Identification	Total Number of Fatigue Cycles to Crack Initiation	True Remaining Fatigue Crack Initiation Life when sent to JENTEK
2-4 (Specimen with a fatigue crack)	1,880,000	0%
3-3	664,000	12%
2-2	1,000,000	35%
2-3	1,380,000	39%
2-5	No crack Initiation till 2,858,000	>77%

5.5 Concluding Remarks

The results are **"Proprietary and Confidential"** and are for limited disclosure to Canadian and United States governments (provided under separate cover). Appendix E details the summary and conclusions of JENTEK Sensors Inc. about the MWM evaluation carried out in this program.

6. EVALUATION OF THE ACOUSTIC EMISSION APPROACH

6.1 Objective

The objective of this task was to evaluate the feasibility of using acoustic emission (AE) approach to detect flaws and monitor crack growth in ship structures.

6.2 Approach

The proposed work was a paper study and the task was subcontracted to Powertech Labs Inc., Surrey, BC and is detailed in Appendix F. The work was carried out by Dr. Ainul Akhtar, Director, Strategic Technologies and consisted of the following main elements:

a) State-of-the-art review
b) Visit to a naval vessel
c) Recommendations

6.3 Overview

Dr. Ainul Akhtar visited the Canadian National Defense Fleet Maintenance Facility Cape Breton located in Victoria, B.C. He had an opportunity to board a warship as well as a supply ship with the intention of examining weld construction in ship structures and to assess the actual environment where the acoustic emission instrumentation and technology will need to be applied. He also held discussions with the naval architecture division and the ship maintenance staff. The final report is based on the issues related to the Canadian Naval vessels but is applicable to both naval as well as merchant vessels. The following sections are a brief overview of the work carried out by Dr. Akhtar.

6.3.1 Acoustic Emission Sensors

Three different types of AE sensors, namely, piezzoelectric sensors, hydrophones and sensors using fiber optics, were investigated.

Piezzoelectric sensors are the most commonly used sensors in AE testing. The frequency range of the sensors depends on the type of application. A higher frequency sensor, e.g., 150 kHz resonant frequency piezzoelectric sensor will be sensitive to frequencies in the range of 100 kHz-300kHz and thus the sensor will not be affected by audible sound (< 20kHz). However, if the higher frequency signal attenuates faster, a greater number of sensors will be required to monitor the same area. Structural details also play an important role in determining the degree of attenuation and the location of transducer. Most acoustic emission equipment can be operated with up to 300 m co-axial cables to carry out the pre-amplified signal from the piezoelectric sensor to the data acquisition system. However, practical difficulties will be encountered in managing large numbers of cables should 100% structural monitoring be the objective for a ship structure. Wireless transmission like telemetry is a proven technology and can be used. However, each sensor must have its own transmitter, or signals from a set of closely spaced sensors can be collected and transmitted to the central recording system. Substantial capital and maintenance costs will be involved should such an AE monitoring system become commercially available.

Hydrophone sensors could be used for large area surveillance for the ship hull through placing the hydrophone submerged in water outside the ship since longitudinal stress waves can propagate in liquid media with little attenuation and shear waves cannot be transmitted. Similarly, they may be used for the internal structures of liquid fuel tanks, liquid cargo tanks and ballast tanks. However, the viability of these schemes remains yet to be tested.

Two types of AE sensors using fiber optics have been reported. The fiber optic sensors may eliminate concerns associated with the coupling of conventional piezzoelectric sensors. The end faces of the fibers remain encased and therefore, can be exposed to adverse environments such as rain or seawater. Moreover, optic fibers may allow for ease of transmission of the signal from many sensors over long distances. Distributed fiber optic sensors could do away with the need for local power supply. However, for the distributed fiber optic devices to be effective AE sensors, they must remain attached to the structure along their entire length. Experiments remain to be carried out to test the effectiveness of these devices on ship structures. As yet, acoustic emission systems involving fiber optic sensors are not commercially available. However, should they become commercially available and the issue of acoustic coupling be resolved, fiber optic systems would be far more suited for global AE monitoring of the ship structure than would an AE system involving piezoelectric sensors.

6.3.2 The Signal-to-Noise Ratio

The biggest drawback of the AE technology has been the signal-to-noise ratio. The author, Dr. Ainul Akhtar, has gone into great detail in addressing this concern. Firstly, different sources of noise that can be encountered on ship structures were identified. The noise sources can be the gas turbines and diesel engines used for propulsion, rudder vibration, sloshing noise in fuel tanks, ballast tanks and liquid cargo, human activity on board, helicopter landing and take off, weather related noise (e.g., rain on the deck) etc. Additional sources of emission, other than those associated with the background noise and the propagation of crack, come into play when there is stable crack growth under dynamic loading. Two of these are crack face rubbing and crushing of the corrosion products.

The simplest approach to address the issue of noise is to select a range of frequencies for monitoring that remain outside the range in which the noise occurs. Resonant frequency transducers offer the possibility of noise reduction but keeping the resonant frequency high means higher signal attenuation and therefore closer spacing. Signal processing methodologies are available now that enable discrimination of an acoustic event based on its characteristics. Event characteristics or wave form analysis are in-turn used to determine whether it is signal or noise. The advantage of such an approach is that the threshold can be kept low and thus eliminate the need for a closer spacing of the piezoelectric sensors.

6.3.3 Conclusions and Recommendations

Global structural integrity monitoring of ships using AE technology is, at present, cost prohibitive and therefore local critical areas should be identified and monitored using piezoelectric sensors. Acoustic emission systems are commercially available to simultaneously carry out the task of local area monitoring for a number of selected sites on the ship. However, the missing link to make local area monitoring an effective tool is the quantification of crack growth from the acoustic emission data gathered on stable crack growth. Therefore, a program should be undertaken to quantify stable crack growth from the AE data gathered through local area monitoring on-board a ship and examine the methodologies available for the discrimination of noise from signal, in the specific operating environment of a ship. Non-critical areas on the structure of the ship like the cracking at the interface between the deck and the exhaust funnels on certain naval class vessels could be monitored first.

Upon achieving the objective of crack growth quantification from the proposed local area AE monitoring on-board a ship, the acoustic emission sensors may be relocated for the monitoring of selected other critical areas, either simultaneously or in succession. Transfer of the crack growth quantification methodology developed in the proposed work would then enable a quantitative assessment of cracks which may or may not be amenable to visual inspection and conventional NDE.

7. EVALUATION OF THE CRACK PROPAGATION GAUGES

7.1 Objective

The objective of this task was to evaluate the feasibility of using crack propagation gauges on irregular complex geometries such as fillet welds so that they could be used to monitor in-situ crack growth on ship structures.

7.2 Background

Crack propagation gauges provide a convenient method for indicating crack growth rate. The gauges consist of a number of resistor strands connected in parallel. When bonded to a structure, progression of a surface crack through the gage pattern causes successive open circuiting of the strands, resulting in an increase in resistance. The gauges come in different patterns. The crack propagation gauge CPA, manufactured by Measurements Group Inc. (www.measurements group.com), was used in the present program. It is 50 mm (2 inches) long, 10 mm (0.4 inch) wide, has a nominal thickness of .043 mm (0.0017 inches), and a fatigue life of greater than 10 million cycles at ± 2000 micro-strain. The standard backing is a glass-fiber-reinforced epoxy matrix. The gauges feature small copper pads on the tabs for ease of soldering. M-bond 600 or 610 adhesives manufactured by Measurements Group Inc. are recommended for installing these gauges. The recommended gauge installation requires the specimen surface to be smooth and degreased. After installation, the gauges need to be clamped for curing. The curing temperature depends on the type of adhesive being used. A curing temperature of 160^{o} C for two hours is recommended for M-bond 600 adhesive used in the present program.

Figure 7.1 shows a schematic of the CPA pattern crack propagation gauge. The CPA pattern incorporates 20 resistor strands. Once the crack passes below the gauge, the individual strands break resulting in an increase in the resistance. A typical plot of the number of strands fractured versus resistance is shown in Figure 7.2.

Figure 7.1: A Schematic of the Crack Propagation Gauge (CPA Pattern)

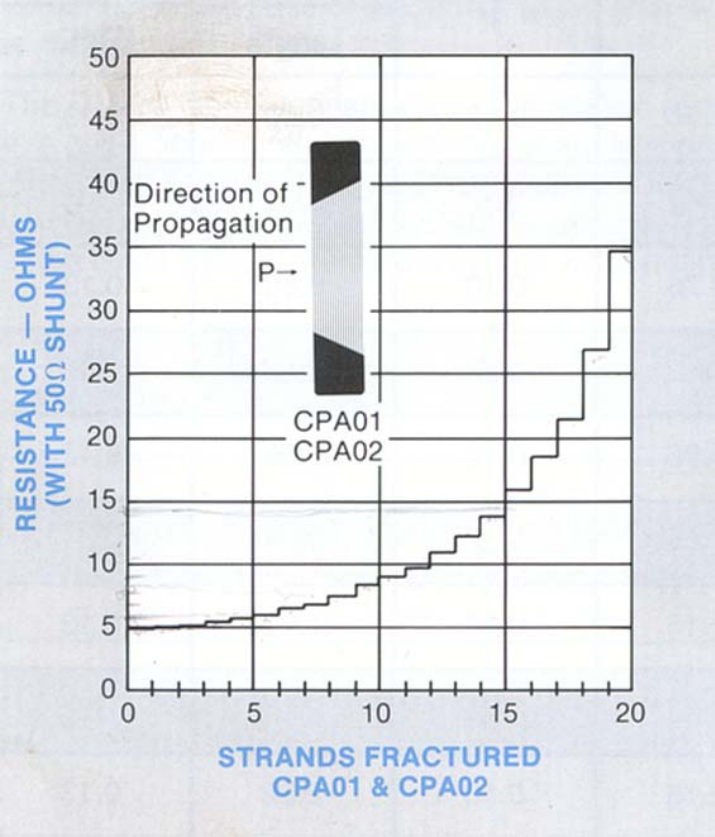

Figure 7.2: A Typical Plot of the Number of Strands Fractured versus Electrical Resistance

7.3 Experimental Program

As discussed earlier, the surface preparation involved for installing crack propagation gauges was quite labour intensive. The M-Bond 600 adhesive, as recommended by the manufacturer, required high temperature curing. The surface preparation desired for gauge installation was almost impossible to achieve on the fillet welds. Moreover, it would have required grounding the weld toe and polishing the surface. Therefore, it was decided to modify the gauge installation procedure and study its impact on the performance of the crack propagation gauges. The modified procedure involved cleaning the surface with a wire brush and emery paper and then degreasing it with a standard solvent. The adhesive selected for the modified procedure was M-Bond 200 that is normally used for the standard resistive strain gauges and does not require any high temperature curing.

Standard middle tension specimen geometry was chosen to evaluate the modified procedure. On one side of the notch the recommended procedure for crack propagation installation using M-Bond 600 adhesive was used and on the other side, the modified procedure using M-Bond 200 adhesive was used to install the gauges. Figure 7.3(a) shows the middle tension specimen with the two gauges installed on either side of the notch and Figure 7.3(b) shows the complete fatigue test set up.

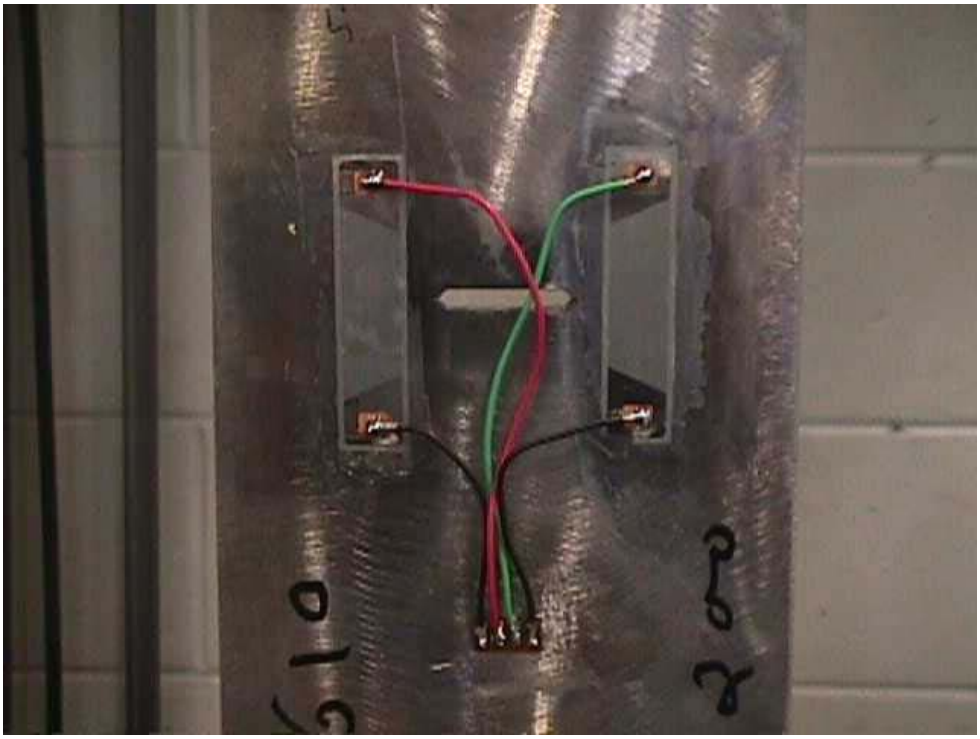

Figure 7.3(a): Photograph of the Middle Tension Specimen with the Two Gauges installed on either Side of the Notch

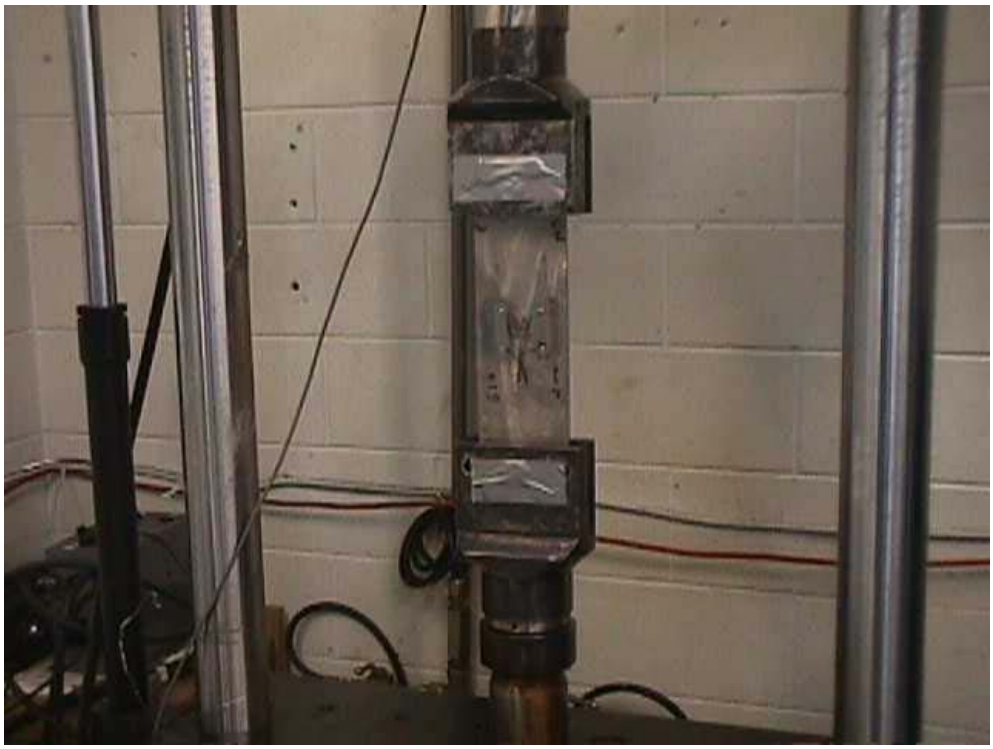

Figure 7.3(b): A Photograph of the Fatigue Test Set up

The fatigue testing was carried out at constant amplitude with a positive stress ratio, R =0.1. A simple electrical circuit was designed to read the change in voltage caused by the change in resistance due to the breaking of the strands in the crack propagation gauges. The data acquisition was carried out with the labview software. Figure 7.4 shows the plot of voltage versus time data acquired for the two gauges during the fatigue testing. Figures 7.5(a) and 7.5(b) are a zoom of Figure 7.4. The stepped increases in the voltages plots are indicative of individual strands fracturing when the crack passes below that strand. Both of the gauges are showing similar behaviour, indicating that the modified procedure developed for installation of crack propagation gauges worked as well as the standard procedure recommended by the gauge manufacturer for their installation.

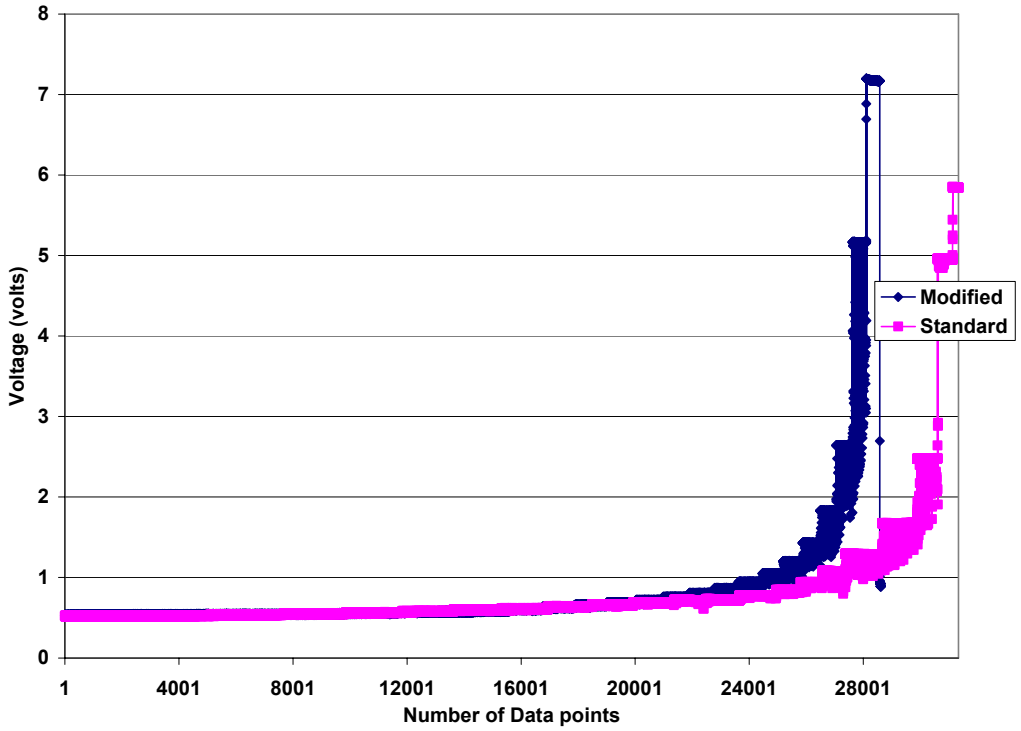

Figure 7.4: Plot of Voltage versus Time during Fatigue Testing for the Two Gauges using Modified and Standard Installation Procedure

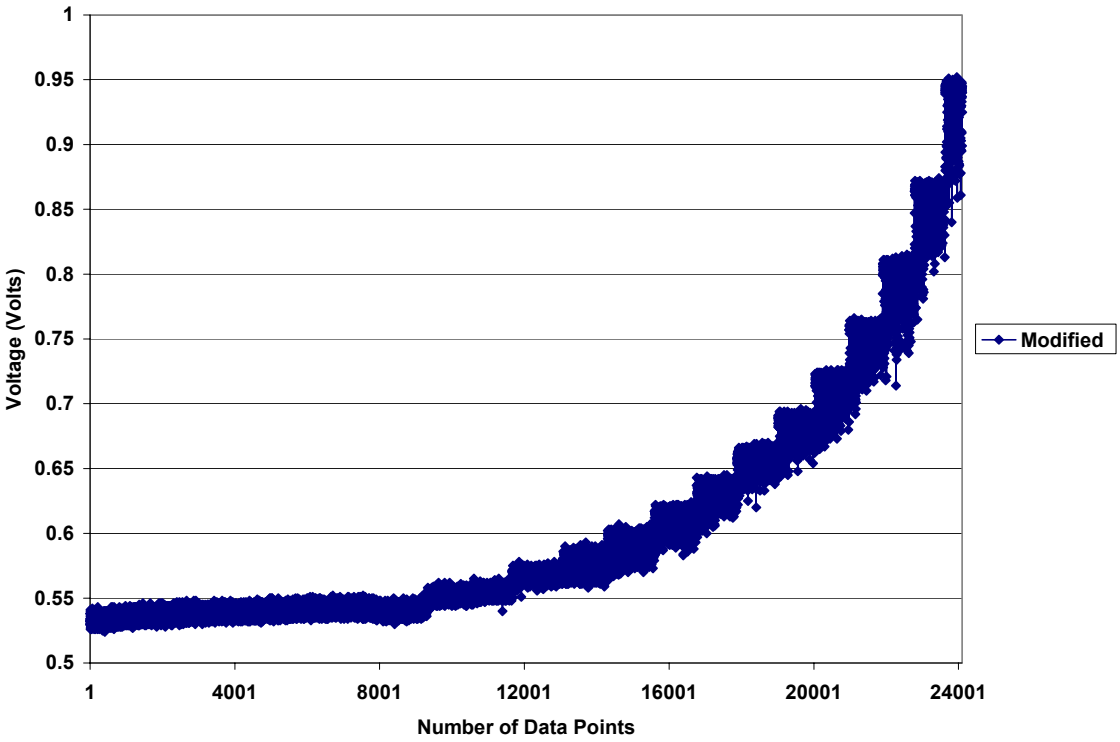

Figure 7.5(a): A Plot of Voltage versus Time for the Gauge using Modified Installation Procedure (Zoom of Figure 7.4)

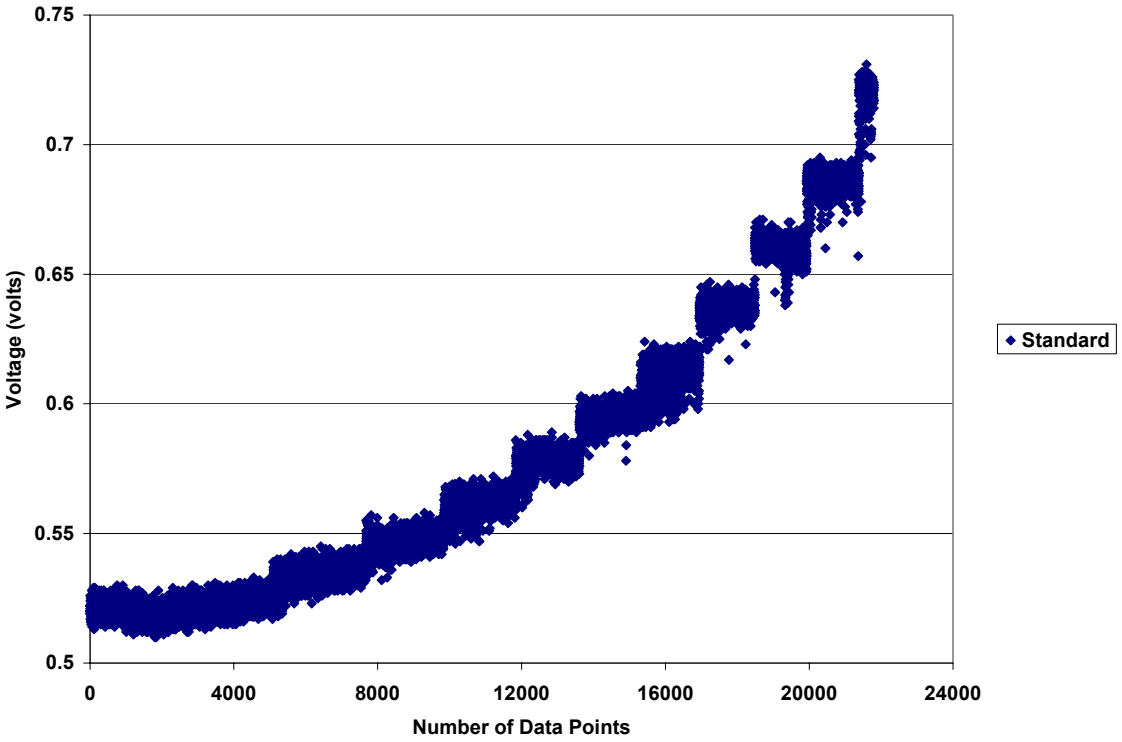

Figure 7.5(b): A Plot of Voltage versus Time for the Gauge using Standard Installation Procedure (Zoom of Figure 7.4)

Cruciform specimens with fillet welds were chosen to investigate the applicability of crack propagation gauges using a modified installation procedure for fatigue crack growth monitoring in ship structures. Figure 7.6 shows the schematic of the specimens. The specimens were subjected to constant amplitude fatigue testing at a positive stress ratio, R = 0.1. The fatigue testing was carried out in a closed loop servo-hydraulic machine with a maximum applied load of 133kN (30,000 lbs) and R ratio =0.1. Magnetic particle inspections were carried out at fillet welds periodically to look for fatigue cracks. Two fatigue cracks were found on the front top weld toe and the other on the back bottom of the specimen. Once the fatigue cracks were found, they were marked and the specimen was removed to install the crack propagation gauges. Two crack propagation gauges were installed ahead (within 2-3 mm) of the two fatigue cracks found at the weld toe. The gauge installation was checked by measuring the electrical resistivity across the gauge. The resistivity was around 6 ohms indicating that first four strands had broken for both the gauges during the installation. Figure 7.7(a) shows the photograph of the gauge installed across the fillet weld and Figure 7.7(b) shows the cruciform specimen installed in the fatigue testing rig. Figure 7.8 shows the plot of the voltage versus number of data points acquired during the fatigue testing for one of the gauges where the crack propagated and resulted in the failure of the specimen. As the figure indicates, the voltage is increasing with time and the behaviour is similar to that obtained on the smooth middle tension specimens. This shows that the crack propagation gauges, as well as the modified installation procedure, could be used to monitor fatigue crack growth on complex surfaces such as the fillet welds in the cruciform specimen used in the present program.

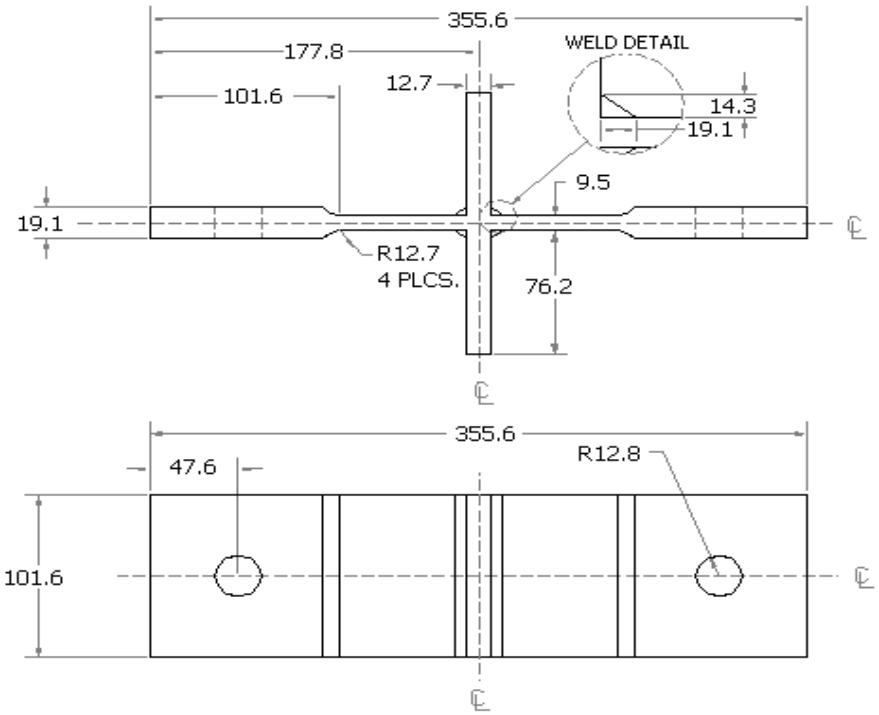

Figure 7.6: Schematic of the Cruciform Specimen

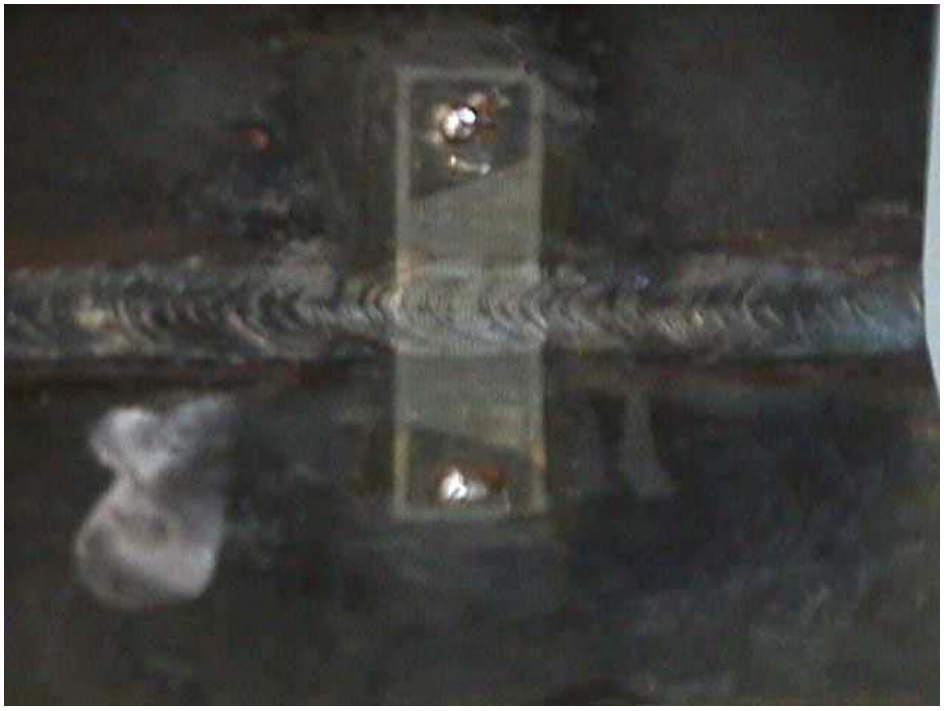

Figure 7.7(a): Photograph showing Crack Propagation Gauge Installed across the Fillet Weld of the Cruciform Specimen

Figure 7.7(b): Photograph of the Cruciform Specimen in the Fatigue Testing Rig

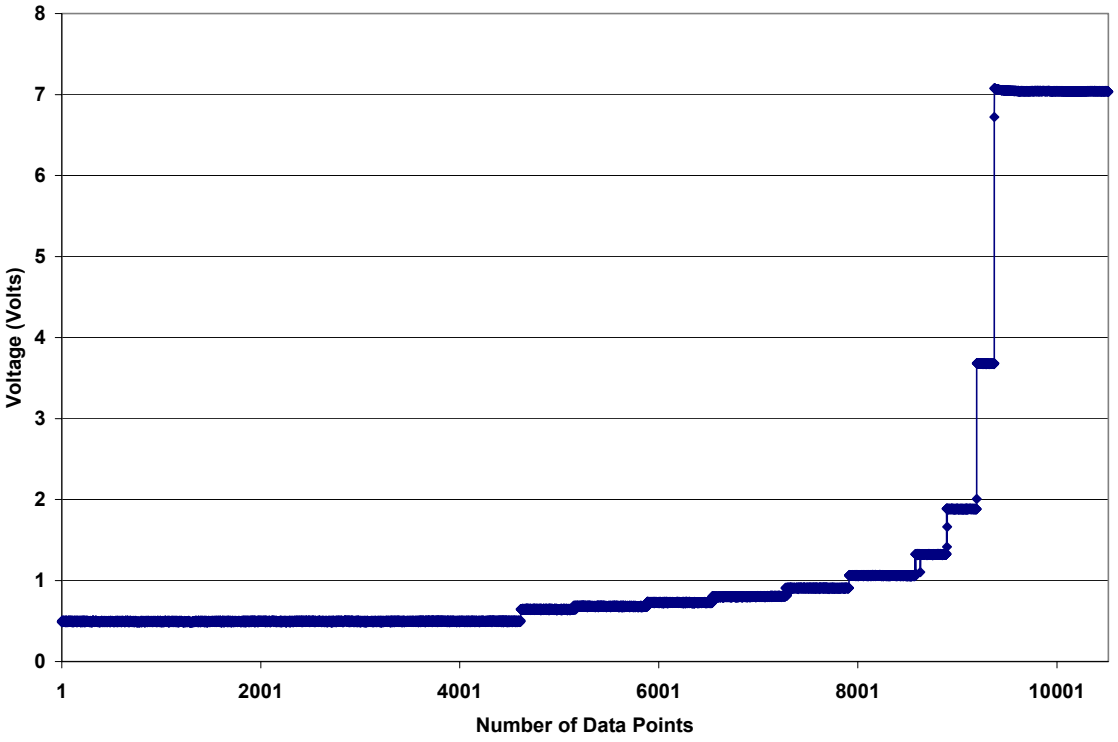

Figure 7.8: Plot of Voltage versus Time during Fatigue Testing of Cruciform Specimen

8. SUMMARY AND CONCLUSIONS

An extensive literature review was carried out to identify potential NDE techniques to address in service NDE of fatigue and fracture properties for ship structures. Specifically, the following three issues were addressed:

- Determination of in-situ fracture toughness of the material
- Establish remaining fatigue crack initiation life
- Detection of cracks and fatigue crack growth measurements

8.1 Determination of In-situ Fracture Toughness of the Material

The ABI technique was selected for evaluation of in-situ fracture toughness determination and the work was carried out at Advanced Technology Corporation, Oak Ridge, TN. The comparison of fracture toughness results from the non-destructive ABI method and destructive method was based on the determination of toughness in accordance with ASTM E1921. This is because it has been demonstrated that the ABI method can be used to develop a master curve for ferritic steel that is in reasonable agreement with the master curve determined by destructive tests in accordance with ASTM E 1921-97. The following summarizes the findings of the current work:

The reference temperature, [i.e., the temperature at which the mean initiation toughness is 100 MPa$\sqrt{m}$ (ASTM E1921)], calculated from the destructive tests for steel A is -77^{o}C compared to -60^{o}C from the non-destructive tests. The difference is within the 20^{o}C scatter band allowed in the standard. A similar comparison for the steel B was not possible due to high toughness (ductile tearing) at the test temperatures of interest from the perspective of service conditions. Therefore, to establish the reliability of the method, it is necessary to carry out testing by performing in-situ indentations on the plate surface at the laboratory scale level to establish the reference temperature. This should be validated by full thickness destructive testing in accordance with ASTM E1921.

For the welds, the fracture toughness results from both methods show agreement for the shielded metal arc (SMA) weld, whereas, for the flux cored arc (FCA) weld the destructive test results indicate lower toughness compared to the non-destructive evaluation. This is because the reference temperature difference, in the latter case, was much greater than the 20^{o}C scatter band allowed in the standard. This is due to heterogeneity of a multi-pass weld through the plate thickness of the butt weld. Considering the NDE requirement of **only the surface of the weld** being available for indentation tests, this is a more challenging task for reliable validation.

8.2 Determination of Remaining Fatigue Crack Initiation Life

Two techniques, the Piezzomagnetism Approach and the MWM were investigated to address the issue.

8.2.1 Piezzomagnetism Approach

The work was carried out at the University of Illinois. The piezzomagnetism approach is still at a laboratory stage. Most of the work in the current program was carried out in the low cycle fatigue regime. The technique at present can identify whether the specimen is within the first 10% or the last 10% of the fatigue life. In the middle 80%, there seems to be no change in the magnetic hysteresis. However, the most significant result of the present work indicated that under high cycle fatigue conditions a magnetic hysteresis was observed even though mechanical hysteresis as an indication of fatigue was nearly absent. Currently, further work is being carried out at the University of Illinois to examine in detail the B-field measurements in high cycle fatigue conditions. The results of this study will be made available to BMT FTL and if the results are encouraging, these will be reported to SSC.

8.2.2 Meandering Winding Magnetometer

The results are **"Proprietary and Confidential"** and are for limited disclosure to Canadian and United States governments (provided under separate cover). Appendix E details the summary and conclusions of JENTEK Sensors Inc. about the MWM evaluation carried out in this program.

8.3 Fatigue Crack Detection and Crack Growth Measurement

The Acoustic Emission Approach and crack propagation gauges were investigated to address the issue.

8.3.1 Acoustic Emission Approach

A paper study was carried out at Powertech Labs Inc. to investigate the feasibility of using the acoustic emission approach to carry out global monitoring of ship structures for fatigue crack detection and crack growth monitoring. The following summarizes their findings.

For acoustic emission monitoring, piezoelectric sensors are the best commercial devices available today. However, these devices are not suited for the global monitoring of a large structure such as a ship. Distributed sensing of acoustic emission is feasible through the use of one or two loops of optic fibers running across a large area. Although the technology of AE detection using fiber optic sensors is proven, it is not yet commercialized.

Should a fiber optic system become commercially available in the future, it will require further development to demonstrate compatibility for use on-board a ship. Thus, the global AE monitoring of a ship structure remains desirable, but a long-term objective.

Monitoring of critical local areas of the ship structure using piezo electric sensors could provide valuable information on reliability and enable scheduling of cost effective repairs. Acoustic emission systems are commercially available to carry out the task of local area monitoring for a number of selected sites on the ship simultaneously. However, the missing link to make local area monitoring an effective tool is the quantification of crack growth from the acoustic emission data gathered on stable crack growth.

Limited experimentation has been done in the past to monitor cracks in ship structure. The objective of such experiments has been to locate the crack rather than to quantify the crack growth. Difficulties were encountered due to noise and it has been suggested that a high threshold setting may be appropriate to overcome the noise generated by rain impingement on the deck. A high threshold setting, however, would require a larger number of sensors to provide coverage for a given area. Other approaches have been used to improve the signal to noise ratio during AE monitoring of other structures such as reinforced concrete decks, bridges and pressure vessels. Wave form characterization as a means of discriminating acoustic events from different sources is deemed most appropriate for application to ship structures.

8.3.2 Crack Propagation Gauges

A small experimental program was carried out at BMT FTL to investigate the feasibility of using crack propagation gauges to monitor crack growth on complex irregular geometries such as fillet welds. Standard middle tension specimen geometry was first used to evaluate the modified (simple) procedure developed at BMT FTL for crack propagation gauge installation. Cruciform specimens with fillet welds were then fabricated to evaluate crack propagation gauges using the modified installation procedure. The crack propagation gauges were successful in monitoring fatigue crack growth on complex surfaces such as fillet welds in the cruciform specimens used in the present program.

9. RECOMMENDATIONS

- The ABI technique for in-situ fracture toughness determination

The ABI technique to evaluate fracture toughness is a promising technique that has demonstrated its success in the context of nuclear pressure vessels. The evaluation of this technique for ship structural steels and their weld metals met with partial success in the current project as described in the summary and the conclusions. This is likely due to a drawback in the experimental approach. It is believed that by focusing on the determination of T_o, (the reference temperature), a more positive evaluation of the technique can be demonstrated for base metal as described above. In light of the importance of the fracture toughness estimates in determining structural integrity, it is recommended that further work should be undertaken with the ABI technique, focusing on base materials in the next stage. Subject to a successful outcome in this stage, further work can continue with weld metals.

For the next stage, dealing with base metal tests, it is proposed that evaluation of this ABI method should not be limited to the operating temperatures, but rather be aimed at determining the reference temperature. The validation can then be performed by full thickness destructive testing in the reference temperature range. Ship plates that have a range of reference temperatures need to be evaluated to assess the reliability of the method in terms of determining the reference temperature from indentations on the plate surface. Depending on the budget, it is best that a range of thicknesses representing ship plates be evaluated with the objective of also covering the significance to through-thickness variability in fracture toughness as this may have a limitation as well.

- Acoustic emission for local area monitoring.

Global monitoring of ship structures is not economically feasible, however, the local area monitoring will still cover large areas compared to the conventional NDE techniques. Therefore, it is recommended that a small experimental program be carried out to investigate the feasibility of using the AE technique on a ship structure as well as to evaluate the effectiveness of wave form characterization as a means of discriminating acoustic events from different sources on a ship structure.

- Crack propagation gauges for crack growth monitoring.

When a known crack exists and the results of the numerical/analytical analyses carried out of the location reveal that the crack will not propagate to the critical size within the next scheduled maintenance, a crack propagation gauge can then be used to monitor the fatigue crack growth and provide in-service crack growth rate. This, in turn, can be used to validate the analytical/numerical assessment.

10. REFERENCES

[1] Symposium Proceedings, "Non-Destructive Characterization of Materials in Aging Systems", Editors: R. L. Crane, et al; Nov–Dec 1997; Boston; published by the Materials Research Society; Vol. 503.

[2] Symposium Proceedings, "Non-Destructive Evaluation of Aging Maritime Applications", Editor: R. B. Mignogna; June 1995; Oakland, California; published by The International Society for Optical Engineering.

[3] Yee, R., Malik, L., Basu, R, and Kirkhope, K.; "Guide to Damage Tolerance Analysis of Marine Structures", Ship Structure Committee Report SSC 402 (SR 1374); prepared by Fleet Technology Limited, 1997.

[4] Non-Destructive Testing, "Quality Control and NDT", Ed. Louis Cartz; Published by ASM, 1995.

[5] Chase, S.B., "A New Fatigue Crack Detection System" in "Structural Materials Technology", an NDT Conference, Eds Scancella, R.J., Callahan, M.E., 1994.

[6] Chase, S.B., "Developing NDT Technologies for the Next Century in Structural Materials Technology", an NDT Conference, Eds. Hartbower, P.E. and Stolarski, P.J., 1996.

[7] Ono, K., "Acoustic Emission." "Fatigue Crack Measurement Techniques and Applications", Eds., K.J. Marsch and R.O. Ritchie, EMAS Publications, West Midlands, U.K., 1991.

[8] Pollock, A.A., "Acoustic Emission Inspection." Non-Destructive Evaluation and Quality Control, Metals Handbook, Ninth Edition, Vol. 17, 278-294, 1989.

[9] Scruby, C.B. and Buttle, D.J., "Quantitative Fatigue Crack Measurement by Acoustic Emission." Fatigue Crack Measurement Techniques and Applications, Eds., K.J. Marsch and R.O. Ritchie, EMAS Publications, West Midlands, U.K., (1991).

[10] Akhtar, A, et al, "Acoustic Emission Testing of Steel Cylinders for the Storage of Natural Gas on Vehicles", NDT & E International; V25; 1992; pp 115-125.

[11] US Patent Application #09/038,850 filed March 12, 1998; Inventors: Lentle, Aldridge and Akhtar.

[12] Tirbonod, B., et al; "Acoustic Emission Measurements during the Local Monitoring of a Defect in ZB2 Pressure Vessel"; NDT International; V24, 1991; pp 3-14.

[13] Leinbach, Jr., R.A., "Non-Destructive Test & Evaluation at the Carderock Division, Naval Surface Warfare Center", "Non-Destructive Evaluation of Aging Maritime Applications", Ed., Mignogna, R.B. Proceedings SPIE, Vol. 2549, 1995.

[14] Pishva, M.R., Bellinger, N.C., Terada, T. and Koul, A.K., "DC-PD Technique for Crack Length Measurements at Elevated Temperatures", Laboratory Technical Report, LTR-ST-1635, National Research Council, Canada, (1987).

[15] Instruction Manual, "Matelect Pulsed DCPD Crack Growth Monitor", Version 6, Matelect Limited, 33 Bedfords Gardens, London, U.K, (1994).

[16] Gangloff, R.P., "Electrical Potential Monitoring of Crack Formation and Subcritical Growth from Small Defects." Fat. Engg. Mater. Struct., Vol. 4, No. 1. (1981).

[17] Hartman, G.A. and Johnson, D.A., "D-C Electric-Potential Method Applied to Thermal/Mechanical Fatigue Crack Growth", Experimental Mechanics, (March 1987).

[18] Hicks, M.A. and Pickard, A.C., "A Comparison of Theoretical and Experimental Methods of Calibrating the Electrical Potential Drop Technique for Crack Length Determination." Int. Journ. of Fracture 20, (1982).

[19] Chang, M., Terada, T. and Koul, A.K, "Calibration of a DCPD Technique for Fatigue Crack Initiation and Short Crack Growth in Double Edge Notched Specimens", Internal Report (unpublished), SML, IAR, National Research Council, Canada, (1992).
[20] Donald, J.K. and Ruschau, J., "Direct Current Potential Difference Fatigue Crack Measurement Techniques", Fatigue Crack Measurement Techniques and Applications, Eds., K.J. Marsch and R.O. Ritchie, EMAS Publications, West Midlands, U.K., (1991).
[21] Burgers, A. and Kempen, P.D., "Automatic Crack Length Measurement by the Electrical P.D. Method with Computer Control", Advances in Crack Length Measurement, Ed. C.J. Beevers, EMAS Publications, West Midlands, U.K., (1982).
[22] Kraus, J.D., "Electromagnetics", McGraw Hill, Third Edition, (1984)
[23] Veropest, I., Aernoudt, E., DeruyttereE, A. and Neyrinck, M., "An ACPD Method for Detection and Measurement of Surface Microcracks during Fatigue Testing of Wires", Advances in Crack Length Measurement, Ed. C.J. Beevers, EMAS Publications, West Midlands, U.K., (1982).
[24] Watt, K.R., "A Consideration of an A.C. Potential Drop Method for Crack Length Measurement", The Measurement of Crack Length and Shape during Fracture and Fatigue, Ed. C.J. Beever, EMAS Publications, West Midlands, U.K., (1980).
[25] Hwang, I.S. and Ballinger, R.G., " A Multi-Frequency AC Potential Drop Technique for the Detection of Small Cracks", Measurement Science Technology, Vol. 3, (1992).
[26] Gendron, S. and Marchand, N.J., "On-Line Damage Assessment of Turbine Airfoil-Like Test Coupons under Simulated Service Conditions", Testing under Simulated Conditions Part 2, Oberflachen Werkstoffe, No. 3, (1994).
[27] Gendron, S., et al, "Thermal Fatigue Damage Accumulation in a Coated Turbine Blade Material Tested under Simulated Service Conditions", Elevated Temperature Coatings: Science and Technology I, Eds., N.B. Dahotre, J.M. Hamikian and J.J. Stiglich, The Minerals, Metals and Materials Society, (1995).
[28] Charlesworth, F.D.W. and Dover, W.D., "Some Aspects of Crack Detection and Sizing using A.C. Field Measurements", Advances in Crack Length Measurement, Ed. C.J. Beever, EMAS Publications, West Midlands, U.K., (1982).
[29] Dover, W.D., et al, "Fatigue Crack Measurements in Offshore Structures", Fatigue Crack Measurement Techniques and Applications, Eds., K.J. Marsch and R.O. Ritchie, EMAS Publications, West Midlands, U.K., (1991).
[30] Tiku, S., Ph.D Thesis, Dept. of Metallurgy, Ecole Polytechnique, Univ. of Montreal, (1997).
[31] Haggag, F. M., "Field Indentation Microprobe for Structural Integrity Evaluation", U.S. Patent 4,852, 397; August 1989.
[32] Byun, T. S., et al, "A Theoretical Model for Determination of Fracture Toughness of Reactor Pressure Vessel Steels in the Transition Region from Automated Ball Indentation Test", Journal of Nuclear Materials, V252, 1998, pp 187-194.
[33] Murty, K. L., "Non-Destructive Evaluation of Deformation and Fracture Properties of Materials Using Stress-Strain Microprobe", in Reference 1.
[34] Vary, A., "Correlations among Ultrasonic Propagation Factors and Fracture Toughness Properties of Metallic Materials", Materials Evaluation, June, 1978.
[35] Sinclair, A. N. and Eng, H. "Ultrasonic Determination of Fracture Toughness" Non-Destructive Characterization of Materials II, Eds. Bussiere, J.F., Monchalin, J.P., Rudd, C.O. and Green, Jr., R.E.

[36] Canella, G. and Taddei, M.; "Correlation between Ultrasonic Attenuation and Fracture Toughness of Steels", Ibid.
[37] Green, Jr., R.E.; "Ultrasonic Nondestructive Materials Characterization", Materials Analysis by Ultrasonics, Metals Ceramics, Composites. Ed. Alex Vary.
[38] Serabian, S.; "Ultrasonic Material Property Determinations", Ibid.
[39] Williamson, G. K., and Smallman, R. E.; Phil. Mag.; V1; Jan. 1956; pp 34-36.
[40] Kurita, M.; "A New Method for Evaluating X-Ray Diffraction Peak Broadening with Engineering Applications"; in Advances in X-Ray Analysis; V31; 1988; pp 277-286.
[41] Kurita, M., and Chiaki, K.; "Use of X-Ray Diffraction using Gaussian Curve Method for Measuring Plastic Strains of Steels"; ibid; V34; 1991; pp 633-642.
[42] Goto, T.; "Material Strength Evaluation and Damage Detection by X-Ray Diffraction"; ibid; V35; 1992; pp 489-501.
[43] Pangborn, R. N., et al; "Dislocation Distribution and Prediction of Fatigue Damage"; Met Trans A; V12A; Jan. 1981; pp 109-120.
[44] Isobe, Y., et al; "An Evaluation Method for Predicting Fatigue Remaining Lives of Structural Components in Nuclear Power Plants with X-Ray Diffraction Technique", Intl. Conf. Fatigue '93, Montreal, 1993.
[45] Pangborn R.N. and Zamrik, S.Y.; "Fatigue Damage Assessment by X-ray Diffraction and Non-Destructive Life Assessment Methodology", Non-Destructive Characterization of Materials IV, Ed. Rudd, C.O., published by Plenum Press, (1991).
[46] Guralnick, S. A.; "Hysteresis and Acoustic Emission as Non-Destructive Measures of the Fatigue Process in Metals"; Illinois Institute of Technology Report RN-5-54249-FR; May 1997.
[47] Goldfine, N. and Clark, D., "Introduction to the Meandering Winding Magnetometer (MWM) and the Grid Measurement Approach", Proceedings SPIE Vol. 2944, 1996.
[48] Goldfine, N. and Washabaugh, A., "Surface- Mounted Eddy-Current Sensors for On-Line Monitoring of Fatigue Tests and for Aircraft Health Monitoring", Presented at the second Joint NASA/FAA/DoD Conference on Aging Aircraft, August 1998.
[49] Goldfine, N.J. and Zilberstein, V.; "Recent Applications of Meandering Winding Magnetometers to Materials Characterization", Presented at 38th Annual British Conf. on NDT, Sept. 1999.
[50] Goldfine, N. et al; "Conformable Eddy Current Sensors and Methods for Gas Turbine Inspection and Health Monitoring", Gas Turbines Technology Conference, Materials Solutions, ASM International, 1998.
[51] Weber, D., and Gurney, T. R.; "Tests to Investigate the Performance of Fatigue Gauges in Conjunction with Fillet Weld Joints in Al-Zn-Mg Alloys"; in Structural Integrity Assessment; Ed. P. Stanley.
[52] Luong, M. P.; "Non-Destructive Evaluation of Fatigue Limits of Metals using Infrared Thermography"; in Reference 1.

[53] Crack Arrest Toughness of Steel Weldments (SR-1384).
[54] Standard Test Method for Determination of Reference Temperature, T_0, for Ferritic Steels in the Transition Range, ASTM E 1921-97.
[55] Standard Test Method for Measurement of Fracture Toughness, ASTME E 1820-96.
[56] Towers, O.L., "Procedures for Fatigue Cracking Fracture Toughness Test Pieces, with Particular Reference to Weldments", The Welding Institute Research Bulletin, April 1982, pp. 112-120.
[57] "Non-Destructive and Localized Measurements of Stress-Strain Curves and Fracture Toughness of Ferritic Steels at Various Temperatures using Innovative Stress-Strain Microprobe™ Technology", DOE-SBIR Phase II Final Report *DOE/ER/82115-2*, under grant number DE-FG02-96ER82115.

SHIP STRUCTURE COMMITTEE PARTNERS AND LIAISON MEMBERS

PARTNERS

The Society of Naval Architects and Marine Engineers

Mr. Joe Cuneo
President,
Society of Naval Architects and Marine Engineers

Dr. John Daidola
Chairman,
SNAME Technical & Research Steering Committee

The Gulf Coast Region Maritime Technology Center

Dr. John Crisp
Executive Director,
Gulf Coast Maritime Technology Center

Dr. Bill Vorus
Site Director,
Gulf Coast Maritime Technology Center

LIAISON MEMBERS

American Iron and Steel Institute
American Society for Testing & Materials
American Society of Naval Engineers
American Welding Society
Bethlehem Steel Corporation
Canada Center for Minerals & Energy Technology
Colorado School of Mines
Edison Welding Institute
International Maritime Organization
International Ship and Offshore Structure Congress
INTERTANKO
Massachusetts Institute of Technology
Memorial University of Newfoundland
National Cargo Bureau
Office of Naval Research
Oil Companies International Maritime Forum
Tanker Structure Cooperative Forum
Technical University of Nova Scotia
United States Coast Guard Academy
United States Merchant Marine Academy
United States Naval Academy
University of British Columbia
University of California Berkeley
University of Houston - Composites Eng & Appl.
University of Maryland
University of Michigan
University of Waterloo
Virginia Polytechnic and State Institute
Webb Institute
Welding Research Council
Worchester Polytechnic Institute
World Maritime Consulting, INC

Mr. Alexander Wilson
Captain Charles Piersall (Ret.)
Captain Dennis K. Kruse (USN Ret.)
Mr. Richard Frank
Dr. Harold Reemsnyder
Dr. William R. Tyson
Dr. Stephen Liu
Mr. Dave Edmonds
Mr. Tom Allen
Dr. Alaa Mansour
Mr. Dragos Rauta
Mr. Dave Burke / Captain Chip McCord
Dr. M. R. Haddara
Captain Jim McNamara
Dr. Yapa Rajapaksie
Mr. Phillip Murphy
Mr. Rong Huang
Dr. C. Hsiung
Commander Kurt Colella
Dr. C. B. Kim
Dr. Ramswar Bhattacharyya
Dr. S. Calisal
Dr. Robert Bea
Dr. Jerry Williams
Dr. Bilal Ayyub
Dr. Michael Bernitsas
Dr. J. Roorda
Dr. Alan Brown
Dr. Kirsi Tikka
Dr. Martin Prager
Dr. Nick Dembsey
VADM Gene Henn, USCG Ret.

RECENT SHIP STRUCTURE COMMITTEE PUBLICATIONS

Ship Structure Committee Publications on the Web - All reports from SSC 392 and forward are available to be downloaded from the Ship Structure Committee Web Site at URL:
http://www.shipstructure.org
SSC 391 and below are available on the SSC CD-ROM Library. Visit the National Technical Information Service (NTIS) Web Site for ordering information at URL:
http://www.ntis.gov/fcpc/cpn7833.htm

SSC Report Number	Report Bibliography
SSC 427	**Life Expectancy Assessment of Ship Structures** A. Dinovitzer 2003
SSC 426	**Post Yield Stability of Framing** J. DesRochers, C. Pothier, E. Crocker 2003
SSC 425	**Fatigue Strength and Adequacy of Weld Repairs** R.J. Dexter, R.J. Fitzpatrick, D.L. St. Peters 2003
SSC 424	**Evaluation of Accidental Oil Spills from Bunker Tanks (Phase I)** T. McAllister, C. Rekart, K. Michel 2003
SSC 423	**Green Water Loading on Ship Deck Structures** M. Meinhold, D. Liut, K. Weems, T. Treakle, Woe-Min Lin 2003
SSC 422	**Modeling Structural Damage in Ship Collisions** Dr. A.J. Brown 2003
SSC 421	**Risk Informed Inspection of MarineVessels** Dr. B.M. Ayyub, U.O. Akpan, P.A. Rushton, T.S. Koko, J. Ross, J. Lua 2003
SSC 420	**Failure Definition for Structural Reliability Assessment** Dr. B. M. Ayyub, P.E. Hess III, D.E. Knight 2002
SSC 419	**Supplemental Commercial Design Guidance for Fatigue** R.A. Sielski, J. R. Wilkins, J.A. Hultz 2001
SSC 418	**Compensation for Openings in Primary Ship Structure** J.J. Hopkinson, M. Gupta, P. Sefcsik 2002
SSC 417	**Prediction of Structural Response in Grounding Application to Structural Design** K.K. Tikka 2001
SSC 416	**Risk Based Life Cycle Management of Ship Structure** Dr. B.M. Ayyub, U.O. Akpan, G. F. DeSouza, T. S. Koko, X. Luo 2001
SSC 415	**Crack Arrest Toughness of Steel Weldments** Dr. L.N. Pussegoda, Dr. L. Malik, B.A. Graville, Y. Han, and Dr. S. J. Kennedy, 2000
SSC 414	**Probability Based Design (Phase 4) Synthesis of the Reliability Thrust Area** P.A. Frieze 2000